



UNIVERSIDAD DE CHILE  
FACULTAD DE CIENCIAS FÍSICAS Y MATEMÁTICAS  
DEPARTAMENTO DE GEOLOGÍA

**ERUPTIVE PARAMETERS AND PRE-ERUPTIVE PROCESSES FOR  
LATE HOLOCENE ACTIVITY CENTRED AT MELIMOYU VOLCANO,  
SOUTHERN CHILE (44°05' S)**

TESIS PARA OPTAR AL GRADO DE MAGÍSTER EN CIENCIAS,  
MENCIÓN GEOLOGÍA

CAROLINA ANDREA GEOFFROY GÓMEZ

PROFESOR GUÍA:  
ÁNGELO CASTRUCCIO ÁLVAREZ  
MIEMBROS DE LA COMISIÓN:  
ÁLVARO AMIGO RAMOS  
MIGUEL ÁNGEL PARADA REYES

SANTIAGO DE CHILE

2017

**RESUMEN DE LA TESIS PARA OPTAR AL GRADO DE:**  
Magíster en Ciencias, mención Geología.  
**POR:** Carolina Andrea Geoffroy Gómez  
**FECHA:** Septiembre 2017  
**PROFESOR GUÍA:** Ángelo Castruccio Álvarez

**PARÁMETROS ERUPTIVOS Y PROCESOS PRE-ERUPTIVOS PARA LA ACTIVIDAD  
HOLOCENA DEL VOLCÁN MELIMOYU, SUR DE CHILE (44°05'S):**

El volcán Melimoyu es un estratovolcán con actividad eruptiva histórica desconocida. Sin embargo, a lo largo de la Carretera Austral y rutas aledañas se observan depósitos de caída asociados a este centro, que evidencian al menos dos erupciones explosivas de importante magnitud ocurridas durante el Holoceno tardío. El depósito más antiguo, datado en ca. 2,8 cal ka AP y conocido en la literatura como MEL1, aparece zonado composicionalmente con piroclastos pumíceos de composición dacítica (64.3-65.4% SiO<sub>2</sub>) predominantemente en la porción inferior-media gradando abruptamente a piroclastos escoriáceos de composición basáltica (49.3-50.4% SiO<sub>2</sub>) en la porción superior. En contraste, el depósito más reciente, conocido como MEL2, y datado en ca. 1,6 cal ka AP, presenta una composición andesítica (59.5-61.3% SiO<sub>2</sub>).

En este trabajo se analizaron depósitos en los alrededores del volcán a más de 20 km del origen. En su mayoría corresponden a la estratigrafía antes descrita, sin embargo, depósitos reconocidos en el sector oeste del volcán son macroscópica y texturalmente diferentes. Algunos fueron asignados al evento MEL2 sobre la base de análisis químicos en el material juvenil, o bien mediante dataciones radiocarbono en paleosuelos subyacentes. Para cada uno de los depósitos identificados se midió espesores y clastos mayores. La compilación de esta información permitió obtener volúmenes no-DRE de ~ 2,6 km<sup>3</sup> para MEL1 y ~ 1,6 km<sup>3</sup> para MEL2. Por otra parte, las alturas de columna obtenidas fueron aproximadamente 30-35 km para MEL1 y 25-30 km para MEL2. En cuanto a la dispersión atmosférica, esta sería E-SE para MEL1, mientras que MEL2 presenta una dispersión principalmente E.

Producto del estudio químico y petrográfico de los piroclastos de MEL1 se reconoció que el reservorio dacítico se habría encontrado a profundidades moderadamente someras de ~ 2 kbar (7 km), donde los cristales, principalmente de plagioclásas y anfíbolas, se habrían formado sin perturbaciones importantes. En contraste, los productos escoriáceos sugieren una inyección de composición basáltica desde profundidades mayores, durante un período relativamente corto, que habría sido el gatillante de la erupción. La composición andesítica de MEL2 puede ser explicada mediante una mezcla de las composiciones dacíticas y basálticas respectivamente de MEL1, y posterior proceso de cristalización fraccionada. Los piroclastos andesíticos de MEL2 no muestran evidencia de recarga de magma, no obstante, se sugiere que procesos de cristalización y saturación de volátiles podrían ser los gatillantes de esta erupción.

## **Escoria y leyenda: la memoria del Peripillán**

Cuentan sobre el sacrificio de una virtuosa mujer, la hermosa Licarayén, quien acabó el maleficio frenando fuego y bullicio.

“Ríos de magma y de lava Peripillán expulsaba”, la geóloga, curiosa, escuchó la misteriosa leyenda que se contaba.

Cada rincón visitó frío, verde o lluvioso y entre cerros numerosos por montones encontró capas de negro color.

¡Qué diversas situaciones esconden las erupciones que han formado aquellas capas por escorias expulsadas en distintas direcciones!

Con su martillo y su lupa observando esas escorias, se fue imaginando historias y estudiando concienzuda.

Para no quedar con dudas seleccionó algunas pocas y de forma rigurosa muestras de escorias tomó, que en su libreta anotó antes de irse orgullosa.

Así empezó a descifrar junto a su fiel microscopio las escorias en acopio y minerales captar.

Y con ellos encontrar las respuestas de un pasado, del trayecto apresurado desde abajo del volcán hasta este gran cielo austral de aquel magma emancipado.

Y del pasado seguro, ideas permitirán entender como el volcán podría actuar a futuro.

Aunque no todo aseguro, queda algo aún por saber.

¿Sirvió que Licarayén haya ofrecido su vida o el volcán será el que olvida, y un día volverá a arder?

## AGRADECIMIENTOS

En primer lugar, a CONICYT, ya que esta tesis se enmarca dentro del proyecto FONDECYT de Iniciación #11130671 y ya que mis estudios fueron financiados por la Beca de Magíster Nacional. Al Centro de Excelencia en Geotermia de los Andes (CEGA, proyecto FONDAP #15090013) por el financiamiento otorgado para congresos y salidas relevantes para mi tesis.

Al Departamento de Postgrado y Postítulo de la Universidad de Chile por su “Ayudas para Estadías Cortas de Investigación Destinadas a Estudiantes Tesistas de Doctorado y Magíster de la Universidad de Chile” que permitió financiar una estadía en Nueva Zelanda para realizar análisis químicos esenciales para el desarrollo de esta investigación.

A mis profesores Álvaro Amigo, Ángelo Castruccio y Miguel Ángel Parada por su dedicación, apoyo y confianza para la realización de este trabajo.

A Brent Alloway por el financiamiento y su apoyo logístico en la pasantía y en las discusiones, y por ser, junto a Walescka Pino-Ojeda, una segunda familia en Nueva Zelanda. A Francisco Gutiérrez por sus aportes en las discusiones.

A los funcionarios del Departamento de Geología, especialmente a Blanca Baccolla y Maritza Acuña que siempre estuvieron muy atentas y cariñosas cuando tuve dudas.

A las chicas del área de comunicaciones del CEGA, quienes, aunque no han ayudado directamente en mi tesis, han aportado enormemente en mi crecimiento durante el último año, ampliando mis conocimientos a otros aspectos importantes de la ciencia y la geología.

A todas las personas de la sala de postgrado, especialmente a quienes han sido mis vecinos y al poder femenino de la sala, con quienes compartí tantas oncecitas y cervezas. A los petrólogos y volcánólogos que han pasado por la sala, por todo su aporte en los resultados/discusiones/figuras y los lindos momentos vividos en las salidas a terreno y en los congresos.

A mis amigos de la vida que se han hecho presente en estos años, aguantando mis mañas y haciéndome reír siempre que lo necesité, especialmente a Levi, Fer, Kota, Oso, Benja, Caro G., Caro B., Fabi, Salo, Pasita, Feñi, Gabi, Rayo, Mari y mis Geogirls. Gracias por todos los cafés, los carretes, las salidas deportivas y las bailables.

Y por supuesto a toda mi familia, principalmente a mis papás y hermanos, por entender mis elecciones, darme ánimo todo el tiempo y distraerme de esta tesis (Los amo ❤).

## TABLA DE CONTENIDO

1.	Introducción .....	1
1.1.	Estructura de esta tesis .....	1
1.2.	Formulación del problema .....	1
1.3.	Ubicación y vías de accesos.....	3
1.4.	Marco geológico.....	3
1.5.	Hipótesis de trabajo.....	5
1.6.	Objetivos .....	5
1.6.1.	Objetivo principal.....	5
1.6.2.	Objetivos específicos.....	5
1.7.	Metodologías .....	6
2.	Eruptive parameters and pre-eruptive processes for Late Holocene activity centred at Melimoyu volcano, Southern Chile (44°05' s).....	9
2.1.	Introduction .....	9
2.1.1.	Geological background.....	12
2.1.2.	Previous research on melimoyu-sourced post-glacial activity .....	12
2.1.3.	Other volcanoes .....	13
2.2.	Methods.....	14
2.2.1.	Sieving and grain-size .....	14
2.2.2.	Dating.....	14
2.2.3.	Eruptive parameters .....	15
2.2.4.	Whole rock chemistry .....	15
2.2.5.	Glass and mineral chemistry .....	16
2.3.	Results.....	19
2.3.1.	Tephra descriptions .....	19
2.3.2.	Dating.....	23
2.3.3.	Eruptive parameters .....	25
2.3.4.	Geochemistry.....	30
2.3.5.	Mineralogy and petrography.....	34
2.3.6.	Thermobarometry.....	45
2.4.	Discussion.....	49

2.4.1.	Last 20 kyrs activity of Melimoyu volcano .....	49
2.4.2.	Eruptive parameters of M1 and M2.....	54
2.4.3.	Pre-eruptive conditions of M1 .....	57
2.4.4.	Relationship between Melimoyu's eruptions.....	60
2.5.	Conclusions .....	66
3.	Bibliografía.....	69
4.	Anexos .....	78

## INDICE DE FIGURAS

Figure 1 Location map for Melimoyu volcano.....	10
Figure 2 Zoom of the western side of Melimoyu volcano.....	19
Figure 3 Stratigraphy of a representative section of deposits to the E side of Melimoyu volcano.....	20
Figure 4 Stratigraphy of sections studied of deposits to the western side of Melimoyu volcano.....	23
Figure 5 The four localities on the western side that preserve Melimoyu pyroclastic units.....	25
Figure 6 Isopach maps of M1, M1s and M2 units.....	27
Figure 7 Isopleth maps of M1p, M1s and M2 units.....	29
Figure 8 Whole-rock compositions of all units found in this study.....	30
Figure 9 Variation diagrams of some major and trace elements showing the whole-rock compositions of M1p, M1s, M2 and one lava from Melimoyu volcano.....	32
Figure 10 Primitive mantle-normalized spider diagram and REE patterns .....	33
Figure 11 Selected backscattered electron images of representative glass shards.. ....	35
Figure 12 Selected major element compositions variations of glass shards from MEL1 and MEL2 tephras collected in time series.....	38
Figure 13 Backscattered electron images of plagioclase phenocrysts in magmas from MEL1 (lower) and MEL2 (upper) eruptions sourced from Melimoyu volcano.. .....	39

Figure 14 Plagioclase phenocrysts and microlites compositions from MEL1 (lower) and MEL2 (upper) eruptions sourced from Melimoyu volcano. ....	40
Figure 15 Backscattered electron images of amphiboles phenocrysts in magmas from M2 (A,B) and M1p (C,D).....	41
Figure 16 Amphiboles phenocrysts composition of M1p and M2 units.....	42
Figure 17 Backscattered electron images of olivines, clinopyroxenes and orthopyroxenes phenocrysts in magmas from M1, M1s and M2 units.....	43
Figure 18 Olivine and pyroxene compositions of the studied samples.....	45
Figure 19 Stability P-T fields.....	46
Figure 20 Temperatures obtained by geothermometry .....	47
Figure 21 A) Ti versus Rb and B) Sr versus Ba graphs modified from Stern et al. (2015). .....	51
Figure 22 La/Yb versus Zr/Nb for the lava flow and tephras of Melimoyu eruptions, and tephra layers of Stern et al. (2015) associated to Melimoyu.....	52
Figure 23 Eruption volumes for volcanic centers of the southernmost part of the SVZ between 42°-46° from Late Glacial and Holocene time.....	54
Figure 24 Mingled pumices of M1 eruption.....	58
Figure 25 An zoning profiles on plagioclases of M1p. ....	59
Figure 26 SiO <sub>2</sub> -K <sub>2</sub> O-FeO wt% variation in glass from M1p, M1s and M2 units. ....	61
Figure 27 Mixing models between M1p and M1s composition to obtain M2 chemistry. .	62
Figure 28 Results of fractional crystallization models.....	64
Figure 29 Holocene eruptions of Melimoyu volcano.....	67

## INDICE DE TABLAS

Table 1 Whole-rock major and trace element compositions determined by XRF and ICP-MS.....	17
Table 2 Granulometric parameters for selected tephra sections .....	21
Table 3 Summary of radiocarbon ages reported in this study and from previous studies. ....	24

Table 4 Eruptive parameters of Melimoyu Holocene eruptions.....	26
Table 5 Ratios of trace elements of M1p, M1s, M2 and samples from western side.....	31
Table 6 Modal mineralogy (vol.%) of Melimoyu eruptions .....	34
Table 7 Summary of the mineralogical characteristics of Melimoyu eruptions. ....	36
Table 8 Summary of pressures and temperatures obtained in this study.....	48
Table 9 Ratios of trace elements of M1p, M1s, M2 and samples from Stern et al. 2015.	
.....	50
Table 10 Distribution coefficients for the phases fractionated in fractional crystallization model. .....	63

## **1. INTRODUCCIÓN**

### **1.1. Estructura de esta Tesis**

La presente tesis se enfoca en el estudio tefrocronoestratigráfico de los depósitos piroclásticos asociados al volcán Melimoyu, y específicamente de dos depósitos de caída de erupciones holocenas del mismo volcán, con énfasis en la estimación de la magnitud y dispersión de estas erupciones, así como de las condiciones pre-eruptivas de las mismas. La estructura de la tesis se basa en dos capítulos:

El capítulo 1 es una introducción. Se presenta la ubicación y marco geológico de la zona, la motivación y objetivos del estudio, la hipótesis de trabajo, además de las metodologías utilizadas.

El capítulo 2 consiste en un manuscrito de artículo científico, escrito en inglés, el cual será posteriormente modificado para ser sometido a una revista científica internacional. El contenido corresponde a los resultados y las discusiones de este estudio planteado.

### **1.2. Formulación del problema**

El volcán Melimoyu ( $44^{\circ}05'S$  -  $72^{\circ}53'W$  – 2400 msnm) se ubica en el segmento sur de la Zona Volcánica Sur (ZVS). En esta región, el registro eruptivo explosivo se acota al período post-glacial, debido a la presencia substancial de hielo y nieve durante el Pleistoceno Superior. Recientemente se han realizado avances significativos en el registro explosivo de los volcanes Chaitén y Michinmahuida (Amigo et al., 2013; Watt et al., 2013b) y del volcán Hudson (Weller et al., 2014).

Sin embargo, la ausencia de erupciones históricas y los difíciles accesos han derivado en que los depósitos piroclásticos de erupciones derivadas de los volcanes situados en el área intermedia de los anteriores, comprendida entre los  $42^{\circ}S$  y  $45^{\circ}S$  (entre ellos, el volcán Melimoyu), continúan pobemente estudiados, siendo solo documentados en estudios tefroestratigráficos regionales de escasa profundidad en las

características eruptivas (Naranjo y Stern, 2004; Watt et al., 2013a; Fontijn et al., 2014; Weller et al., 2015).

A pesar de ello, tales volcanes son considerados activos y además se asocian a registros holocenos de magnitud importante y, de esta manera, son monitoreados en la actualidad. En consecuencia, un objetivo importante es entender los procesos asociados a sus ciclos eruptivos así como las dimensiones que han alcanzado sus erupciones identificadas. Adicionalmente, dado que esta zona estuvo glacialmente cubierta hasta inicios del Holoceno, varios autores han postulado una posible relación entre la desglaciación y un aumento de la actividad eruptiva (Singer et al., 1997, 2008; Nyland et al., 2013, Watt et al., 2013a). No obstante, Alloway et al. (2017a), indican que habría un sesgo temporal dado que los depósitos eruptivos anteriores a la última glaciación serían más difíciles de preservar.

En particular, el volcán Melimoyu presenta dos erupciones de importante magnitud conocidas, de edades menores con respecto a la última desglaciación, por lo que no se explicarían por la relación postulada. Además, la erupción de mayor tamaño y más antigua conocida del volcán Melimoyu, se caracteriza por mostrar bimodalidad en su composición química, la cual varía desde una composición dacítica a basáltica; mientras que la erupción más reciente y de menor tamaño tiene una composición andesítica. Estas características han llevado a formular preguntas con respecto a cuáles serían los procesos gatillantes para sus erupciones y cuál es la relación que existe entre los magmas que formaron estas erupciones. Específicamente saber si existe una relación parental entre el basalto y la dacita de la primera erupción, y cuál sería el origen de la composición intermedia de la segunda erupción, buscando determinar qué procesos, mezcla y/o cristalización fraccionada, estarían principalmente involucrados en su formación.

Un estudio tefrocronoestratigráfico, volcanológico y petrológico de un conjunto representativo de depósitos piroclásticos corresponde al pilar fundamental para mejorar el registro post-glacial de erupciones explosivas en el volcán Melimoyu y en la ZVS para entender mejor los procesos pre-eruptivos y su respectiva influencia en el comportamiento eruptivo, y permitir la ejecución de análisis particulares más profundos en esta zona a futuro.

### 1.3. Ubicación y Vías de Accesos

El volcán Melimoyu está ubicado en la región Aysén del General Carlos Ibáñez del Campo, Chile. Los poblados más cercanos desde el este son La Junta (40 km) y Puyuhuapi (37 km), desde el norte Raúl Marín Balmaceda (34 km) y desde el oeste Melimoyu (19 km). Existe un acceso levemente marcado a la base del volcán desde el norte, por la ruta a Raúl Marín Balmaceda, siguiendo el Río Correntoso. También existen rutas poco marcadas que se acercan al volcán, desde el poblado de Melimoyu. Los depósitos de caída asociados a las dos erupciones conocidas de este volcán se reconocen en el segmento de la Carretera Austral (Ruta 7) inmediatamente al este del volcán, algunos sectores de la ruta a Raúl Marín Balmaceda (Ruta X-10) y camino a Lago Verde y límite con la República Argentina (Ruta X-13).

### 1.4. Marco Geológico

La Zona Volcánica Sur (ZVS) es un segmento de arco volcánico continuo de 1400 km de largo que se extiende entre los 33.3°S y los 46°S, y que es generado por la subducción de la placa oceánica de Nazca bajo la placa continental Sudamericana. Comprende más de 70 centros volcánicos que han estado activos durante el Pleistoceno y Holoceno (Stern et al., 2007). La estructura cortical más importante en la región es el Sistema de Fallas Liquiñe-Ofqui (LOFZ, sigla en inglés), la cual se extiende por más de 1000 km (Hervé, 1976, Hervé et al., 1993; Cembrano et al., 1996; 2000; 2002). La LOFZ resulta de la combinación entre la subducción oblicua y el impacto del *Chile Rise* contra el continente. López-Escobar et al. (1995) sugiere que existe una fuerte conexión entre la LOFZ, que es paralela al arco, y la ubicación de los centros volcánicos en la ZVS.

El volcán Melimoyu está ubicado en el segmento sur de la ZVS. La mayoría de los volcanes en este segmento se encuentran localizados a lo largo o al oeste de la LOFZ, excepto por el volcán Hudson (Naranjo y Stern, 1998). Varios conos de escoria monogenéticos se encuentran también alineados a lo largo de la LOFZ (Gutiérrez et al.,

2005). Los volcanes cuaternarios de este segmento de la ZVS se encuentran sobre una porción del Batolito Nor-Patagónico, el cual está compuesto principalmente de tonalitas y granodioritas. Este complejo intrusivo data del Cretácico al Mioceno tardío, tiene ~1000 km de largo y se extiende a lo largo del segmento sur de la ZVS (41°S–46°S), se formó por eventos magmáticos episódicos durante un intervalo de 125 Ma (Pankhurst et al., 1999). En el segmento sur de la ZVS la corteza es relativamente delgada (<35 km) y la composición de los estratovolcanes es muy variable, incluyendo basaltos, andesitas, dacitas e incluso riolitas.

Otros volcanes cercanos al volcán Melimoyu para los cuales se ha reportado actividad holocena son los siguientes (de norte a sur): Corcovado, Yanteles, Mentolat además de los grupos de los conos monogenéticos de Palena y Puyuhuapi. Las erupciones que se han reportado para estos volcanes son de tamaño moderado a grande y sus composiciones químicas fluctúan desde basaltos a dacitas (Naranjo y Stern, 2004). Las erupciones de los grupos de conos son medianas en tamaño y mayoritariamente de composición basáltica (Heusser et al., 1992, Watt et al., 2011). De acuerdo con la tefroestratigrafía regional de Naranjo y Stern (2004), el volcán Corcovado tendría 3 erupciones explosivas menores a medianas con edades entre 6.9 ka y 9.2 ka AP. No obstante, en un trabajo reciente Alloway et al. (2017a) postula que la erupción más antigua del volcán Corcovado, estaría asociada al volcán Michinmahuida, ubicado más al norte. El volcán Yanteles tendría una gran erupción fechada en 9.2 ka AP. Para el volcán Mentolat se habría reportado una erupción de 7.0 ka AP y recientemente, se han descrito varias erupciones para este volcán con edades de 3.9, 11.1-11.5 ka AP (Mella et al., 2004; Stern et al., 2015) y una erupción de >17.3 ka AP (Weller et al., 2014; Stern et al., 2015). Por otro lado, los grupos volcánicos Palena y Puyuhuapi, están formados por conos de escoria basálticos sin erupciones mayores reportadas. Ambos grupos se encuentran ubicados a lo largo de la LOFZ. Los conos de Palena corresponden a cinco conos de escoria con orientación NNE (González-Ferrán O., 1995). Los conos de Puyuhuapi corresponden a centros aislados de conos de escoria y lavas basálticas, cubriendo un área de alrededor de 9 km<sup>2</sup> que tiene alineación NE-SW. Para el grupo Palena, una tefra escorácea se dató en 11.5 ka AP (Heusser et al., 1992; Watt, 2010) y para el grupo volcánico Puyuhuapi una tefra escorácea se dató estratigráficamente alrededor de 9.0 ka AP (Watt et al., 2011).

## 1.5. Hipótesis de trabajo

El registro eruptivo observable del volcán Melimoyu es mayor a lo hasta ahora documentado. Por otra parte, las erupciones reconocidas para este mismo volcán corresponden a erupciones de magnitud mayor a lo originalmente planteado. Existe una relación entre los tres magmas que componen las erupciones conocidas, donde predomina el proceso de cristalización fraccionada en la evolución desde un magma basáltico a composiciones más diferenciadas.

## 1.6. Objetivos

### 1.6.1. Objetivo principal

Esta tesis tiene como objetivo principal mejorar el registro eruptivo de la actividad post-glacial del volcán Melimoyu y los parámetros eruptivos de sus erupciones principales, así como reconocer los procesos magmáticos que ocurrieron previos a estas erupciones. Para así contribuir al entendimiento de la generación de grandes erupciones explosivas post-glaciales en la parte sur de la ZVS.

### 1.6.2. Objetivos específicos

- (a) Establecer reconstrucción geocronológica del periodo post-glacial para el volcán Melimoyu.
- (b) Cuantificar las dos erupciones mayores del volcán Melimoyu.
- (c) Determinar condiciones pre-eruptivas en las dos erupciones mayores.

## 1.7. Metodologías

Se estudiaron alrededor de 30 secciones de depósitos piroclásticos y una colada de lava en los alrededores del volcán Melimoyu. Estas secciones se encuentran en la Carretera Austral, en las rutas principales a Lago Verde y Raúl Marín Balmaceda, y en algunas rutas rurales. En cada punto visitado se describieron las características principales, se midieron los espesores, clastos mayores y se tomaron muestras de clastos mayores y de material representativo. Cuando fue posible también se recolectó muestras del suelo subyacente al depósito piroclástico. Aproximadamente 180 muestras de piroclastos fueron obtenidas y secadas en horno a alrededor de 80°C en el Laboratorio de Sedimentología en la Universidad de Chile. Aquellas muestras que correspondían a material representativo fueron además analizadas granulométricamente, ya sea por tamizaje mecánico con tamices en intervalos de un phi ( $\phi$ ), entre  $-4\phi$  (16mm) y  $+4\phi$  (1/16mm); o por espectrometría de difracción láser (LDS, sigla en inglés) para las muestras más finas ( $<4\phi$ ) utilizando el Malvern Mastersizer Hydro 2000G del Departamento de Geología de la Universidad de Chile.

(a) Para establecer la reconstrucción geocronológica, dos muestras de suelo con material orgánico se secaron a temperatura ambiente ( $<35^{\circ}\text{C}$ ), con las cuales se determinaron edades  $^{14}\text{C}$  por Espectrometría de Masas con Aceleradores (AMS, sigla en inglés). Edades que fueron luego calibradas con el software OxCal4.2 (Ramsey, 2009). También se hicieron análisis de elementos mayores, trazas y pérdida por calcinación (LOI, sigla en inglés) en 16 muestras de depósitos piroclásticos y en una lava. Los análisis fueron realizados por el Espectrómetro de Fluorescencia de Rayos-X ThermoARL (XRF, sigla en inglés) y el Espectrómetro de Masa por Plasma de Acoplamiento Agilent 7700 (ICP-MS) en el Laboratorio Peter Hooper GeoAnalytical en la Universidad del Estado de Washington (WSU).

(b) Para cuantificar las erupciones mayores del volcán, fue necesario determinar ciertos parámetros físicos. En primer lugar, para la determinación de la altura de la columna e intensidad eruptiva, se midió en terreno, pómez y líticos mayores en cada punto de muestreo. Los clastos mayores se volvieron a estimar en

laboratorio según dos métodos: promedio aritmético de los ejes más largos de los 5 clastos mayores y promedio geométrico de los tres ejes de los 5 clastos mayores promediados luego aritméticamente. También se estimó la densidad de los juveniles cubriendo algunos clastos con parafina líquida, luego sumergiéndolos en agua y midiendo volumen y peso de estos clastos. Con esos datos se construyeron curvas isópletas y se analizó la información a partir de éstas mediante el modelo de Carey y Sparks (1986), usando un algoritmo implementado por Biass et al. (2015). Para la determinación del volumen emitido, se estimaron los espesores mayores en cada punto de muestreo, lo que permitió generar curvas isópicas. Los volúmenes se estimaron mediante dos modelos de decaimiento: modelo de decaimiento exponencial de Pyle (1989,1995) modificado por Fierstein y Nathenson (1992) para uno o dos segmentos; y modelo de decaimiento Weibull propuesto por Bonadonna y Costa (2012).

(c) Para determinar condiciones pre-eruptivas de las dos erupciones mayores, se procedió a analizar 20 secciones transparentes-pulidas efectuadas en los laboratorios en Vancouver Petrographics Ltd, Canadá y en el Departamento de Geología, Universidad de Chile, Chile. La caracterización petrográfica, a través de Microscopio Óptico y Microscopio Electrónico de Barrido (SEM, según sus siglas en inglés), permitió describir las texturas presentes al mismo tiempo que identificar las fases minerales presentes en las muestras analizadas. Además, se obtuvieron imágenes del vidrio y de los minerales con un detector de electrones retrodispersados (BSE, según sus siglas en inglés). Adicionalmente, fue considerado el análisis de 12 muestras recolectadas en la zona por el Prof. Brent Alloway (Universidad Victoria de Wellington, VUW, Nueva Zelanda), las cuales representan diferentes niveles dentro de las dos erupciones principales (9 de MEL1 y 3 de MEL2). Por otra parte, se analizó la química de elementos mayores en vidrio y en minerales identificados usando la Microsonda JEOL Superprobe JXA-8230 en la VUW. Derivado de lo anterior, se pudo establecer el tipo de geotermómetros y geobarómetros de utilidad para este caso de estudio. Las fases minerales que fueron usadas para geotermobarometría corresponden a anfíbolas, ortopiroxenos, clinopiroxenos, olivinos y plagioclásas, a través de los geotermómetros y geobarómetros de Ridolfi y Renzulli (2012) en anfíbolas para MEL1 (parte pumícea) y MEL2. El geotermómetro B de Holland y Blundy (1994) fue usado en pares de anfíbolas y plagioclásas en contacto en MEL1 (parte pumícea).

El geotermómetro de ortopiroxeno-líquido, ecuación 28a de Putirka (2008) fue utilizado en MEL1 (parte pumícea) y MEL2. Para MEL1 (parte escorácea) se usaron los geotermómetros de Putirka (2008) de olivino-líquido (ecuación 22), clinopiroxeno-líquido y clinopiroxeno (ecuaciones 33 y 32d respectivamente). También se usó el geotermómetro de olivino-augita de Loucks (1996) para el único par olivino-clinopiroxeno encontrado. Por último, el geobarómetro en clinopiroxeno (ecuación 32a en Putirka, (2008)) se utilizó para MEL1 (parte escorácea).

Finalmente se realizaron algunos modelos de mezcla directa con la química de elementos mayores y modelos de cristalización fraccionada. Para esto, se consideraron coeficientes de partición de elementos traza de algunas de las fases minerales presentes en las muestras, para las cuales se utilizó la ecuación que define el modelo de cristalización fraccionada o fraccionamiento de Rayleigh:

$$C_L = C_0 F^{(D^{-1})}$$

Donde  $C_L$  corresponde a la concentración final del elemento traza en el líquido luego del fraccionamiento,  $C_0$  es la concentración inicial de este elemento,  $D$  es el coeficiente de distribución total de la asociación mineral, que se calcula ponderando el coeficiente de partición de cada fase involucrada en el fraccionamiento con la proporción de fraccionamiento de cada fase. Por último,  $F$  corresponde a la fracción de líquido restante luego de la cristalización.

## **2. ERUPTIVE PARAMETERS AND PRE-ERUPTIVE PROCESSES FOR LATE HOLOCENE ACTIVITY CENTRED AT MELIMOYU VOLCANO, SOUTHERN CHILE (44°05' S)**

### **2.1. Introduction**

Explosive eruptions can produce a wide range of products and their study allows the understanding of volcanic processes. The characterization of pyroclastic fall deposits could reveal relevant information about volcanic history, eruptions dynamics and the pre-eruptive system.

Lowe and Alloway (2014) described that tephrochronological studies involving mapping, characterization, and dating are critical for developing a comprehensive record of past explosive eruptions and recurrence rates. Where mapping and characterization implies the use of distinctive physical properties as color, bedding characteristics, lithic, crystal componentry; in combination with stratigraphic associations studies in field. Also, includes characterization using mineralogical or geochemical analytical methods, often both, in the laboratory. And for tephras erupted within the past c. 60,000 calendar years, as in the case of this study, the radiocarbon ( $^{14}\text{C}$ ) technique remains the most important method for dating. Likewise, the collection of field measurements such as deposit thickness and particle size distribution can get insights on the size of the eruptions and plume dispersal. From these data, it is possible to estimate eruptive parameters such as emitted volume, intensity and column height.

In addition, the analysis of chemistry and textural characteristics of juvenile clasts can offer keys to understand processes occurring within the sub-volcanic system prior to eruption. Temperature and pressure estimates can be constrained by geothermometry and geobarometry using the chemistry of coexisting minerals and/or glasses. The extent, distribution and timing of crystallization and degassing, can be determined using textural and chemical analysis (Blundy and Cashman, 2008). Additionally, modelling of sub-volcanic systems involving matching of the phase assemblage and phase compositions of erupted magma linked to geophysical and geochemical observations

can provide a detailed and coherent picture of volcanic systems (Cashman and Sparks, 2013).

The southern part of the Southern Volcanic Zone (SVZ) is poorly understood in terms of styles of eruptions, frequency, volume and magmatic processes that lead to eruptions. Recent eruptions at Hudson (1991, Naranjo and Stern 1998, Kratzmann et al., 2009) and Chaitén (2008, Alfano et al., 2011; Pallister et al., 2013; Alloway et al. 2017a) have revealed that eruptions in this scarcely populated area can bring serious hazards to the people of Chile and Argentina. These eruptions have revealed that it is necessary to carry out detailed studies at volcanoes of this area to better understand magmatic processes and eruption styles at individual volcanoes to be better prepared in terms of hazard assessment. Furthermore, this zone was glaciated up to Holocene and numerous authors have pointed out a relationship between deglaciation and increased eruptive activity since then (Singer et al., 1997, 2008; Nyland et al., 2013, Watt et al., 2013a). However, as Alloway et al. (2017a) points out, there is a temporal bias towards post-glacial eruptive activity as late last glacial to Last Glacial Maximum eruptive deposits are seldom preserved.

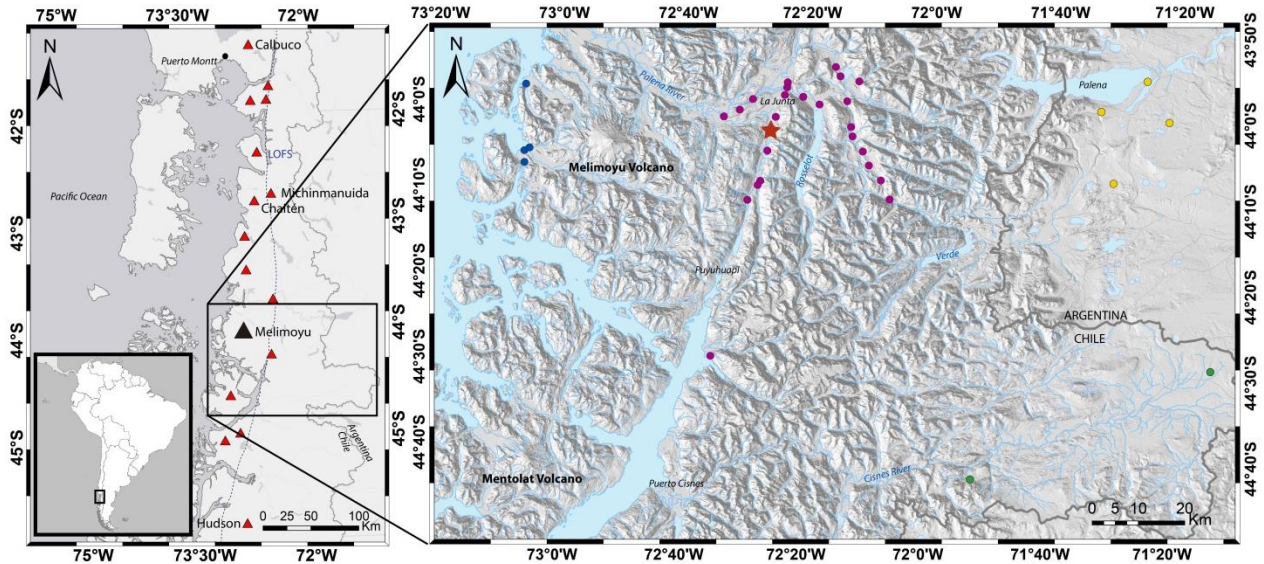


**Figure 1** Location map for Melimoyu volcano. A: Map of the southern part of the Southern Volcanic Zone (SVZ), the main trace of the Liquiñe-Ofqui Fault Zone (LOFZ) as a dashed line. Volcanoes that have been active in the Holocene are marked with red triangles. Melimoyu is marked by the black triangle. B: The region around Melimoyu (MEL). Localities where deposits from MEL1 and MEL2 are found are marked with a magenta circles, and deposits found in the W side are marked with blue circles. Approximate location of sampling sites of Stern et al. 2015 and distal sampling sites of Naranjo and Stern 2004 are marked with green and yellow points respectively. The red star indicates the Santa Ana section showed in Fig.3.

Recently, there have been significant advances in the record of explosive eruptions of volcanoes in this part of Chile such as Chaitén, Michinmahuida (Amigo et al., 2013; Watt et al., 2013b; Alloway et al. 2017b), and Hudson (Weller et al., 2014). However, the pyroclastic deposits of eruptions from the volcanoes located in the intermediate area between 42° S and 45° S are still poorly studied, with its main characteristics being only superficially documented in few regional works (Fontijn et al., 2014; Naranjo and Stern, 2004; Watt et al., 2013a; Weller et al., 2015).

Melimoyu volcano (44°05'S - 72°53'W, 2400 m.a.s.l) is a poorly-studied active stratovolcano, located in a very remote area in the southern segment of the (SVZ) in Chile (Fig.1). Melimoyu forms a permanently ice-covered stratovolcano with an elongation of 10 km in an E-W direction, with a 1 km diameter summit crater. There is no record of historic activity for this volcano. However, in road sections eastwards of Melimoyu Volcano, two closely-spaced tephra fall deposits are prominently expressed beneath the present-day ground surface. These deposits are related to late Holocene aged Plinian eruptions described as MEL1 (lower) and MEL2 (upper) (Naranjo and Stern, 2004). Lapilli constituents of MEL1 exhibit a distinct upward gradation from yellow pumice to black scoraceous material and appear to be compositionally zoned. On the other hand, MEL2 above is uniformly composed of yellow pumiceous lapilli and coarse ash, and doesn't appear to be as compositionally zoned as MEL1 below.

The aim of this work is to refine the volume and distribution of both eruptions and to evaluate pre-eruptive conditions of these two compositionally distinct Melimoyu eruptions, using petrology and mineral and glass chemistry together with compositional modeling. This information provides insights into the complexity of its sub-volcanic system as well as to identify the likely style and magnitude of eruptions that could reasonably be expected in the future.

### 2.1.1. Geological background

Melimoyu volcano is located in the southern segment of the SVZ. Most of the southern SVZ volcanoes are located along or to the W of the Liquiñe-Ofqui Fault Zone (LOFZ), except for Hudson volcano (Naranjo and Stern, 1998). Numerous monogenetic mafic cinder cones are also roughly aligned along the LOFZ trend (Gutiérrez et al., 2005). The Quaternary volcanoes of the southern SVZ are located on a portion of the Northern Patagonian Batholith composed mainly of tonalites and granodiorites. This Cretaceous to late Miocene intrusive complex, which is ~1,000 km in length and extends across the length of the southern SVZ (41°S–46°S), was formed by episodic magmatic events over a 125 Myr time interval (Pankhurst et al., 1999).

In this region, the eruptive record is restricted to the post-glacial period, due to the substantial presence of ice and snow during the Uppermost Pleistocene, and deglaciation starting from ~19 to 14 ka (Clark et al., 2009; Denton et al., 2010). In the Southern SVZ the crust is relatively thin (<35 km), and composition in stratovolcanoes vary from basalts, andesites, dacites to rhyolites.

### 2.1.2. Previous research on Melimoyu-sourced post-glacial activity

Two prominent closely-spaced lapilli and coarse ash layers of presumed Melimoyu-source were first identified during pioneering cover-bed reconnaissance work undertaken by Naranjo and Stern (2004). On the basis of acquired radiocarbon dates both layers occurred during the late Holocene. Eruption MEL1 occurred at ~2.8 ka, while, MEL2 occurred at ~1.6 ka. The authors also estimated no-DRE volumes of 1.4 km<sup>3</sup> and 0.5 km<sup>3</sup> for MEL1 and MEL2 respectively. In both cases, tephra distribution is only reported to the E of the volcano, but there are not studies on the W of the volcano.

Further south, Stern et al., (2015) analyzed 18 tephras from lake cores and glacial-lacustrine sediments from an outcrop in the upper Río Cisnes valley (44°30'-44°42'S), at ca. 120 km SE from the volcano. Based on their petrography and chemistry, six of those tephras were correlated to Melimoyu volcano. In particular, two ash layers are

chronologically correlated to MEL2 (dated at 1.8 ka and 1.7 ka). Additional ash layers attributed by the authors to Melimoyu are reported older than MEL1 (4.7, 8.3 and 19.7 ka) with no subaerial correlations described so far.

### 2.1.3. Other volcanoes

Other volcanoes close to Melimoyu where Holocene eruptions have been reported are (from N to S) Corcovado, Yanteles, Palena and Puyuhuapi volcanic groups and Mentolat. The stratovolcanoes eruptions reported are medium to large size, varying from basaltic to dacitic compositions (Naranjo and Stern, 2004). Volcanic groups eruptions are medium size with basaltic compositions (Heusser et al., 1992, Watt et al., 2011).

According to the regional tephrostratigraphy of Naranjo and Stern (2004) Corcovado has 3 small to medium size explosive eruptions bounded between 6.9 ka and 9.2 ka BP (the oldest one associated to Michinmahuida volcano after Alloway et al., 2017a); Yanteles one large size explosive eruption at 9.2 ka BP. For Mentolat it is reported one eruption at 7.0 ka BP. Recently, several new eruptions for Mentolat have been described. Eruptions at 2.5, 3.9, 11.1-11.5 ka BP are reported (Mella et al., 2004; Stern et al., 2015), and the eruption MEN0 from Weller et al., (2014) also reported by Stern et al., (2015) with an age of >17.3 ka BP.

Palena and Puyuhuapi volcanic groups are composed by basaltic cinder cones with no major eruptions. They are located along the LOFZ. Palena Volcanic Group, correspond to five cinder cones oriented along a NNE trend (Gonzalez-Ferran O, 1995). Puyuhuapi volcanic group, which corresponds to isolated centers of scoraceous cones and basaltic lavas, cover an area of around 9 km<sup>2</sup> that is aligned in a NE-SW trend. For Palena volcanic group one scoraceous tephra was dated at 11.5 ka BP (Heusser et al., 1992; Watt, 2010) and for Puyuhuapi volcanic group one scoraceous tephra was stratigraphically dated at 9.0 ka BP (Watt et al., 2011).

## 2.2. Methods

More than 30 sections of pyroclastic deposits and lava outcrops were described and sampled (Fig. 1). Sections are usually along the main NS route in the region (Carretera Austral) and routes to Lago Verde (near the border with Argentine) and Raul Marín Balmaceda (in the Pacific coast) in addition to rural roads and rainforest near Melimoyu village. The access was done in 4x4 vehicles and boats. However, the access to the volcano edifice was not possible due to the lack of trails and the dense rainforest cover. In most sections, measurements of deposit thickness and maximum clast size of pumice, scoria, and lithics were made. 180 samples were collected in order to determine its bulk granulometric distribution, as well as chemical and petrographic analyses. In some places, paleosol samples were also collected for radiocarbon dating.

### 2.2.1. Sieving and grain-size

Both bulk and maximum clast samples were dried in an oven at no more than 80°C for around 48 hours. Granulometric analyses of the coarse fraction were done on samples sieved at one-phi ( $\phi$ ) intervals from -4 $\phi$  (16 mm) to +4 $\phi$  (1/16 mm). Each fraction was then weighed on a balance, and weight percentages were calculated. Grain-size distributions of the fine fraction of the samples (< 4 $\phi$ ) were quantified using laser diffraction spectrometry (LDS), using a Malvern Mastersizer Hydro 2000G at the Geology Department of the University of Chile. The refractive indices for size-distribution calculation were 1.48 and 1.50; based on the high SiO<sub>2</sub> content of the ash, the absorption index was set to 0.10, as discussed by Horwell (2007).

### 2.2.2. Dating

Organic material in soils above and below the deposits were collected in the field and dried at low temperature (<35°C). Two samples have been <sup>14</sup>C-dated by Accelerator

Mass Spectrometry (AMS) analyses. The ages were calibrated with the OxCal4.2 software (Ramsey, 2009) by using the Southern Hemisphere calibration curve SHCal13 (Hogg et al., 2013). Ages are given as calibrated ranges before present (BP, where present is 1950) at the 95.4% confidence level.

### 2.2.3. Eruptive parameters

In order to estimate the volume of the studied eruptions, isopach maps were built. We used the exponential thickness decay model of Pyle (1989, 1995), modified by Fierstein and Nathenson, (1992), with one or two segments. And compared on results with the Weibull function proposed by Bonadonna and Costa (2012).

Eruption column heights were estimated using the Carey and Sparks (1986) model, based on the maximum pumice and lithic isopleths, by using the MATLAB script of Biass et al. (2015). Maximum clast size was determined from calculating the geometric mean of the three axes of each one of the five largest clasts found at an outcrop, and the arithmetic mean of the five largest clasts found at an outcrop (considering only the largest axe). Densities of juveniles were determined by covering some clasts with liquid paraffin, then immersing them in water, and measuring volume and weight of these clasts.

To determine the eruptive rate ( $Q$ ) from the height of column ( $H_t$ ), the following relationship between those parameters was used (Sparks et al., 1997):  $H_t = 1.67Q^{0.259}$ . The estimates were then used to calculate the approximate intensity ( $I$ ) of these eruptions, using the relationship  $I = \log_{10} [Q] + 3$ .

### 2.2.4. Whole rock chemistry

Whole-rock major and trace element compositions and loss-on-ignition content of the tephras were obtained for sixteen samples (seven from MEL1, three from MEL2 and six others from the western side of Melimoyu volcano) in addition to one lava sample

(Table 1) by ThermoARL X-ray Fluorescence Spectrometer (XRF) and Agilent 7700 Inductively Coupled Plasma Mass Spectrometry (ICP-MS). The analyses were performed at the Peter Hooper GeoAnalytical Laboratory at Washington State University (WSU). This ICP-MS allows to analyze 14 REEs and 13 additional trace elements. Long term precision for the method is typically better than 5% ( $RSD = SD/Mean\ Result \times 100$ ) for the REEs and 10% for the remaining trace elements. The suite of elements analyzed on XRF includes 10 major and minor elements, plus 19 trace elements. More details of preparation techniques and analytical methods are available from WSU GeoAnalytical Lab (<http://cahnrs.wsu.edu/soe/facilities/geolab/>).

#### 2.2.5. Glass and mineral chemistry

Around 20 polished thin sections were obtained at Vancouver Petrographics Ltd, Canada and at Thin Section Laboratory at Department of Geology, University of Chile, Chile. In addition, 12 samples previously collected by Brent Alloway (Victoria University of Wellington, New Zealand) were jointly analyzed with results incorporated into this thesis. They represent material channel sampled upward through each deposit (1-9 for MEL1 and 10-12 for MEL2) at the Pte. Los Cesares Section. These samples were crushed and mounted as circular resin probe mounts at the VUW's lab. Major element mineral and glass analyses were obtained at VUW, using a JEOL Superprobe (JXA-8230). Back-scattered electron (BSE) images were taken of glasses and crystal phases to identify zoning patterns and locate the analytical spots. An accelerating voltage of 15 kV, beam current of 12 nA and a focused beam were employed for mineral analyses. For glass, an accelerating voltage of 15 kV, beam current of 8 nA and a 10 µm defocused beam were used. Secondary standards were run at the start and end of each day to monitor calibration during the analysis. All glass analyses are normalized to 100 wt. % anhydrous and total Fe is reported as FeO. Minerals analyses with <93 wt. % were discarded.





## 2.3. Results

### 2.3.1. Tephra Descriptions

The observed stratigraphy of volcanic deposits on the eastern side is similar to the reported by Naranjo and Stern, (2004). There are two lapilli tephra levels, the lower one is a yellow pumiceous to black scoracious level and the upper one is an orange pumiceous level. Instead, to the western side some fairly reworked ash deposits were found and were described and sampled in order to improve the registry of Melimoyu Holocene history. Fig 2 shows location of sections described. Deposits were observed from ca. 20 to 60 km eastward. Closer areas to the volcano remain unknown. Fig. 3 shows a generalized stratigraphic column, indicating MEL1 and MEL2 events and Fig. 4 shows sections described in the western side.

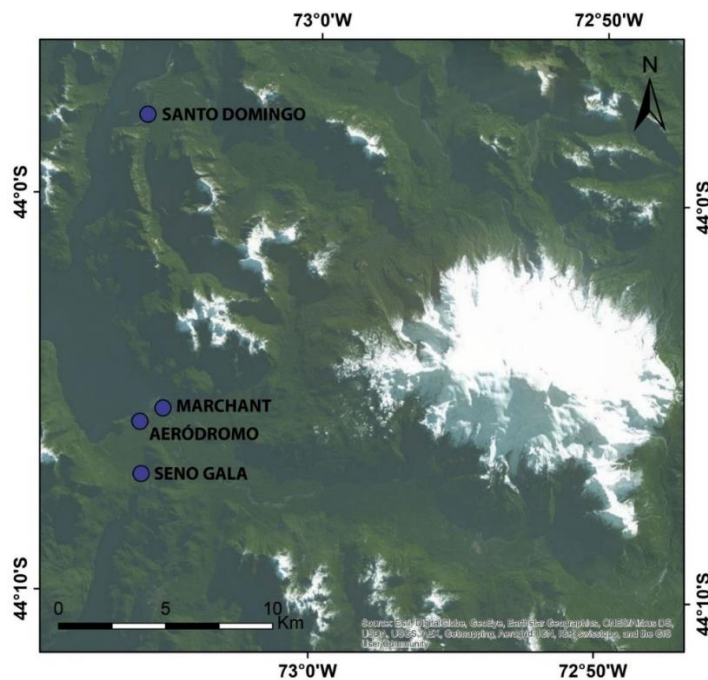


**Figure 2** Zoom of the western side of Melimoyu volcano. Location of sections described and sampled on this area are marked with blue circles.

MEL1 is the largest and oldest event (~2.8 ka BP) from Melimoyu volcano described by Naranjo and Stern, (2004). Usually deposits are found at ~20 to ~60 km from the volcano at Carretera Austral, routes to Lago Verde and Raul Marín Balmaceda. This eruption produced a major pumice fall deposit that usually rests on top of a well-developed organic rich paleosol. Most outcrops show a sharp contact on the base and top, but in some sections the top of the deposit has been reworked.

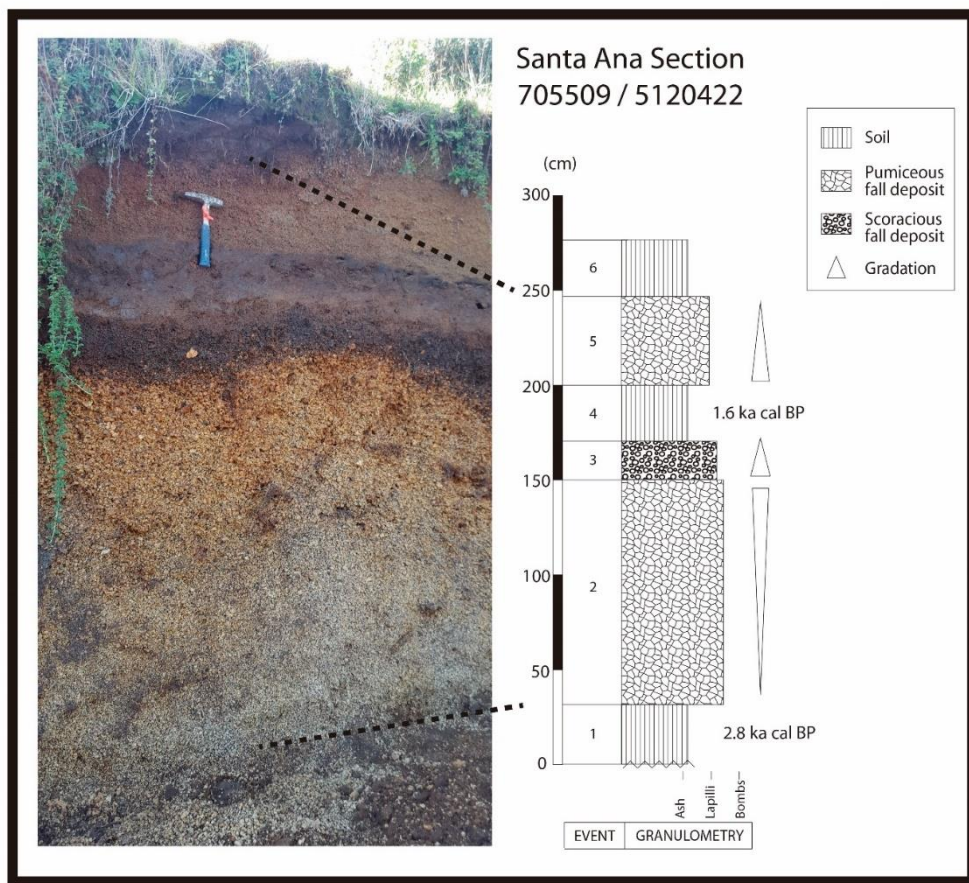


**Figure 3 Stratigraphy of a representative section of deposits to the E side of Melimoyu volcano. Approximate ages are given as calibrated ranges in thousand years (ka) before present (BP), where present is 1950. Locality of the column is labelled on the map of Fig 1.**

Thickness variations of the deposits and the trend of clast sizes shows an E-SE dispersion. The thickest deposit of this unit is found ~30 km E of the edifice, SE of the village La Junta, with a thickness of 115-135 cm and juveniles with 3-5 cm diameter. The thinnest deposit is found around ~60 km E from the edifice and consist in 10-cm deposit

thick and <1cm juvenile diameter at one of the most distal preserved point that is near Puyuhuapi.

The deposit is characterized for being a yellow weathered fall deposit (named M1p in this work), well to moderately sorted, inverse-graded, with pumice-rich angular clasts, with < 20% of variable lava and some intrusive lithics (more details of granulometry are shown in Table 2). There is a gradation to a black deposit (here after called M1s), well to moderately sorted and normally-graded, with angular scoria and < 30% of lava lithics. Between both deposits, some pumice-scoria mingled clasts are found. In the most distal outcrops the scoracious part can be absent and the gradation is not clear. MEL1 deposits are typically capped by a well-developed paleosol. This paleosol separates MEL1 deposits from those of the overlying MEL2 event.

**Table 2 Granulometric parameters for selected tephra sections at different distances from vent.**

Sample Name	Distance from the volcano and direction	Thickness cm	Md $\phi$	Md mm	$\sigma\phi$	$\alpha\phi$	MP/ML	Lithics
<b>M1p</b>								
AGO14-4B	25 km/N76°E	75	-5.08	33.84	1.16	1.38	70/25	dark lava>granitoid>red lava
MEL115-1C	33 km/N103°E	65	-3.54	11.62	2.46	0.35	57/13	dark lava>> granitoid
MEL115-22B/C/D	55 km/N91°E	58	-1.21	2.31	1.4	-0.11	21/3	dark lava
MEL115-6B	62 km/N100°E	10	-1.61	3.05	1.32	0.09	11/6	dark lava
<b>M1s</b>								
AGO14-4D	25 km/N76°E	12	-3.97	15.66	1.88	0.59	31/13	dark lava >> grey lava
MEL115-1F	33 km/N103°E	20	-2.88	7.38	1.6	0.24	35/7	dark lava >> granitoid
MEL115-22F	55 km/N91°E	9	-1.65	3.14	1.3	0.04	13/9	dark lava
MEL115-6C	62 km/N100°E	8	-1.38	2.61	1.06	-0.05	10/5	dark lava
<b>M2</b>								
AGO14-4F	25 km/N76°E	50	-2.79	6.9	2	0.32	24/6	dark lava>grey lava >>granitoid
MEL115-1J	33 km/N103°E	40	-2.77	6.62	2.04	0.51	17/4	dark lava
MEL115-22I	55 km/N91°E	8	-0.57	1.48	1.47	0.31	5/1	dark lava
MP' = Geometric mean of the three axes of each one of the five largest pumice clasts; 'ML' = Geometric mean of the three axes of each one of the five largest lithic clasts								

MEL2 deposit (~1.6 ka BP) is also described by Naranjo and Stern, (2004) and corresponds to a smaller fallout deposit stratigraphically above MEL1 (renamed as M2). It is more widely dispersed and preserved along Carretera Austral and route to Raul

Marín Balmaceda. Best preserved outcrops show less defined contact on the base and top than MEL1. Diffused contact and rework deposits are observed moving away from the volcano.

The thickness of the deposits and the clast sizes shows an important E dispersion component. Thickness of ~ 50 cm and juvenile diameter of 2-3cm at 25 km from source at the route to Raul Marín Balmaceda. Thickness of ~8-cm and juveniles with <1cm diameter at the most distal preserved point at the route to Lago Verde, ~55km from source.

This deposit corresponds to an orange weathered fall deposit that normally shows no gradation or in some points normal gradation. It is well sorted, with pumice-rich angular clasts, with some lava lithics (less than 10%). The MEL2 deposits are usually capped by a well-developed soil that includes reworked pumice clasts and where the current surface is developed.

Also, one outcrop of lava was observed in the route to Raul Marín Balmaceda. It is a well-preserved lava that correspond to aa type with a more massif center which was sampled. The vent could be the principal cone or one of adventitious cone observed at the NE side of the Melimoyu volcano.

To the western side, four sections were described in total. Samples were taken for chemistry and dating in four and two sections respectively. In general, deposits are fine materials with clasts of no more than 15 mm of diameter. In section “Aeródromo”, two deposits were recognized: a grey well sorted deposit with pumice unrounded clasts; and a red moderately sorted deposit, with pumice unrounded clasts in a fine matrix. Three deposits in section “Santo Domingo” were identified: a grey deposit with angulate and rounded clasts with clear-cut contacts, a grey deposit with fine clasts with clear-cut contacts, and a grey deposit with fine material and diffuse contacts. We observed two deposits in section “Rio Marchant”: a grey level with fine material and a second level with some sub-angulate clasts with the largest clasts at the base. In section “Seno Gala”, there are two continuous levels; the upper level is normally-graded with sub-rounded clasts, and the lower level is inverse-graded and composed of larger clasts. Granulometry indicates that at least a deposit of section “Seno Gala” could correspond to a fall deposit, considering the good sorting and subrounded clasts.

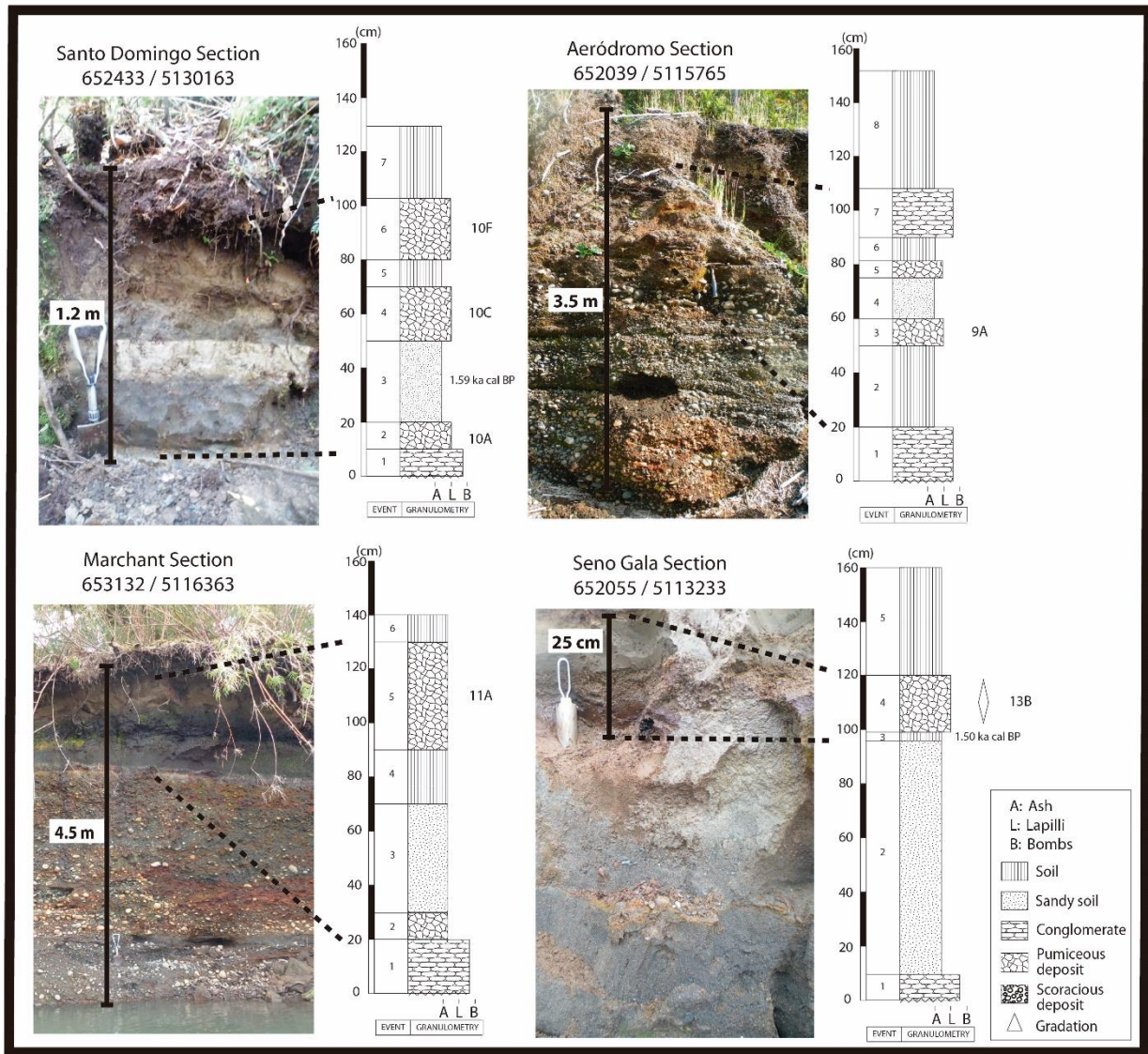


**Figure 4 Stratigraphy of sections studied of deposits to the western side of Melimoyu volcano. Ages are given as calibrated ranges in thousand years (ka) before present (BP), where present is 1950. Sample name of levels chemically analyzed are labelled. Locality of these columns are labelled on the map of Fig 2.**

### 2.3.2. Dating

Estimates of ages from this study and previous works are presented in Table 3. Data of previous works were re-calibrated to be reported, except for data from Stern et al. (2015) that were already presented calibrated. Radiocarbon ages funded from Iniciativa Científica Milenio grants P202-51 and NC120066 and FONDECYT 1151469

are reported. Two deposits from sections “Santo Domingo” and “Seno Gala” of the western side of the volcano (10B and 13A samples respectively) dated in this study represent volcanic activity been occurred 1.50-1.59 cal. ka BP (95.4% confidence level). These records show events with ages similar to M2 eruption.

**Table 3 Summary of radiocarbon ages reported in this study and from previous studies.**

Sample Name	Material	Coordinates or Location	Event	Conventional age ± error BP	Calibrated age range BP	Observation	References
MEL115-13A	Charcoal fragments	652055/5113233	Undetermined/ Probably M2	1,650 ± 30	1,568-1,416	Wood under deposit Paleosol under deposit	This Study
MEL115-10B	Organic soil	652433/5130163	Undetermined/ Probably M2	1,730 ± 30	1,629-1,533		This Study
a	Organic material	Mallín El Embudo	Undetermined/ Probably M2		1,743 ± 40		Stern et al. (2015)
T-04B	Organic soil	44°09.1'S/72°28'W	MEL2	1,750 ± 80	1,755-1,423		Naranjo and Stern (2004)
a	Organic material	Lago Shaman	Undetermined/ Probably M2		1,827 ± 40		Stern et al. (2015)
UCIAMS-145940	Charcoal fragments	Sendero de Montana	MEL1	2,505 ± 20	2,710-2,379		Alloway and Moreno (unpublished data)
UCIAMS-145939	Charcoal fragments	Pte. Los Cesares	MEL1	2,715 ± 20	2,845-2,748		Alloway and Moreno (unpublished data)
T-07	Charred material	44°03.6'S/72°25.8'W	MEL1	2,740 ± 70	2,995-2,716		Naranjo and Stern (2004)
T-04F	Charcoal fragments	44°09.1'S/72°28'W	MEL1	2,790 ± 70	3,056-2,746		Naranjo and Stern (2004)
f	Organic material	Lago Shaman	Undetermined/ Probably from Melimoyu		4,275 ± 50		Stern et al. (2015)
b	Organic material	Mallín El Embudo	Undetermined/ Probably from Melimoyu		4,492 ± 40		Stern et al. (2015)
g	Organic material	Lago Shaman	Undetermined/ Probably from Melimoyu		8,357 ± 40		Stern et al. (2015)
CIS 263-A	Organic material	Las Barrancas	Undetermined/ Probably from Melimoyu		>19,670		Stern et al. (2015)

Based on dating and chemistry (more detail of chemistry will be described in section 1.4.4), a correlation between sections described in the western side of the

volcano was made (Fig. 5). We determined that one level of each section could represent M2 eruption. The other deposit in ‘Aeródromo’ section could correspond to a fall deposit of another eruption, and others deposits from ‘Santo Domingo’ and ‘Marchant’ sections would be reworked pyroclastic levels.

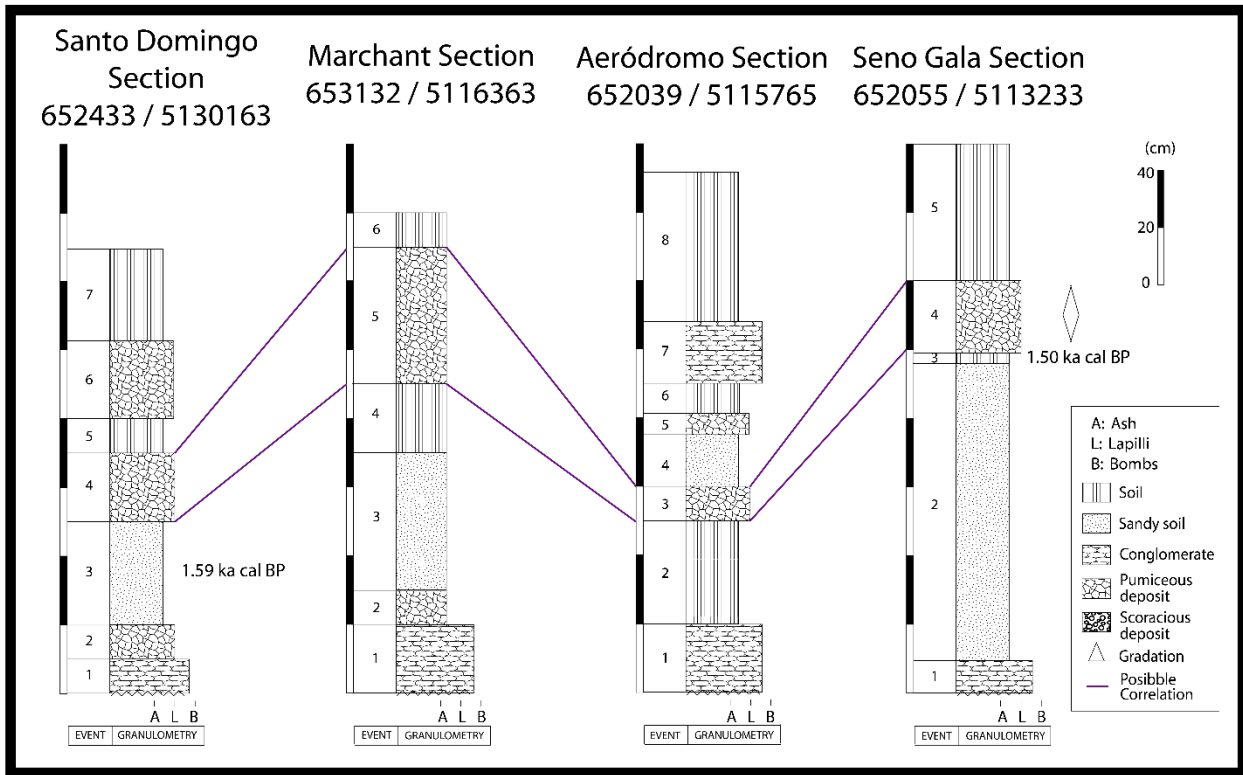


**Figure 5** The four localities on the western side that preserve Melimoyu pyroclastic units. Correlation between those sections are based on chemical characteristics or datation of paleosols.

### 2.3.3. Eruptive parameters

Estimates of eruption volumes and column heights are presented in Table 4, along with the dispersal direction for the different units. As mentioned before, MEL1 eruption was separated into two units M1p and M1s, considering the contrast of composition, and then eruptive parameters for each unit were obtained. To delineate isopachs and isopleths we considered thickness and clast-size measures on 24, 18 and 17 sections for M1p, M1s and M2 respectively.

Three isopach curves for units M1s and M2, and four isopach curves for unit M1p were plotted (Fig. 6). According to both methods described before, similar volumes for each eruption were obtained, except for M2 in which by the method of Bonadonna and Costa, (2012) it is obtained a considerable larger volume. For M2, we included the section “Seno Gala” that, as described before, has similar ages and chemistry that M2 and characteristics for being considered a fall deposit. And for M1p we included a layer described near Puyuhuapi village, which has similar glass color and mineralogy that M1p. Based on those methods we obtained no-DRE volumes of ~1.9-2.1 km<sup>3</sup> for M1p, ~0.5-0.6 km<sup>3</sup> for M1s, ~0.9-1.6 km<sup>3</sup> for M2.

**Table 4 Eruptive parameters of Melimoyu Holocene eruptions.**

Unit/Eruption	Volume (km <sup>3</sup> )	Volume (km <sup>3</sup> )	Volume (km <sup>3</sup> )	Column height (km)	Column height (km)	Dispersal direction
M1p	2.1	1.9	1.9	29-41	30-41	E-SE
M1s	0.6	0.5	0.5	28-43	30-43	E
M2	0.9	1	1.6	26-31	27-31	E
References	One slope, Fiersten and Nathenson, 1992	Two slopes, Fiersten and Nathenson, 1993	Bonadonna and Costa, 2012	G3/5	5PM	

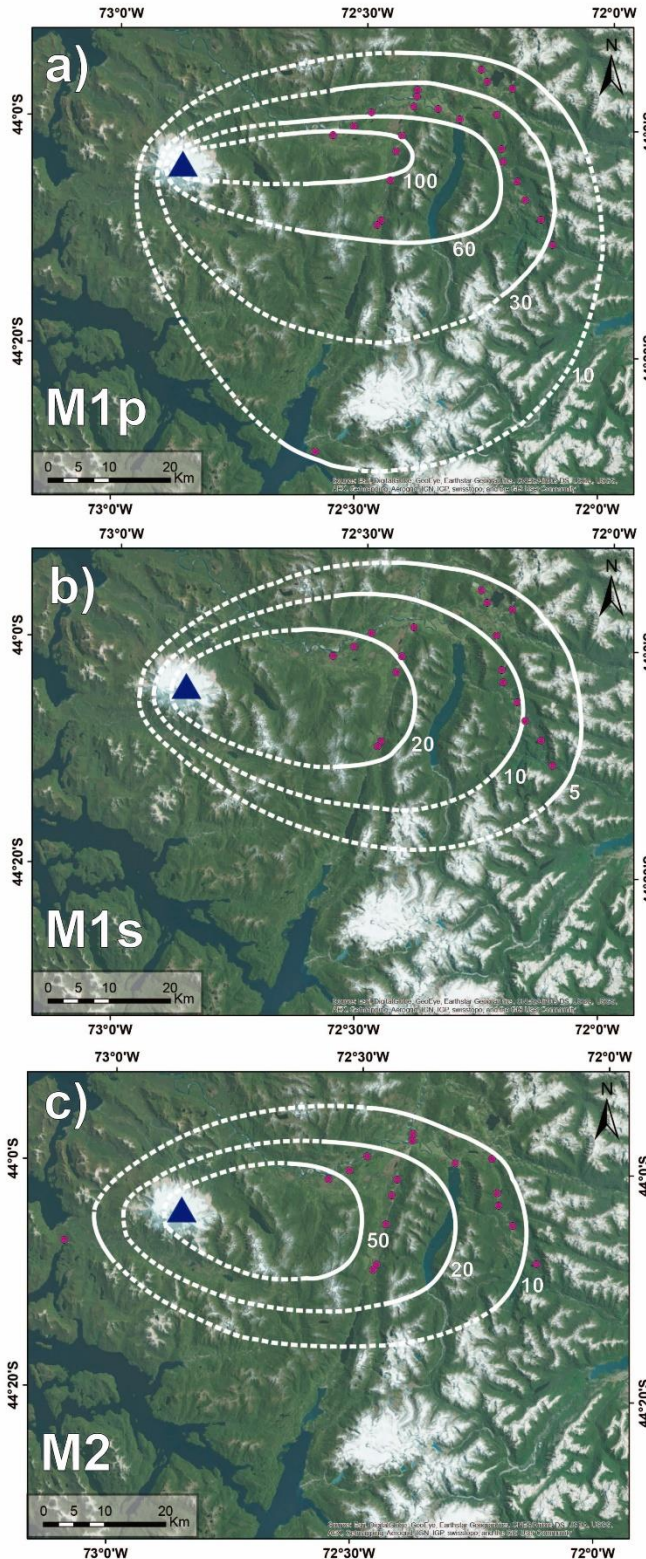


**Figure 6** Isopach maps of M1, M1s and M2 units, with thickness in cm: a. M1p; b. M1s; c. M2. Dashed lines are extrapolated contours. Magenta dots indicate sites where thickness and major clasts measurements were done. Melimoyu volcano is indicated as blue triangle.

To perform isopleths, we considered densities of about  $500 \text{ kg/m}^3$  for juvenile clasts of the M1p and M2 units, and  $1300 \text{ kg/m}^3$  for juvenile of M1s unit, based on density measurements by determining weights of some clasts of each unit sealed in wax, using the Archimedes principle. For lithics the conventional density value of  $2500 \text{ kg/m}^3$  was used. The data allowed to generate at least two isopleths for maximum juvenile and lithic clasts for the three units. Major-size clast measurements were done using two methods described before.

Column heights of 29-41 km for M1p, 28-42 km for M1s and 26-31 km for M2 were calculated considering lithics and juveniles, per the G3/5 and 5PM methods. Nevertheless, the highest values were discarded, because isopleths that gave those highest results were obtained with few control points. Hence, we considered the lack of additional control points could produce crosswind overestimation. Therefore, the plume heights obtained were *ca.* 30- 35 km for M1p, 30-35 km for M1s and 26-30 km for M2.

Considering the heights obtained for the MEL1 eruption, eruptive rates were about  $7.0 - 13.0 \times 10^4 \text{ kg/s}$  for both M1p and M1s units and for MEL2 eruption eruptive rates of  $4.0 - 7.0 \times 10^4 \text{ kg/s}$  were obtained. Hence, intensities of eruptions correspond to 8 for both eruptions. Combining volume and column height information, eruptions will be classified as IEV=5, i.e. Plinian eruptions. Dispersion from E to SE is observed in M1p, and dispersion principally to E is observed in M1s and M2 units. (Fig. 7).

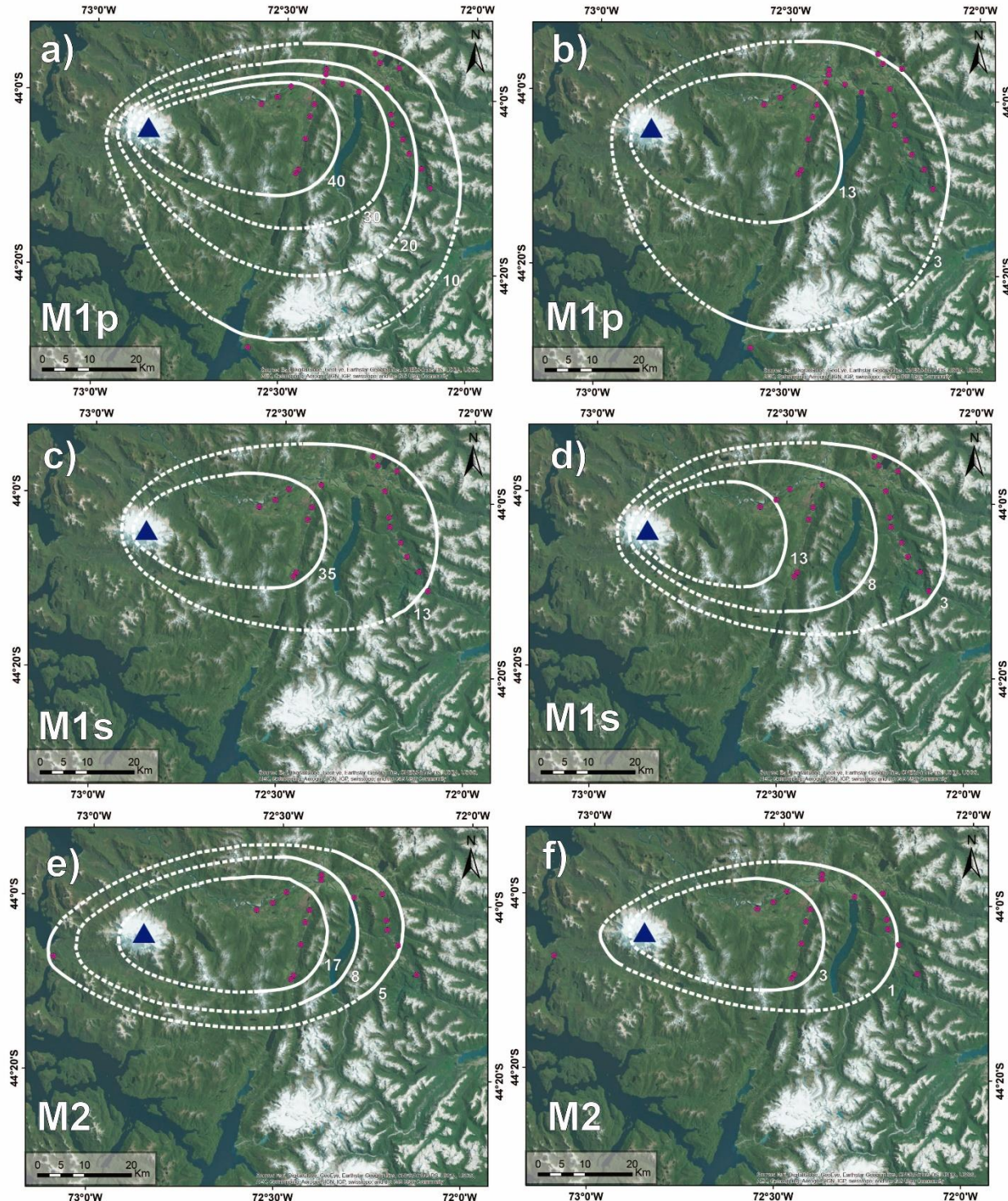


**Figure 7** Isopleth maps of M1p, M1s and M2 units, with major clasts size in mm: a. M1; b. M1s; c. M2. Dashed lines are extrapolated contours. Magenta dots indicate sites where thickness and major clasts measurements were done. Melimoyu volcano is indicated as blue triangle.

### 2.3.4. Geochemistry

The whole-rock composition (Fig. 8) of analyzed samples ranges from basalts to trachydacite (49.27–65.38% SiO<sub>2</sub>). Major and trace elements analyses of samples of the products of M1p, M1s, M2 and deposits of western side are in Table 1. All the samples correspond to the calcalkaline serie. LOI of samples from western side deposits are very high in most of them (up to 20%). For this reason, and in order to determine if those events correspond to one of known eruptions or to a different event, we consider immobile elements to compare. Harker diagrams show chemical values of samples 9A and 13B are systematically similar to M2. Furthermore, ratios of trace elements as Zr/TiO<sub>2</sub>, Nb/Y, Zr/Nb and La/Yb allow recognizing same similitudes between 9A, 13B samples (from sections “Aeródromo” and “Seno Gala” respectively) to M2 (Table 5).

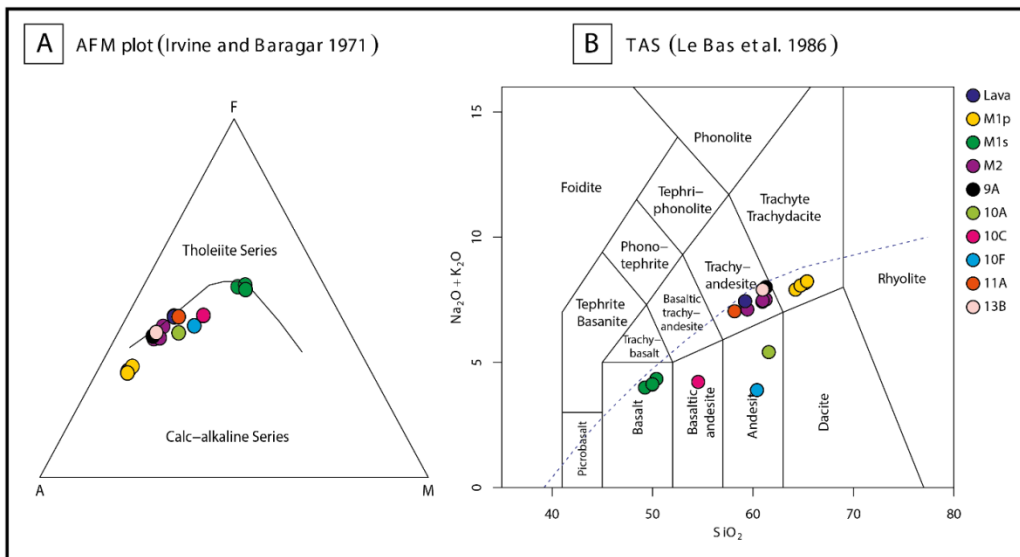


**Figure 8 Whole-rock compositions of all units found in this study.** A: AFM diagram (Irvine and Baragar, 1971) showing calc-alkaline trend of the Melimoyu samples. B. Total alkali vs. silica TAS (Le Bas et al., 1986). 9A sample is from ‘Aeródromo’ section; 10A, 10B, 10C samples are from ‘Santo Domingo’ section; 11A sample is from ‘Marchant’ section; 13B sample is from ‘Seno Gala’ section.

The analyzed deposits of the two known eruptions are basalts to trachydacite. M1p is the most evolved product and corresponds to trachydacite (64.3-65.4% SiO<sub>2</sub>, 5.7-5.9 Na<sub>2</sub>O, 2.2-2.4 K<sub>2</sub>O), M1s is the most mafic magma and has a basaltic composition

(49.3-50.4% SiO<sub>2</sub>, 3.3-3.6 Na<sub>2</sub>O, 0.7-0.8 K<sub>2</sub>O). M2 has an intermediate composition and correspond to a trachyandesite (59.5-61.3% SiO<sub>2</sub>, 5.2-5.4 Na<sub>2</sub>O, 1.9-2.1 K<sub>2</sub>O).

**Table 5 Ratios of trace elements of M1p, M1s, M2 and samples from western side.**

	Zr/TiO <sub>2</sub>	Nb/Y	Zr/Nb	La/Yb
<b>M1p</b>				
AGO14-4C	443	0.52	18.2	9.4
ABR15-1C	440	0.53	18.2	9.3
ABR15-1B	429	0.53	18.3	9.2
ABR15-1D	421	0.54	18.2	9.0
<b>M1s</b>				
AGO14-4D	85	0.30	18.0	6.9
ABR15-1E	95	0.34	18.1	6.6
ABR15-1F	84	0.33	18.1	6.5
<b>M2</b>				
AGO14-4G	280	0.39	18.9	8.4
ABR15-5A	255	0.39	18.7	7.7
ABR15-5C	312	0.41	19.4	8.1
<b>W Side</b>				
MEL115-9A	316	0.46	17.6	8.9
MEL115-10A	140	0.32	20.7	6.8
MEL115-10C	132	0.39	18.4	6.7
MEL115-10F	113	0.36	18.7	6.0
MEL115-11A	232	0.46	17.3	8.8
MEL115-13B	306	0.43	17.9	8.8

The overall trend of major element chemistry of M1p, M1s and M2 eruptions are linear trends as FeO, MgO and CaO all decrease as SiO<sub>2</sub> increases, instead Na<sub>2</sub>O and K<sub>2</sub>O increase with SiO<sub>2</sub>. (Fig. 9). That is less clear for Al<sub>2</sub>O<sub>3</sub> and P<sub>2</sub>O<sub>5</sub>, for which there is even a kink in pattern on SiO<sub>2</sub>. Most of Harker diagrams of trace elements versus SiO<sub>2</sub> move away from a linear trend.

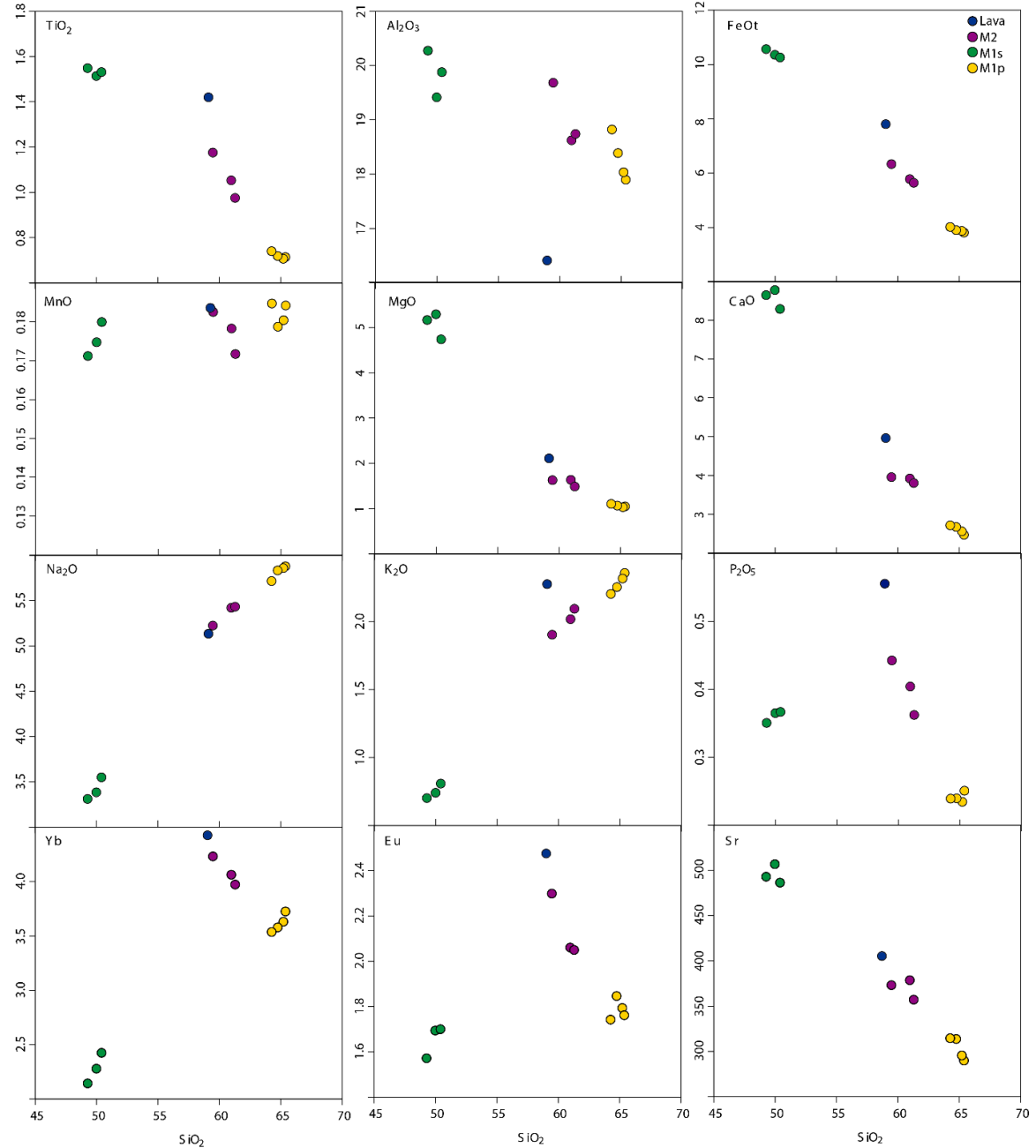


**Figure 9 Variation diagrams of some major and trace elements showing the whole-rock compositions of M1p, M1s, M2 and one lava from Melimoyu volcano.**

Regarding spider diagrams, all samples display Rb, Nb, negative anomalies, Pb positive anomalies. M1p and M2 show Sr and Ti negative anomalies, however M1s has positive and no anomalies respectively. Patterns of REE are similar for three units, with a more evident concave-up form for M1p and M2, showing a depletion of MREE and

HREE. LREE of M1p and M2 are similar, but M1p is more depleted in MREE and HREE, being located between in M2 and M1s (Fig. 10).

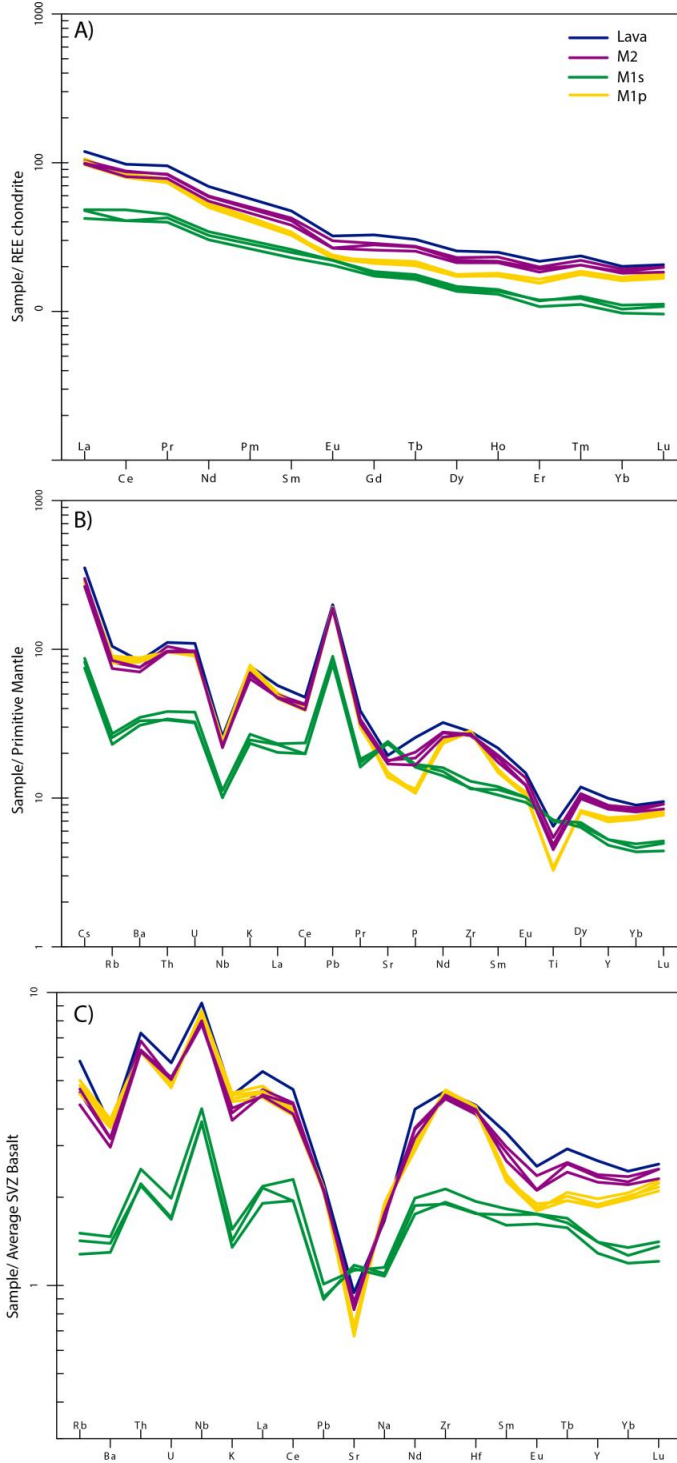


**Figure 10** Primitive mantle-normalized (Sun and McDonough, 1989) spider diagram (a) and REE patterns (Nakamura, 1974) (b), and Average SVZ Basalt (Sellés et al. 2004) spider diagram(c) of samples from M1p, M1s, M2 and one lava of Melimoyu volcano. Trace element concentrations lower than detection limit were omitted (see Table 1).

### 2.3.5. Mineralogy and Petrography

The 25 samples investigated in this study are pumice-scoriae fine lapilli (4 - 8 mm) and coarse lapilli (>32 mm). The pumice and scoriae clasts are vesicular (~55-70 vol. % vesicles) and crystal poor (<10% phenocrystals). M1p and M2 clasts are microlite-poor (<1%), instead M1s clasts are microlite-rich with no visible glass (Fig. 11). A summary of volumetrically percentage is shown in Table 6.

**Table 6 Modal mineralogy (vol.%) of Melimoyu eruptions**

Unit	M1p	M1s	M2
Composition	Trachydacite	Basalt	Trachy-andesite
SiO <sub>2</sub> wt. % (whole rock)	64.3-65.4	49.3-50.4	59.5-61.3
SiO <sub>2</sub> wt. % (glass)	68.1-70.2	50.9-54.4	60.7-64.7
Vesicles (vol.%)	>55	>45	>70
Phenocryst			
(vol.%)			
Plagioclase	4.1	4.6	1.1
Amphibole	0.9	—	0.2
Olivine	—	1.6	<0.1
Clinopyroxene	—	1.2	<0.1
Orthopyroxene	0.2	—	0.2
Oxide	0.2	0.1	0.1
Biotite	—	—	<0.1
Total phenocrysts	5.4	7.5	1.6
Total phenocrysts (vesicle-free)	12	14	5
Groundmass			
(vol.%)			
Plagioclase	<0.1	>90	<0.1
Olivine	—	?	—

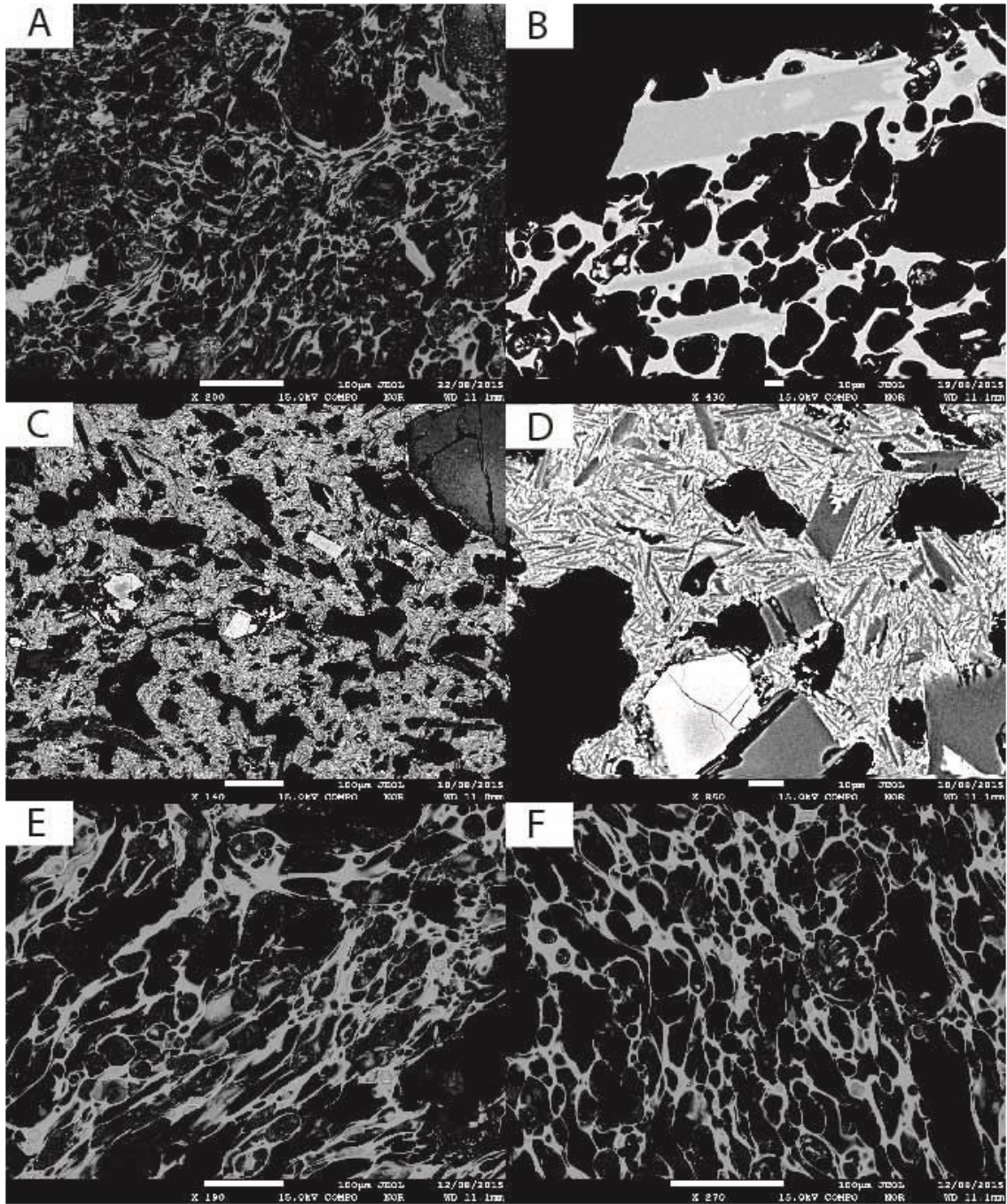


**Figure 11** Selected backscattered electron images of representative glass shards from M1p (A,B), M1s (C,D) and M2 (E,F). Vesicles are in black, while the glass and microlites groundmass are in grey.

Mineral phases range from microlites ( $\sim 10 \mu\text{m}$ ) to phenocrysts of 2 mm in length and include plagioclase, amphibole, and rare orthopyroxene and Fe-Ti oxides for M1p; plagioclase, olivine, clinopyroxene, with rare Fe-Ti oxides for M1s; plagioclase,

amphibole, olivine, clinopyroxene, orthopyroxene and Fe-Ti oxides for M2. A summary of the petrography of each sample is given in Table 7.

**Table 7 Summary of the mineralogical characteristics of Melimoyu eruptions.**

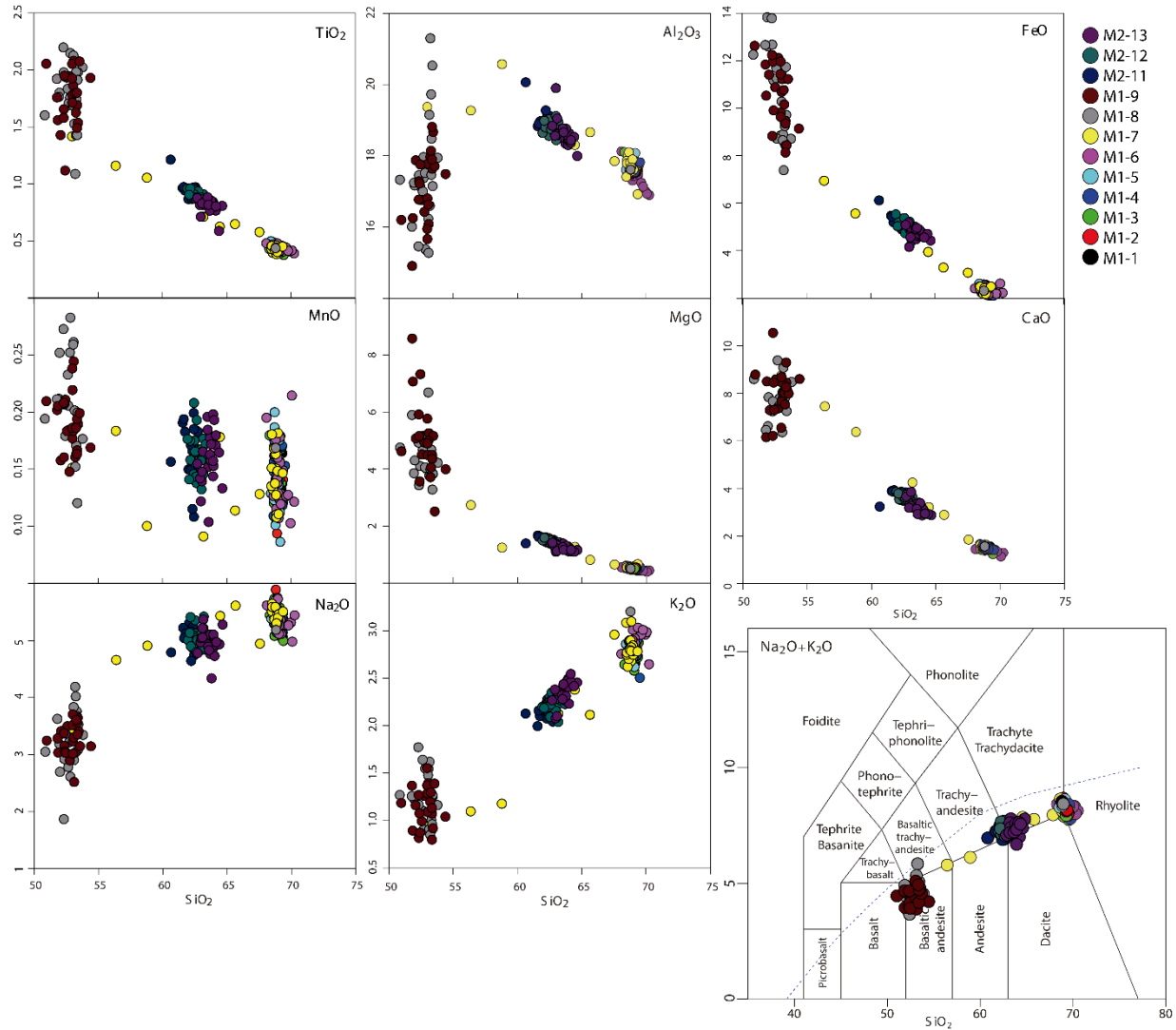
M1p				
Mineral phase	Size (mm)	Structurality	Intracrystalline textures	Occurrence and relationship with other phases
<b>Plagioclase</b>	0.8-2.0	Subhedral-Euhedral	Oscillatory, normal or inverse-zoned rim (An 27-56)	Isolated crystals, Forming clots with amphibole or orthopyroxene
<b>Amphibole</b>	0.2-1.3	Anhedral-Subhedral	Resorption textures (core)	Isolated crystals, Forming clots with plag
<b>Orthopyroxene</b>	0.3-1.0	Anhedral-Subhedral	Resorption textures (#Mg 72-74, En 67-70 Fs 28-31 Wo 2-4)	Clots with plag, oxides
<b>Oxide</b>	<0.2mm	Anhedral-Subhedral		Isolated crystals, clots or inclusions

M1s				
Mineral phase	Size (mm)	Structurality	Intracrystalline textures	Occurrence and relationship with other phases
<b>Plagioclase</b>	0.4-1.2	Subhedral-Euhedral	Patches, Normal or Oscillatory-zoned (An 61-87), microlites (An53-72)	Isolated crystals
<b>Olivine</b>	0.4-1.4	Anhedral-Subhedral	Resorption Textures, zoned (Fo 75-84 )	Isolated crystals, clots with ol, clots with cpx
<b>Clinopyroxene</b>	0.4-1.6	Subhedral	Resorption Textures, zoned (#Mg 0.82-0.90, En 42-46 Fs 8-12 Wo44-45)	Isolated crystals, clots with ol
<b>Oxides</b>	<0.2	Anhedral-Subhedral		Isolated crystals, clots or inclusions

M2				
Mineral phase	Size (mm)	Structurality	Intracrystalline textures	Occurrence and relationship with other phases
<b>Plagioclase</b>	0.3-1.4	Subhedral-Euhedral	Unzoned, Oscillatory or Inverse-zoned (An 38-58 )	Isolated crystals
<b>Amphibole</b>	0.5-1.6			
<b>Olivine</b>	0.1	Anhedral-Subhedral	Fo 73	Clots with cpx
<b>Clinopyroxene</b>	0.2-0.6	Anhedral-Subhedral	Zoned (#Mg82-88, En44-47Fs9-11Wo42-45)	Clots with ol
<b>Orthopyroxene</b>	0.4-0.5	Anhedral	(#Mg57-60, En52-56Fs40-44Wo4)	Oxides inclusions, clots with plag
<b>Oxide</b>	<0.2	Anhedral-Subhedral		isolated crystals, clots or inclusions
<b>Biotite</b>	<0.5	Subhedral		Isolated crystals

Glass data compositions have been shown Melimoyu eruptions to be trachydacite-rhyolite (M1p; 68.1-70.2% SiO<sub>2</sub>, 5.0-5.9 Na<sub>2</sub>O, 2.5-3.0 K<sub>2</sub>O), trachyandesite-trachydacite-dacite (M2; 60.7-64.7% SiO<sub>2</sub>, 4.3-5.4 Na<sub>2</sub>O, 2.0-2.5 K<sub>2</sub>O) and basalt-basaltic andesite-basaltic trachyandesite (M1s; 50.9-54.4% SiO<sub>2</sub>, 2.5-3.7 Na<sub>2</sub>O, 0.8-1.6 K<sub>2</sub>O). With increasing SiO<sub>2</sub>, there is a steady decrease in CaO, FeO, MgO, TiO<sub>2</sub>, Al<sub>2</sub>O<sub>3</sub> and with a corresponding increase in Na<sub>2</sub>O and K<sub>2</sub>O (Fig. 12). Samples form a discontinuous trend from basaltic to rhyolitic glass compositions, where outermost data corresponds to the older eruption M1p-M1s and the center correspond to the younger eruption M2. There is limited scatter within each sample, indicating that the glass composition is relatively homogeneous, excepting for M1s where measures were made on the profusely microlitic groundmass. Glass shard and minerals major element analyses are presented in Table I and II in Supplementary data.



**Figure 12 Selected major element compositions variations of glass shards from MEL1 and MEL2 tephra collected in time series. MM-1 (base) to MM-7 correspond to M1p, MM-8 and MM-9 correspond to M1s (top), MM-11 (base) to MM-13 (top) is M2.**

## Plagioclase

Plagioclase is the most common mineral phase within Melimoyu eruptions (Fig. 13). Crystals are generally euhedral to subhedral and range in size from ~0.4 to 2 mm. Plagioclase crystals are typically individual crystals in both eruptions, but occasionally form clots with amphibole or orthopyroxene and Fe-Ti oxides in M1p. Plagioclase textures are: normal, inverse or oscillatory zoned in M1p; patchy textured in core, normal or oscillatory zoned in M1s; oscillatory, inverse or unzoned in M2.

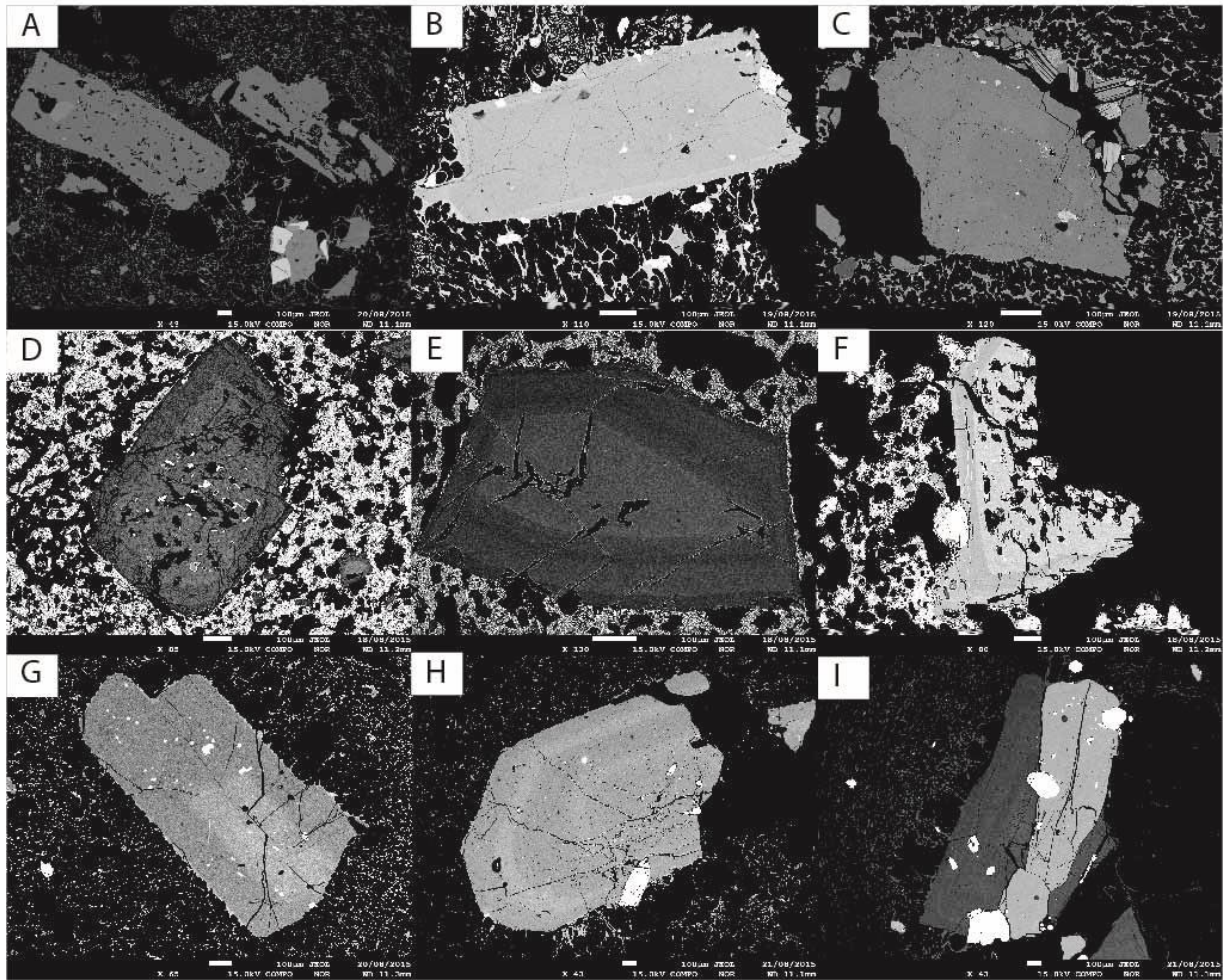


**Figure 13** Backscattered electron images of plagioclase phenocrysts in magmas from MEL1 (lower) and MEL2 (upper) eruptions sourced from Melimoyu volcano. A-C: M2, D-F: M1s, G-I: M1p.

Plagioclase compositions (Fig. 14) range from core ( $\text{An}_{33-55}$ ) to rims ( $\text{An}_{26-55}$ ) in M1p, in high-frequency zoning that usually extends from crystal rim to core. On the basis of core compositions and textures, three types of plagioclases are found. First group: with core composition of  $\text{An}_{34-38}$  and oscillatory zoning; second group: core compositions of  $\text{An}_{45-49}$  and normal or oscillatory zoning; and third group core compositions of around  $\text{An}_{56}$ .

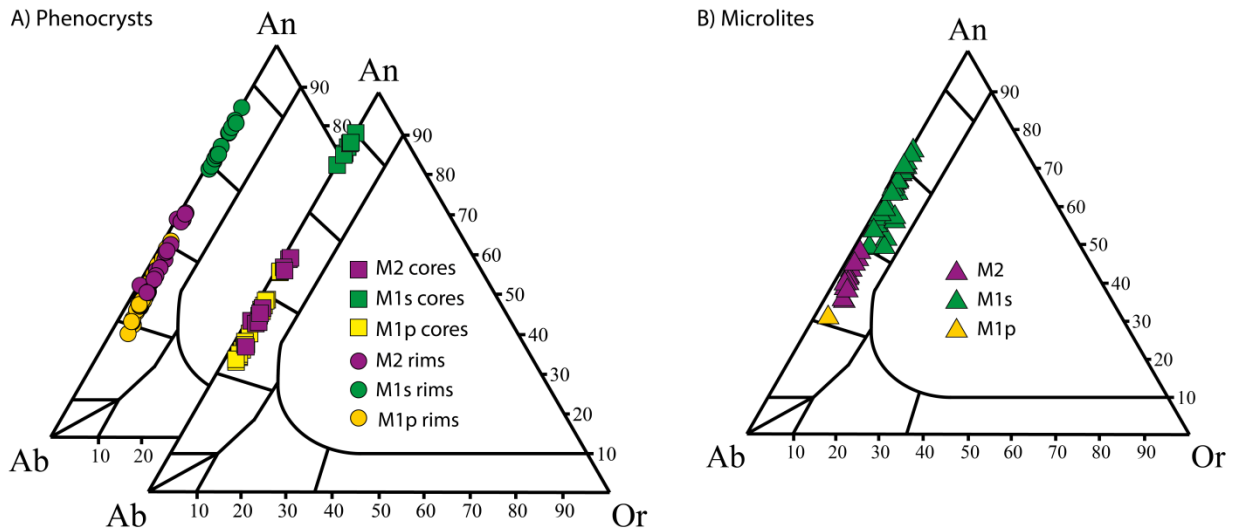


**Figure 14 Plagioclase phenocrysts and microlites compositions from MEL1 (lower) and MEL2 (upper) eruptions sourced from Melimoyu volcano.**

For M1s, core compositions are more restricted and calcic ( $\text{An}_{82-89}$ ), cores generally show resorptions, and crystals usually display low-frequency zoning to rims ( $\text{An}_{68-84}$ ). Also in M1s, the groundmass is profusely microlited, those plagioclase microlites are less anorthitic than phenocrystals with compositions of  $\text{An}_{53-72}$ .

Plagioclase compositions range from core ( $\text{An}_{36-58}$ ) to rim ( $\text{An}_{37-57}$ ) in M2. In general, variations in compositions is <20 mol% in anorthite content for both eruptions.

### Amphibole

Amphibole is present in M1p and M2 (Fig.15). It is most abundant as anhedral to subhedral individual crystals 0.2 mm to 1.3 mm, and 0.5 mm to 1.6 mm in size in M1p and M2 respectively. In both eruptions amphiboles is found as isolates crystals, but in M1p can be found forming clots with plagioclase and oxides.

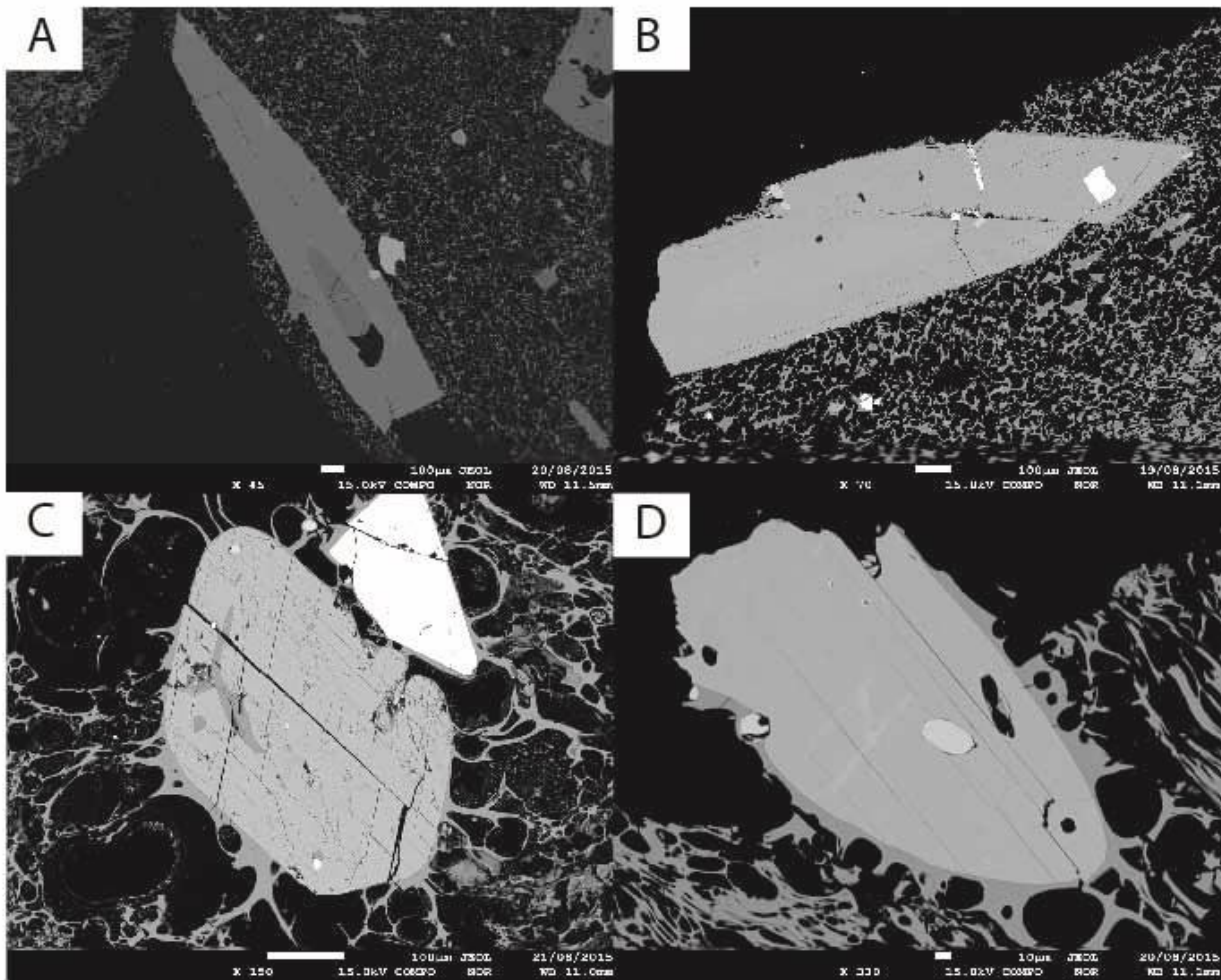


**Figure 15** Backscattered electron images of amphiboles phenocrysts in magmas from M2 (A,B) and M1p (C,D).

Structural formulae of amphiboles were calculated using the method of 13 cations excluding Ca, Na and K (13eCNK) described by Leake et al. (1997). Amphibole compositions (Fig. 16) in M1p are principally magnesio-hastingsite and around 20% of them are tschermakitic pargasite, and range in composition around Mg# = 80-90, and few crystals are in compositions Mg# = 64-74.

In M2, all amphiboles are magnesio-hastingsite, with compositions around Mg# = 77-82. Amphiboles are mostly unzoned, even though there are some variations between measured core and rim, and they show resorption textures in core in both eruptions.

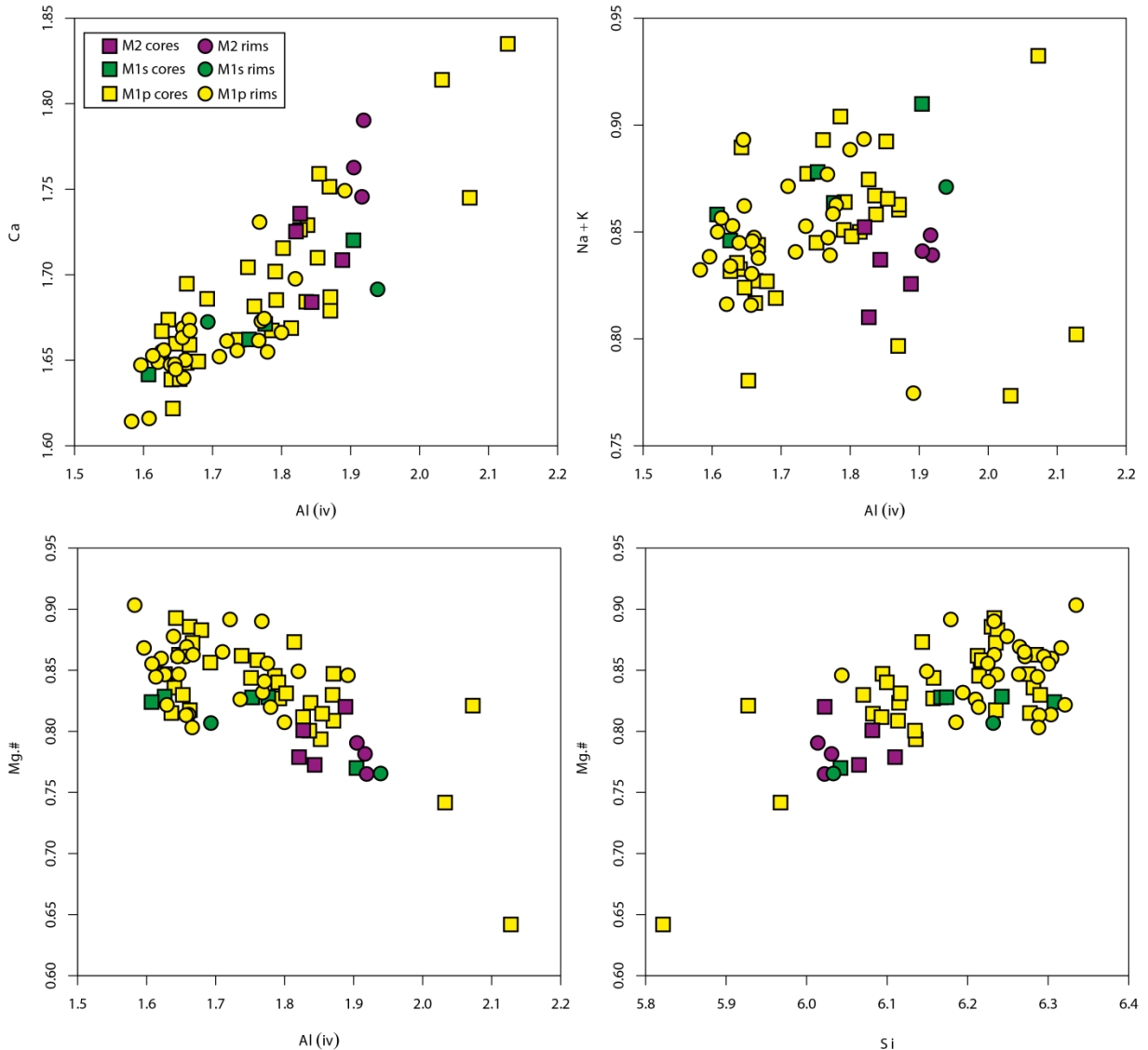


**Figure 16 Amphiboles phenocrysts composition of M1p and M2 units. Amphiboles marked with green circles and squares correspond to amphiboles found in mingled clasts between M1p and M1s units.**

### Clinopyroxene

Clinopyroxene phase is found in M1s and M2 (Fig. 17). Clinopyroxene crystals in M1s range in size from 0.4 to 1.6 mm in length and occur as isolated crystals or can form clots with olivine.

Crystals are primarily subhedral and are compositionally restricted to Mg# = 82-90. Most of crystal exhibit a rim (compositions vary between En<sub>42-46</sub>, Fs<sub>8-12</sub>, Wo<sub>44-45</sub>), and some of them present resorption textures in rim. Crystals can be divided in two groups

(Fig. 18): first group with a clear rim compositionally less #Mg, En, Wo and more Fs; and second group without a rim, but compositionally with more #Mg, En, Wo and less Fs.

Some crystals of clinopyroxene are found in M2, forming clots with olivine, and are compositionally zoned (#Mg = 82-88, En<sub>44-47</sub>, Fs<sub>9-11</sub>, Wo<sub>42-45</sub>).

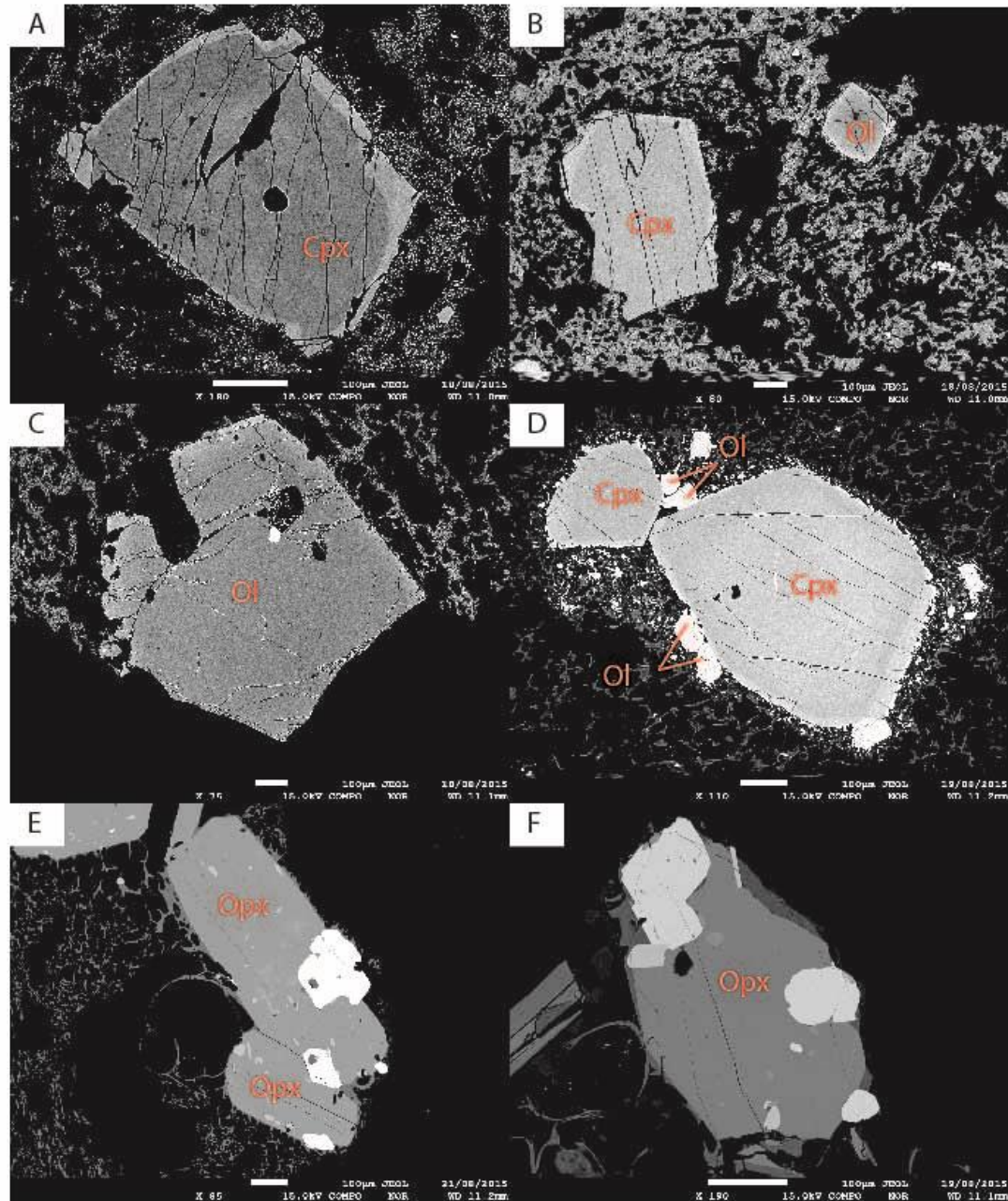


**Figure 17** Backscattered electron images of olivines, clinopyroxenes and orthopyroxenes phenocrysts in magmas from M1, M1s and M2 units. A: Clinopyroxene from M1s, B: Clinopyroxene-Olivine from M1s, C: Olivine from M1s, D: Clinopyroxene-Olivine from M2, E: Orthopyroxene from M1, F: Orthopyroxene from M2.

## **Orthopyroxene**

Orthopyroxene crystals are present in M1p where they form anhedral to subhedral crystals 0.3 – 1 mm in size and in M2 where they form anhedral crystals 0.4 – 0.5 mm in size (Fig. 17).

In M1p there is a little compositional variation (Fig. 18) ( $\#Mg = 72\text{-}74$ ,  $En_{67\text{-}70}$ ,  $Fs_{28\text{-}31}$ ,  $Wo_{2\text{-}4}$ ), no zoning and resorption textures, and orthopyroxene usually form clots with plagioclase and Fe-Ti oxides.

In M2 there is also a little compositional variation ( $\#Mg = 57\text{-}60$ ,  $En_{52\text{-}56}$ ,  $Fs_{40\text{-}44}$ ,  $Wo_4$ ) and no zoning. Crystals form clots with plagioclases, and it is common to find oxides inclusions.

## **Olivine**

Olivine crystals are present in M1s and M2 and are typically anhedral to subhedral (Fig. 17), showing resorption textures and zoning in M1s.

In M1s, olivine is present as isolated crystals or forming clots with other olivines or clinopyroxene, crystals sizes are 0.4-1.4 mm. The compositions of olivines cores are  $Fo_{79\text{-}84}$  and rims are  $Fo_{75\text{-}80}$  (Fig. 18). Some olivine microlites are found with compositions of  $Fo_{75\text{-}78}$ .

In M2, olivines form clots with clinopyroxenes, and crystals sizes are ~0.1mm and compositions are ~ $Fo_{73}$ .

## **Fe-Ti Oxide**

The main Fe-Ti oxide phase is titanomagnetite, although ilmenite is also present on three magmas but specially in M1p and M2. Titanomagnetite occurs as individual crystals, clusters of crystals and as inclusions mainly in orthopyroxene. Crystals are typically subhedral to anhedral in shape, and <0.2 mm in size.

## **Biotite**

There are some biotite crystals present in M2. Those are individual crystals and subhedrals, and <0.5 mm in size.

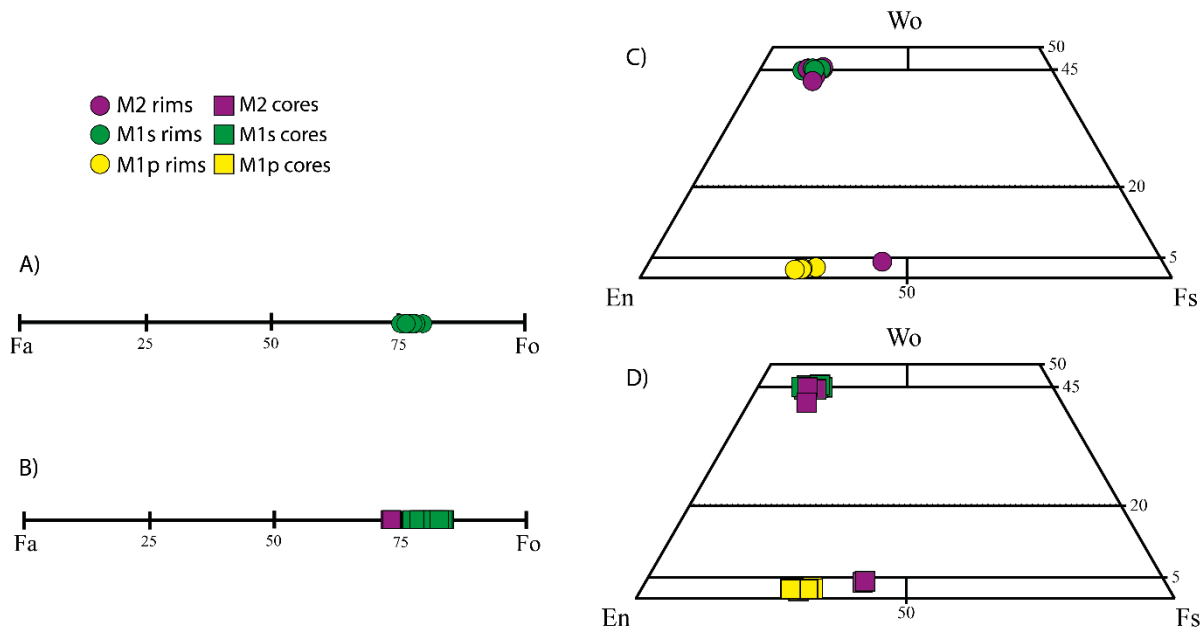


**Figure 18 Olivine and pyroxene compositions of the studied samples. Compositions of olivine phenocrysts rims (A) and cores (B) of M1s and M2. Compositions of orthopyroxene and clinopyroxene phenocrysts rims (C) and cores (D) of M1s and M2 units.**

### 2.3.6. Thermobarometry

In order to delimitate the temperature of magmas and the depth of the magma chambers, we used thermometers and barometers based in geochemistry of minerals and glass. In those cases that H<sub>2</sub>O glass composition was also needed, and temperatures depends on pressures or vice versa, values had to be constrained by iteration between geothermometers and geobarometers and also the hygrometer of Lange et al., (2009), testing different H<sub>2</sub>O percentages. Fig. 19 shows P-T conditions obtained for the three units with amphiboles for M1p and M2, and with clinopyroxenes for M1s. There is a summary of temperatures and pressures on Table 8, and a summary of temperatures with errors is shown on Fig. 20.

#### M1p

The orthopyroxene-liquid geothermometer (equation 28a in Putirka, 2008) and the amphibole geothermometer (Ridolfi and Renzulli, 2012) were used. The amphibole-plagioclase geothermometer of (Holland and Blundy, 1994) was used also for pairs in

contact. One orthopyroxene rim satisfied the equilibrium conditions with Fe/Mg values of 0.22 and the other four had Fe/Mg values of ~ 0.19.

Temperatures of ~ 930-1010 ± 39°C were obtained with the five orthopyroxene rims. With amphiboles, temperatures of around 830°C in core (735-897 ± 23.5 °C) and around 830°C in rim (752-895 ± 23.5°C) were obtained. With plagioclase-amphibole geothermometer, temperature of ~882°C (850-902 ± 40°C) was obtained.

Pressures were obtained with geobarometer in amphiboles (Ridolfi and Renzulli, 2012), pressures of around 2 kbar (1.4-2.4 kbar ± 11.5%) in core and 1.8 kbar (1.4-2.3 kbar ± 11.5%) in rim.

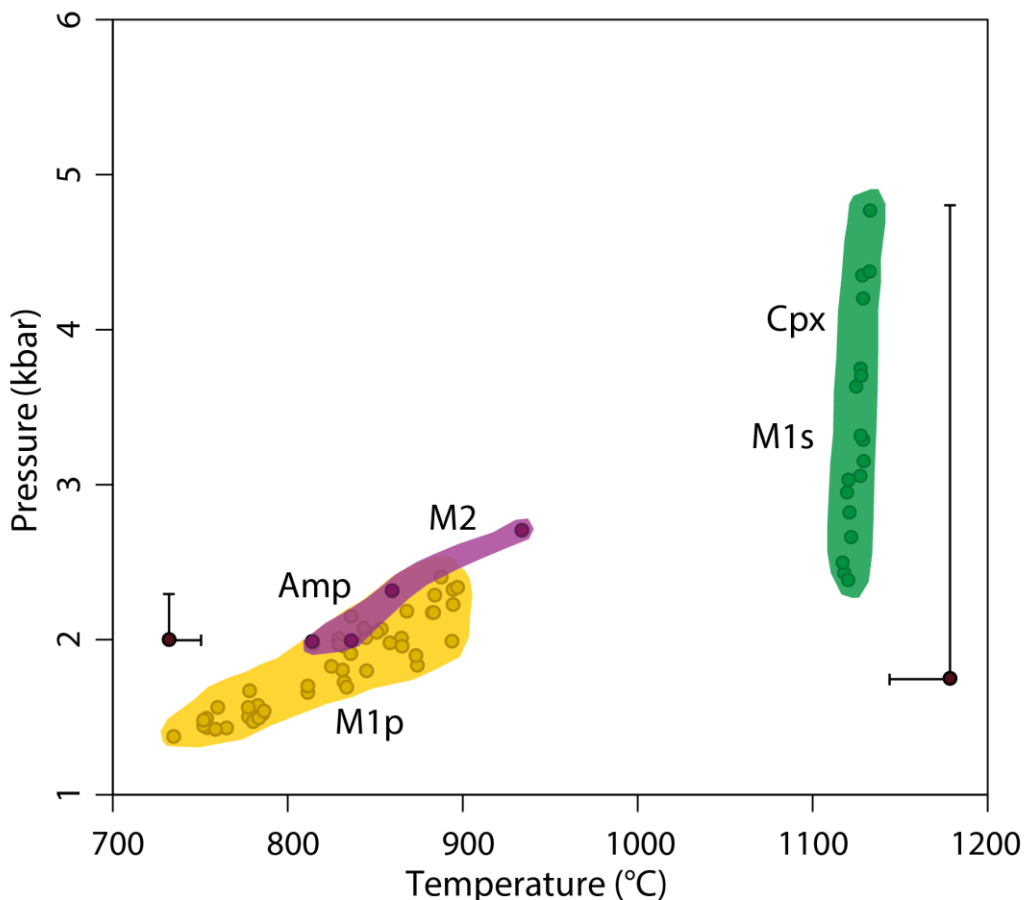


**Figure 19** Stability P-T fields of amphiboles in M1p (yellow field) and M2 (magenta field) obtained with Ridolfi and Renzulli (2012). And stability P-T fields of clinopyroxenes in M1s (green field) obtained by equation 32a of pressure of Putirka (2008) and equation of temperature of Putirka et al. (2003). Error bars are shown.

## M1s

The olivine–liquid geothermometer (equation 22 in Putirka, 2008) and clinopyroxene geothermometer (Putirka et al., 2003) were used in M1s. The olivine-augite geothermometer (Loucks, 1996) was used with the only pair olivine-clinopyroxene that was found. The equilibrium mineral-liquid conditions were tested using Putirka, (2008) in terms of Fe/Mg values. Eleven olivines rim and one core satisfied the equilibrium conditions with Fe/Mg values of 0.26 – 0.29.

Equilibrium temperatures of  $\sim 1080\text{--}1150^\circ\text{C} \pm 43^\circ\text{C}$  were obtained with olivines. For clinopyroxenes, temperatures of  $\sim 1118\text{--}1133^\circ\text{C} \pm 33^\circ\text{C}$  for cores and  $\sim 1117\text{--}1132^\circ\text{C} \pm 33^\circ\text{C}$  for rims were obtained. By using rim crystals of the olivine-clinopyroxene pair, temperature of  $1100^\circ\text{C} \pm 6^\circ\text{C}$  was obtained.

Pressures were obtained in clinopyroxene with equation 32a of Putirka, (2008), considering temperatures obtained with Putirka et al. (2003). Pressures between 2.4 – 4.8 kbar  $\pm 3.1$  kbar were obtained for clinopyroxenes cores and rims.

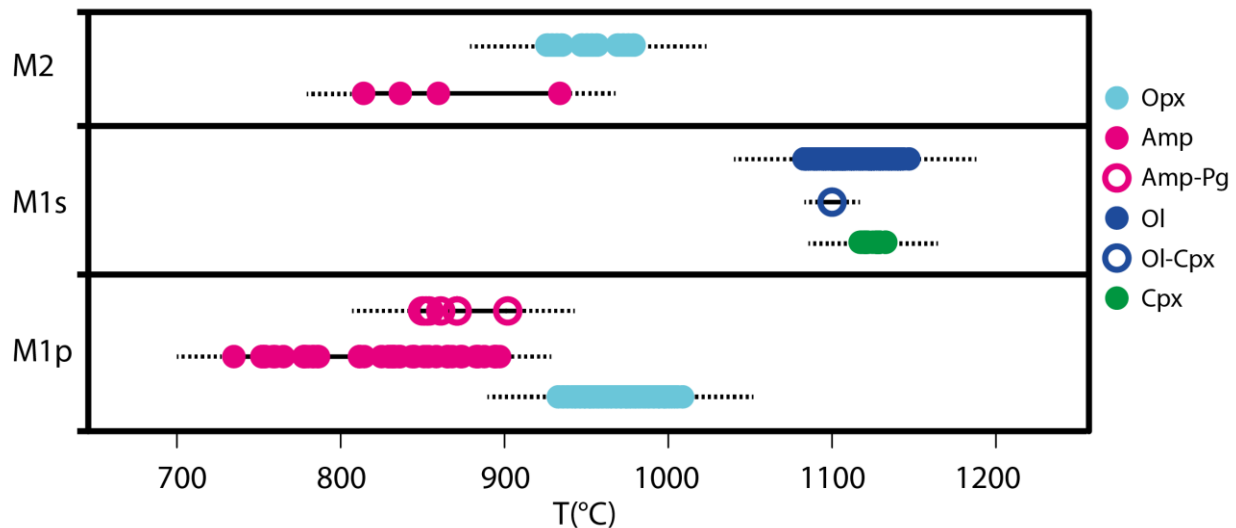


**Figure 20** Temperatures obtained by geothermometry of Amphiboles (Ridolfi and Renzulli, 2012); Orthopyroxenes (Putirka, 2008), Clinopyroxenes (Putirka et al., 2003), Olivines (Putirka, 2008); Olivine-Clinopyroxene (Loucks, 1996); Amphiboles-Plagioclases (Holland and Blundy, 1994). Dashed lines indicate errors.

## M2

The orthopyroxene-liquid geothermometer (equation 28a in Putirka, 2008) and the amphibole geothermometer (Ridolfi and Renzulli, 2012) were used. Two orthopyroxene cores satisfied the equilibrium conditions with Fe/Mg values of 0.34-0.35.

Temperature of  $\sim 920\text{-}980 \pm 39^\circ\text{C}$  was obtained with two orthopyroxene cores. With amphiboles, temperatures of around  $820 \pm 23.5^\circ\text{C}$  in core and around  $890 \pm 23.5^\circ\text{C}$  in rim were obtained.

Pressures were obtained with geobarometer in amphiboles (Ridolfi and Renzulli, 2012), pressures of around 2 kbar  $\pm 11.5\%$  in core and 2.5 kbar  $\pm 11.5\%$  in rim.

**Table 8 Summary of pressures and temperatures obtained in this study.**

	M1p		M1s		M2		References
Temperatures	core	rim	core	rim	core	rim	
Orthopyroxenes		930-1010			920-980		T( $\pm 39^\circ\text{C}$ ; Putirka, 2008)
Amphiboles		735-897			820-890		T( $\pm 11.5\%$ ; Ridolfi and Renzulli, 2012)
Amp-Plag		850-902					T( $\pm 40^\circ\text{C}$ ; Holland and Blundy, 1994)
Olivines			1080-1150				T( $\pm 43^\circ\text{C}$ ; Putirka, 2008)
Clinopyroxenes			1117-1133				T( $\pm 33^\circ\text{C}$ ; Putirka et al., 2003)
Ol-Cpx			1100				T( $\pm 6^\circ\text{C}$ ; Loucks, 1996)
Pressures	core	rim	core	rim	core	rim	
Amphiboles	1.4-2.4				2.0-2.5		P( $\pm 11.5\%$ kbar; Ridolfi and Renzulli, 2012)
Clinopyroxenes			2.4-4.8				P( $\pm 3.1$ kbar; Putirka, 2008)

## 2.4. Discussion

### 2.4.1. Last 20 kyr activity of Melimoyu volcano

Compared with other volcanoes in the region, the stratigraphy of Melimoyu volcano indicates an intermittent post-glacial eruptive activity and low frequency. After new data obtained in this work from the western side of the volcano, it was possible to compare the chemistry of these deposits found there and to correlate some of them with the M2 event. Layer “13B” of section “Seno Gala” has chemistry and age comparable to M2. Although paleosols below layers “9A” of the section “Aeródromo” and “11A” of the “Marchant” section have not been dated, the chemical signature of their juvenile material suggests that they could be linked to M2. Finally, layer “10C” of section “Santo Domingo” has the same age, but a slightly different composition, but considering high LOI obtained in the chemical analysis, it could be also related to M2. Moreover, those layers aren’t the only pyroclastic levels found on the western side of Melimoyu volcano. Besides them, two levels in “Santo Domingo”, one level in “Marchant” and one level in “Aeródromo” were recognized. The presence of other pyroclastic deposits on these sections suggests the existence of others post-glacial eruptions apart from M1 and M2.

Stern et al. (2015), also attributed deposits derived from explosive activity to Melimoyu, based on traces elements in whole rock chemistry and mineralogy. They considered two different chemical groups described in previous works (e.g. López-Escobar et al., 1993, 1995): Type-1 or Low Abundance and Type-2 or High Abundance groups. These groups are based on concentrations of the incompatible elements K<sub>2</sub>O, Rb, Ti, Ba, Zr, Sr, Y, Nb and La, as well as La/Yb and Ba/La ratios. Maca, Cay and Yanteles stratovolcanoes, and the Palena group are Type-1, while Hudson and Melimoyu volcanoes and Puyuhuapi group are Type-2.

**Table 9 Ratios of trace elements of M1p, M1s, M2 and samples from Stern et al. 2015.**

Code	Unit	~age BP	Nb/Y	Zr/TiO2	Zr/Nb	La/Yb	Ti/Rb	Ref
AGO14-2	Lava	-	0.41	224	17.0	8.9	126	This study
AGO14-4C	M1p		0.52	443	18.2	9.4	75	This study
ABR15-1C	M1p		0.53	440	18.2	9.3	77	This study
ABR15-1B	M1p	2800	0.53	429	18.3	9.2	81	This study
ABR15-1D	M1p		0.54	421	18.2	9.0	87	This study
AGO14-4D	M1s		0.30	85	18.0	6.9	561	This study
ABR15-1E	M1s	2800	0.34	95	18.1	6.6	534	This study
ABR15-1F	M1s		0.33	84	18.1	6.5	638	This study
AGO14-4G	M2		0.39	280	18.9	8.4	122	This study
ABR15-5A	M2	1600	0.39	255	18.7	7.7	150	This study
ABR15-5C	M2		0.41	311	19.4	8.1	110	This study
CS5054	Shaman a	1440	0.57	153	14.0	9.4	259	Stern et al. 2015
CS5059	Shaman f	4610	0.51	205	13.8	10.9	124	Stern et al. 2015
CS5060	Shaman g	8280	0.46	201	16.2	8.5	149	Stern et al. 2015
CS5051	Embudo a	2090	0.63	148	12.5	9.0	270	Stern et al. 2015
CS3817	Embudo b	4810	0.48	280	20.1	10.4	123	Stern et al. 2015
CS3847	Cis-263-a	19670	0.37	157	17.2	10.6	252	Stern et al. 2015

They determined that layers “a” from Shaman and “a” from Mallín El Embudo correspond to M2, layers “f” from Shaman and “b” from Mallin El Embudo correspond to an older eruption of ~4.6-4.8 ka, layer “g” from Shaman and the sample CIS-263a to older eruptions of ~8.3 and >19.7 ka respectively that haven’t been described before.

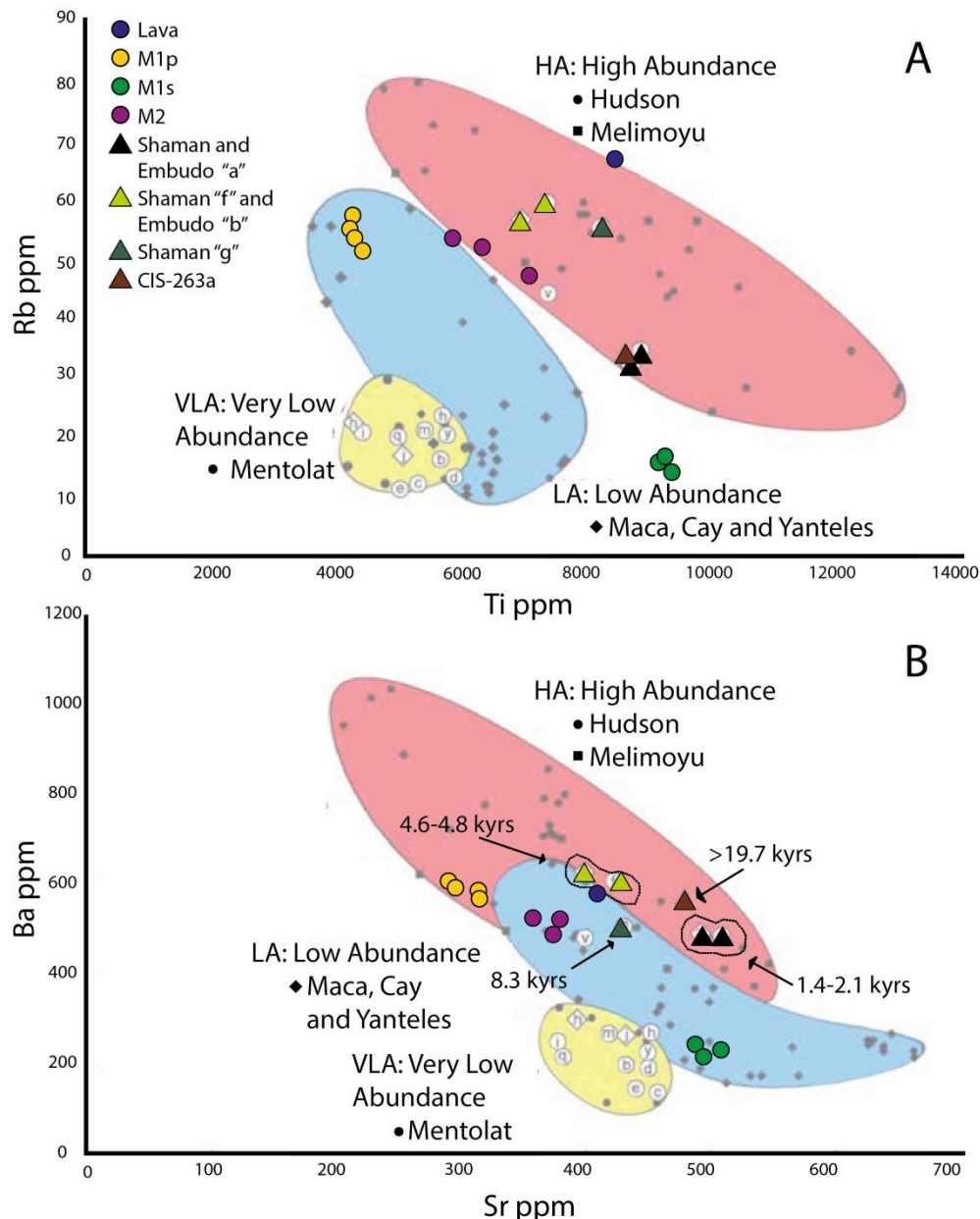


**Figure 21** A) Ti versus Rb and B) Sr versus Ba graphs modified from Stern et al. (2015) to include Melimoyu tephra and lava samples of this study and to highlight layers associated to Melimoyu from Río Cisnes Valley. Line separating the fields of High-, Medium-, and Low-K convergent plate boundary magmas are from Peccerillo and Taylor (1976).

We analyzed plots shown on their work after adding whole rock chemistry of M1p, M1s and M2 of this study (Fig. 21). We determined their correlations aren't conclusive with respect to the origin of those deposits because evidence of the three different fields is not clear. Moreover, layers attributed by Stern et al. (2015) to M2 slightly differ compared with chemistry of M2 eruption than other deposits attributed to a possible older eruption of Melimoyu. Moreover, if we look at the described mineralogy, layers considered to be from Melimoyu, are the only ones without containing amphiboles, which is contradictory with mineralogy observed in this work, where amphibole is the dominant phase after plagioclase both in M1 and M2. Besides, it draws attention that on none of those sediments cores studied by Stern et al. (2015) layers associated to M1 were observed. And yet this eruption is larger than M2, and had a dispersion to SE, i.e., more on the direction of Río Cisnes valley. However, in order to try a better correlation, we analyzed some traces elements ratios (Table 9). From these ratios, Zr/Nb in particular (Fig. 22), seems to be a better ratio to define origin of events since all deposits of Melimoyu have similar  $\sim$  17-19 values. Based on this; Shaman "g", CIS-263a and Embudo "b" are candidates to be from Melimoyu eruptions.

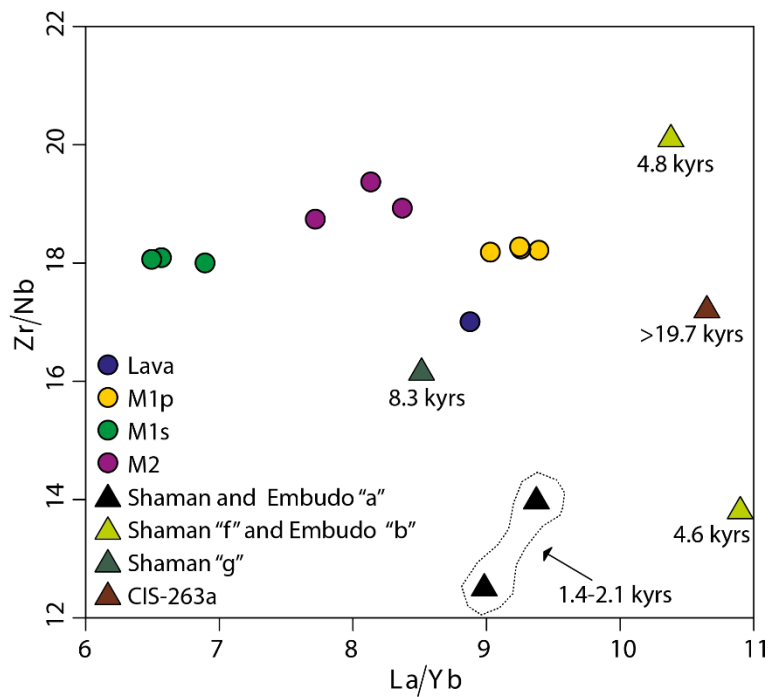


**Figure 22** La/Yb versus Zr/Nb for the lava flow and tephras of Melimoyu eruptions, and tephra layers of Stern et al. (2015) associated to Melimoyu.

Therefore, we suggest the eruptive registry of Melimoyu volcano could be extended considering deposits of the western side from this work and layers described and dated by Stern et al., (2015), adding their possible events of ~4.6-4.8, ~8.3 and >19.7 ka, helping to enhance the poorly constrained Holocene activity of this volcano.

After observing the record of eruptions from the Southern segment of the SVZ (Fig. 23), we could verify that other volcanoes have a broader registry of eruptions. Most of volcanoes in the area have associated deposits of eruptions between 2 ka and 10 ka BP. Hence, most of them could be associated with the final retreat of low-altitude ice at 11.4 ka (Watt et al., 2013a). Mentolat and Hudson have eruptions older than 16 ka BP (Weller et al., 2013; Weller et al., 2014). But in Melimoyu, the record was limited to < 3 ky. It is reasonable to expect that Melimoyu has also Holocene eruptions older than the two known M1 and M2. Considering that, and even including events of ~4.6-4.7, ~8.3 and >19.7 ka, a possible explanation for this lack of recorded eruptions is that some important erosive events occurred in the area around 44° S that could erode deposits of previous eruptions. Southern South America is the only landmass to cross the southern westerly wind belt (WWB), which is a significant control on global ocean circulation and climate (Kilian and Lamy, 2012). Southern westerlies dominate the climate of southern South America. Changes in the position and/or intensity of the Westerlies could cause large changes in precipitation and temperature for a given location (Douglass et al., 2005). In the same ~ 44 ° area but during Pliocene-Pleistocene transition, Herman and Brandon (2015) identified an erosion hotspot and showed that this hotspot coincides with location of maximum precipitation that follows westerlies during glacial periods. Then, migration of the WWB has played an important role in determining the distribution of erosion since 2-3 Ma. Considering the migration of WWB during the Holocene and its effects on erosion, that could be an explanation of the lack of registry of more Melimoyu eruptions. There are some works that model westerlies after last glacial maximum (Rojas et al., 2009; Rojas and Moreno, 2011) but it could be necessary studies of tephrochronology in sediment cores on lakes adjacent to Melimoyu that will provide better records than what can be currently observed in the soil-forming environment. Very detailed eruptive records are being recognized from closed lake basins and bogs (Alloway et al., 2017a), for example, Lago Teo near Chaitén township (Moreno et al.,

2015) that indicate a detailed multiple-sourced eruptive record extending over the last 11,000 cal age BP. On the other hand, considering that, even Melimoyu is a large volcano, it is a volcanic edifice with low slopes and several lavas morphologies. So another possibility to explain the absence of more explosive registry is that Melimoyu may be characterized by more effusive activity.

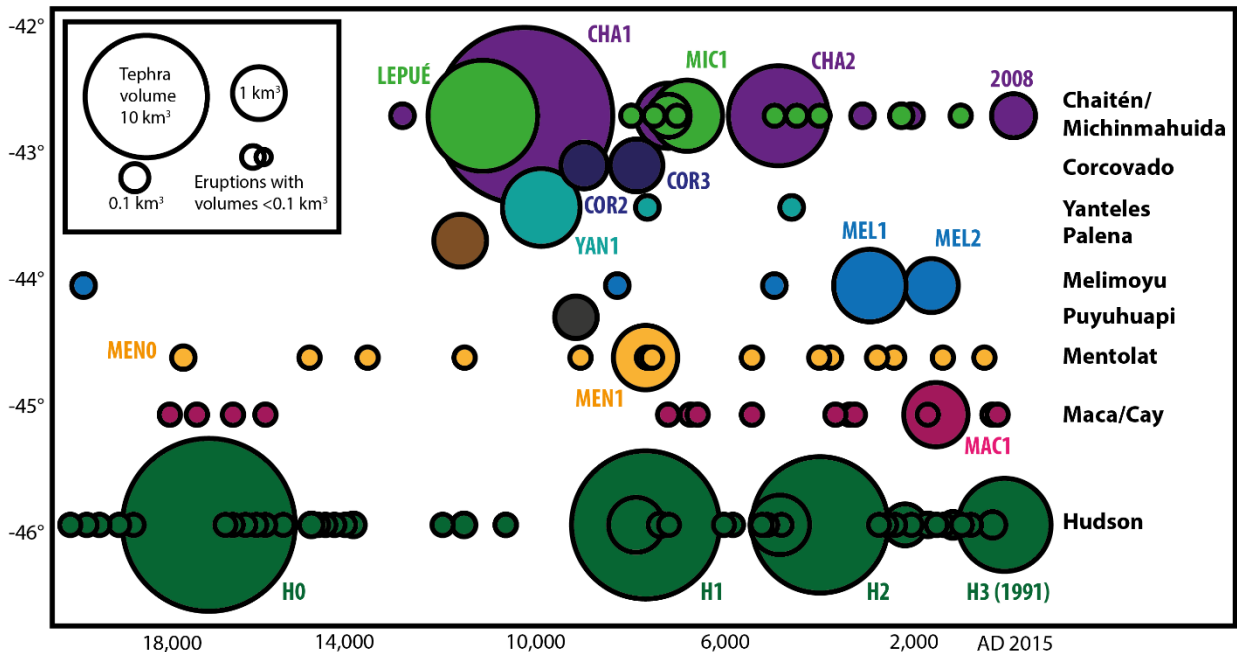


**Figure 23 Eruption volumes for volcanic centers of the southernmost part of the SVZ between 42°-46° from Late Glacial and Holocene time. Modified from Watt et al. (2013a) and Weller et al. (2015). Including changes of source of COR1 by Alloway et al. (2017a, 2017b).**

#### 2.4.2. Eruptive parameters of M1 and M2

Regarding eruptive parameters, volumes obtained here are bigger than estimated in Naranjo and Stern (2004), where they estimated volumes of eruptions in the southern SVZ of  $<1\text{km}^3$ , except for Hudson volcano. If we compare 10cm isopachs between this work and Naranjo and Stern (2004), it is found that for M1, our distribution is slightly wider in the N-S axes, but considerably smaller on the E-W. In this study, although no new points were obtained in Argentina, the analysis of thicknesses of sections from Naranjo and Stern (2004) reveals that the only section that has a layer with a thickness

higher than 10 cm could be due to local effects, as three others have thickness around 5 cm and major clasts of 5 mm that is consistent with the data of this work. Otherwise, the authors didn't adjust their 10-cm isopach including the layer higher than 10 cm, so it could be supposed that authors thought this layer may not have been primary.

For this reason, we considered the eastern limit of their 10cm isopachs should be rather a 5cm isopach. Regarding eruption M2, values of isopachs are slightly larger than those of Naranjo and Stern (2004), considering new control points obtained in this work, including those of the western side of the volcano.

As regards methodologies to measure volume, by the Weibull function of Bonadonna and Costa (2012) a considerably larger volume for M2 (~60%) was obtained instead of the similar values observed for M1p and M1s, comparing with the exponential thickness decay model of Fierstein and Nathenson, (1992). This could due to the lack of data in proximal and especially distal deposits. As the Weibull method is supposed to reduce the uncertainty due to the absence of data, as it does not depend on integration limits, we determine this value is a more realistic volume for M2. With respect to the measurement of major clasts, it is important to consider that we used two methods. The method of the maximum axis of five largest clasts that has been widely used and the G3/5 that is one of best methods according to Bonadonna et al. (2013). In this case, we didn't recognize noticeable differences, but for future works it will be useful to unify the methodologies and use the 50th percentile of twenty largest clasts and complement with the G3/5 method as it is recommended by Bonadonna et al. (2013).

Therefore, in this study we added new sections of tephras described and update the volume values obtained by Naranjo and Stern (2004), despite the difficulty of access in that area. We could reduce uncertainties to the E of the Carretera Austral comparing with isopachs of Naranjo and Stern (2004), but there are still uncertainties especially to the S. It is important to consider, as mentioned by Alloway et al. (2017a), that secondary remobilisation and over-thickening affecting thickness and gran-size parameters are common occurrences in this region due to its high rainfall of ~2400 mm per year. These conditions, and new data especially from lakes core, have changed preliminary downwind distribution estimations from different vents. In the case of M1 and M2, there is a lack of data in the Carretera Austral to the S (N of Puyuhuapi). This is evidenced by

the abrupt break in thickness in that area, opposed to the N of Melimoyu where the decrease of thickness is more gradual. That may be due to recurrent landslides in the area, due to the steep topography that characterized this region, which could preclude to find finer deposits. For these reasons no-DRE volumes of those Melimoyu eruptions ( $\sim 2.0 \text{ km}^3$  for M1p,  $\sim 0.6 \text{ km}^3$  for M1s, and  $\sim 1.6 \text{ km}^3$  for M2) are minimums. With respect to the estimation of column height, we observed that the range of height obtained was wide, but it was because of differences in the shape of isopleths, more than a difference between lithic and juvenile isopleths or between both methods used to measure largest clasts. Plume heights obtained were constrained to ca. 30- 35 km for M1p, 30-35 km for M1s, and 26-30 km for M2. It draws attention that M1s having a thickness considerable smaller than M1p, it had a similar height of column. However, considering that M1p has an inverse grading and M1s a normal grading, those heights would reflect the height of column at the moment of transition in type of clasts composition and this moment would have the highest intensity of the eruption.

Finally, if we consider volcanic activity of the last 3000 years in the southern part of SVZ, Melimoyu would be one of the most active volcanoes in the area along with Hudson and Chaitén volcanoes. Melimoyu volcano would be the only one with two high explosive eruptions closely spaced in time, that combining volume and column height information, they will be classified as IEV=5 (Newhall y Self, 1982), i.e. Plinian eruptions. Dispersion from E to SE is observed in M1, and dispersion principally E is observed in M1s and M2 units that differ slightly from the mainly NE dispersion obtained by Naranjo and Stern (2004). It is important to consider those dispersions of tephras as in case of an eruption; fall deposits will affect probably La Junta, Raul Marín Balmaceda, Melimoyu village, Puyuhuapi, Lago Verde. Furthermore, due to the difficult access, we couldn't find other products of M1 and M2, but looking at the dimension of eruptions it is reasonable to expect that other types of products were erupted during those eruptions. Besides, pyroclastic density currents morphologies were recognized by photo-interpretation, as well as some lahars deposits to the northern and western side of the volcano.

### 2.4.3. Pre-eruptive conditions of M1

Pumice lapilli of M1 commonly exhibit distinctive black and yellow bands of glass that evidence magma mingling (Fig. 24). Analysis of both bands reveals different compositions indicating that both basaltic and dacitic compositions correspond to the same eruption. These clasts have domains of microlite-rich basaltic glass in sharp contact with microlite-poor, brown transparent dacitic glass. Microlite-rich domains may represent magma starting to have an intense vesiculation caused by the initiation of the eruption and the decompression of the chamber (Scandone and Giacomelli, 2001) and may have been syn-eruptively or pre-eruptively mingled with the more evolved magma. Compositional zoning in magmas erupted within volcanic arcs has been investigated at several localities worldwide. In particular, in the SVZ recent studies include eruptions of Quizapu (Hildreth & Drake, 1992; Ruprecht et al., 2012) and Hudson (Kratzmann et al., 2009) volcanoes. Chemical heterogeneities of volcanic deposits are attributed to zoned reservoirs formed by *in situ* fractional crystallization of mafic magma (Smith, 1979; Wolff et al., 1990) or by intrusion of mafic magma into a silicic magma body (e.g. Bacon & Druitt, 1988). However, the origin of this zoning remains controversial (Eichelberger et al., 2001, 2000; de Silva, 2001), therefore, relationship between M1p and M1s composition was one of the key issues of this work. In order to understand that, we analyzed glass chemistry, mineral textures and P-T conditions.

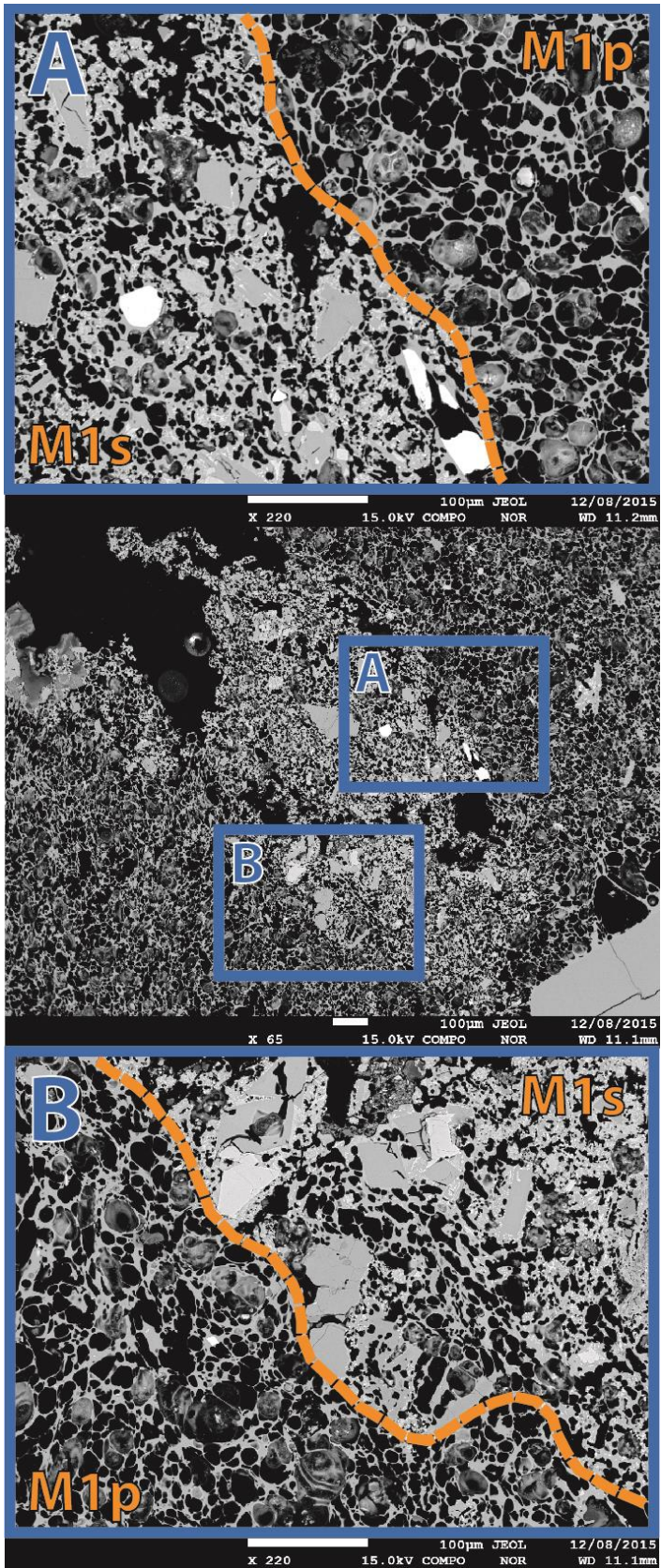


**Figure 24 Mingled pumices of M1 eruption. Selected backscattered electron images of representative glass of limit between M1p and M1s showing differences on glass textures. A and B images show a zoom of the limit of mingling on this eruption.**

Evidence for phenocryst-melt disequilibrium is commonly present in the phenocrysts found in M1s. Plagioclase phenocryst display oscillatory zoning and patchy textures, as well as olivine and clinopyroxene present resorption textures in rim. These textures are indicative of disequilibrium during the history of phenocryst growth and may be the result of change in temperatures, magma composition, or pressure due to ascent from a deeper reservoir. Instead, there is no clear evidence for disequilibrium in phenocrysts found in M1p. Although, plagioclase in M1p show oscillatory zoning, composition variation occurs in a range smaller than 20% of An and there is a lack of a more anorthitic rim that could suggest a final heating before eruption (Fig. 25). Moreover, amphiboles and orthopyroxenes don't present a clear zoning, however, amphiboles show resorption textures in core that could be associated to perturbations of temperature or compositions due to convection into the magma chamber.

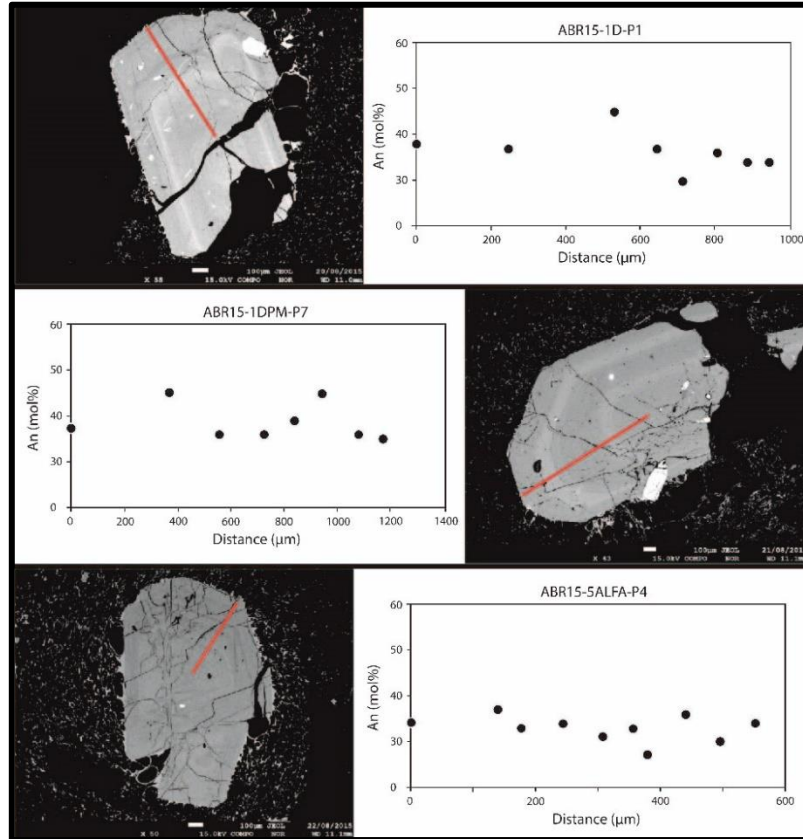


**Figure 25** An zoning profiles on plagioclases of M1p. X axis represent the distance to the core. Even oscillatory zoning is common; An variation is less than 20%.

Geobarometers has high errors, especially those used for M1s. Even so P-T conditions obtained could suggest that M1s magma was emplaced in the deepest part of the same magma chamber or in a deeper reservoir than M1p reservoir. Considering that chemical compositions and mineralogy are to contrasting and that there is no evidence of crystal mush zone or settling of crystals, it is hasty to suggest an in situ fractional crystallization. Besides, minerals in M1s as plagioclases and olivines, show textures like patchy and resorption respectively that could be associated to a change of pressure, that is an ascent from deeper reservoir. Then, the most likely option to form these deposits with two contrasting compositions is an injection of this more primitive magma. Another issue was if this processes occurred during a long time or just before eruption. M1p glass composition is homogeneous, thus there is no evidence of stratification from base to top. Besides, as mentioned before, zonation in crystals are poor contrasting and there are not rims that reflect an important input of temperature or variation of composition. Consequently, the most acceptable option is that both magmas could be cogenetic and M1s was formed below M1p. An injection of M1s could be enough rapid to not having generated a mixing but causing the mingling observed. Therefore, this new pulse of more mafic magma could be triggered this eruption.

#### 2.4.4. Relationship between Melimoyu's eruptions

Around 1200 years after M1, the event which generated deposit M2 occurred, with an intermediate andesitic composition. Andesites are commonly found at subduction zones (Taylor and McLennan, 1985), however, their origin is poor constrained. There are many ways in which an andesite could form: direct melting of the mantle at water-saturated conditions, partial re-melting of altered basaltic crust, crystal fractionation of arc basalts in crystal magma chambers and mixing of mafic magmas with high Si crust magmas (Lee and Bachmann, 2014). But which of these mechanisms dominates is unclear and depends of each case. To form the andesitic composition of M2 there are two most probably hypotheses: mixing between remnant of M1p and M1s after the eruption, or a crystal fractionation from M1s basaltic composition.

As mentioned in the result section, harker diagrams of M1p, M1s and M2 show linear trends as we expected for mixing processes in most of major elements, but harker trace elements diagram show kink in patterns. This implies that it's not possible to explain M2 composition only with mixing and this is more evident in spider diagrams, where it is observed that M1p and M2 have similar values of some trace elements, instead others like high earth rare are more enriched in M2. On the other hand, glass chemistry of M2 shows a clear variation through the deposit. Fig. 26 show different levels equidistant from bottom to top, which permit to recognize variation of glass chemistry. It is observed that M1p has a relatively constant and restricted composition, chemistry of M1s has a wider range due to its very microlitic groundmass, and an increase of SiO<sub>2</sub>-K<sub>2</sub>O and decrease of FeO upwards is observed in M2. Hence M2 has not a complete homogenous composition like is observed in M1.

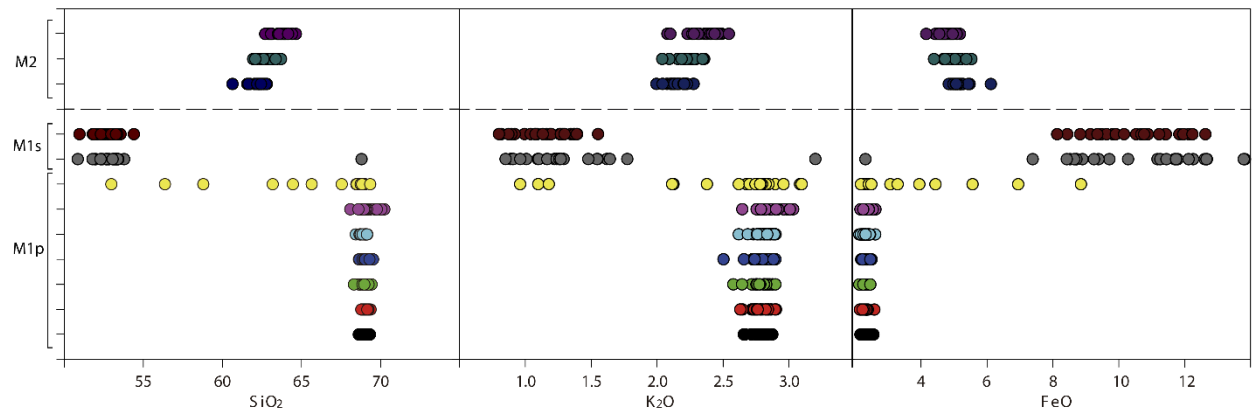


**Figure 26 SiO<sub>2</sub>-K<sub>2</sub>O-FeO wt% variation in glass from M1p, M1s and M2 units.** M1p has a relatively constant range. M1s has a wider range due to its characteristic of been profusely microlitic. Yellow circles represent mingled clasts between M1p and M1s. M2 compositions becomes more evolved to the top.

Considering that previous eruption had bimodal composition and the most obvious processes could be mixing, and the fact that after harker and spider diagrams couldn't be the only process involved, we tried to model direct mixing and a posterior fractionated crystallization. We demonstrated that M2 major element contents could be explained by a mixing between remnant of M1p and M1s of around 70-80% of M1p and 30-20% of M1s (Fig. 27). After that, if we applied the factor of best mixing combination (that is 77% of M1p and 23% of M1s) to trace elements, there is still a difference of ~5 to 25% with real

trace elements composition. For this, we used Rayleight equations of fractionated crystallization,

$$C_L = C_0 F^{(D^{-1})}$$

Where  $C_L$  correspond to final concentration of the trace element on the melt after fractionation,  $C_0$  is the initial concentration of this element,  $D$  is the distribution coefficient of the mineral association (weighing of partition coefficient of each phase by the fractionation ratio of phases),  $F$  is the concentration of residual melt after crystallization. In the model, trace elements that satisfy these conditions were used: high ppm concentrations, low analytical errors and wide coefficient distribution reference data (Table. 10). Trace elements chosen were La, Ce, Nd, Eu, Yb, Ba, Nb, Rb, Sr, Zr. And we considered mineralogy that is observed in M2, ie, Amphiboles, Orthopyroxenes, Magnetites. Additionally, we included a model with Biotite since it is a mineral that was found in M2 in very low proportions.

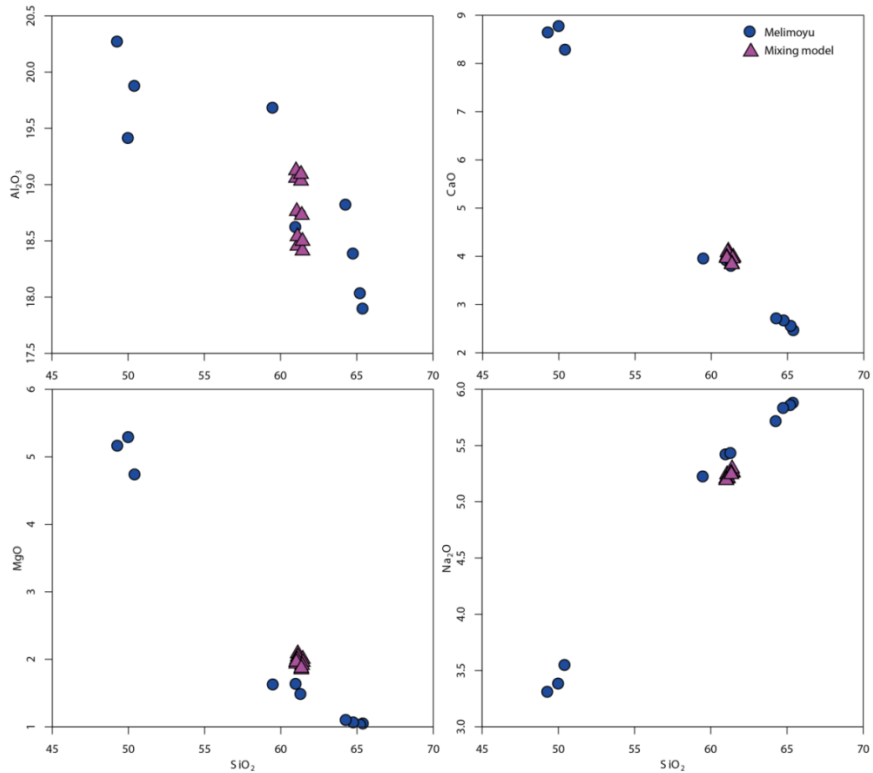


**Figure 27** Mixing models between M1p and M1s composition to obtain M2 chemistry. Blue circles represent whole rock chemistry of M1p, M1s and M2, and magenta triangles represent the best mixing models considering around 77% of M1p dacite and 23% of M1s basalt.

Those elements compositions could be described with models of ~22-27% crystallization (Fig. 28) of plagioclase (50-55%), amphiboles (35-40%) ± orthopyroxenes (2-6%), magnetites (3-8%), biotite (~2%) With this crystallization it is possible to reduce the difference observed between M2 composition and the andesite modeled by mixing of ~5-25% to less than 1-2% (with few elements that have higher errors of maximum 8%).

**Table 10 Distribution coefficients for the phases fractionated in fractional crystallization model. References are: 1) Matsui et al. (1977); 2) Ewart & Griffin (1994); 3) Luhr & Carmichael (1980); 4) Gill (1981); 5) Nash and Crecarft (1985); 6) Schnetzler & Philpotts (1970); 7) Fukimaki et al. (1984); 8) Brenan et al. (1995); 9) Bacon & Druitt (1988); 10) Philpotts & Schnetzler (1970); 11) Irvin and Frey (1978); 12) Green and Pearson (1985); 13) Pearce and Norry (1979); 14) Higuchi & Nagasawa (1969); 15) Dunn & Sen (1994).**

Phase	Amphibole	Plagioclase	Orthopyroxene	Magnetite	Biotite
Rock type	Andesite	Andesite	Andesite	Andesite	Dacite-Rhyolite
La	0.435 0.5	0.21 0.302	0.031 0.26	0.22 0.45	0.272
Reference	1 12	3 7	1 9	3 3	14
Ce	0.22 0.53	0.295	0.028 0.05	0.2 0.12	0.377
Reference	8 9	6	7 4	4 3	1
Nd	0.189 0.62	0.023 0.08 0.16	0.028 0.049	0.25	0.044
Reference	6 8	6 3 3	7 6	3	6
Eu	0.358	0.31 0.36	0.028 0.12	0.42 0.22 0.25	0.328
Reference	6	4 3	7 12	3 3 4	1
Yb	0.462	0.004 0.1	0.09 0.46	0.25 0.47	0.179
Reference	6	15 9	11 4	4 3	6
Ba	0.387	0.56	0.23	0.01 0.4	13.9
Reference	1	2	3	4 3	2
Nb	0.2	1.3	0.78	1	6.367
Reference	8	2	2	14	5
Rb	0.4	0.3	0.029	0.01 0.15	2.24
Reference	9	9	10	4 2	14
Sr	0.2 0.188	1.31	0.024	0.01 0.11	0.363
Reference	12 10	10	10	4 2	1
Zr	1.4	0.2	0.1 0.13	0.2 0.38	0.59
Reference	13	9	4 2	13 2	2

These results not necessarily prove a specific origin, but demonstrate that andesitic magma produced by Melimoyu can be explained by processes of mixing and

fractionation from dacites and basalts as M1p and M1s. Considering that M1 and M2 are separated by ~1200 years and that mixing and crystallization processes could occur in that time scale (Costa and Chakraborty 2004, Hawkesworth et al. 2004).

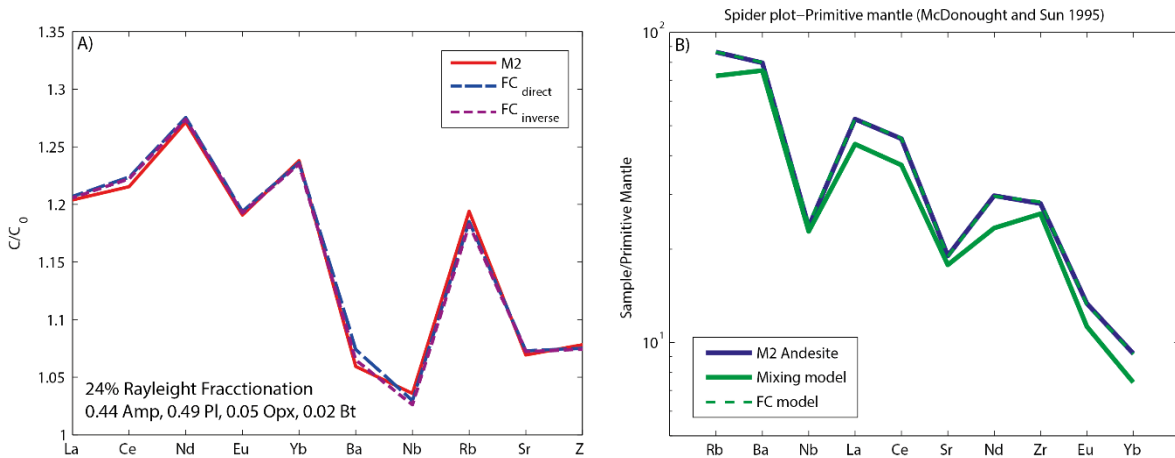


**Figure 28 Results of fractional crystallization models.** A) Diagram showing  $C/C_0$  (M2 modelled/M2 whole rock chemistry) of the best fractional crystallization model. B) Spider diagram showing the results of the trace elements modes of fractional crystallization. Primitive Mantle composition from McDonough and Sun (1995).

With respect to the triggering mechanism of the M2 eruption, there is no evidence of a new pulse of magma as for M1, and then is more difficult to recognize which mechanism was responsible. The analysis of amphiboles (Ridolfi and Renzulli, 2012), H<sub>2</sub>O% on melts around 4.2 to 5.7 was obtained. By the empirical solubility laws (Parfitt and Wilson, 2008), H<sub>2</sub>O that can be dissolved in magma at around 2 kbar is ~5.8 wt% for rhyolites and ~4.5 for basalts. Considering that this eruption has an intermediate composition, the H<sub>2</sub>O conditions showed by amphiboles are near to saturation. Additionally, considering the importance of the gaseous phase in this magma (>70% of vesicles) and the crystallization of biotite that required conditions near to saturation of H<sub>2</sub>O (Scaillet and Evans, 1999), could be suggested that volatile oversaturation could be a trigger for this event, as it was suggested by Castruccio et al. (2016) in Calbuco volcano for the 2015 eruption. As showed by Tait et al. (1989) this process could be achieved by small amounts of crystallization. Regardless, for more conclusive results it will be useful the study of fluid inclusions on future works.

Something that drew attention is the poor crystallinity of this magma comparing to M1p and M1s, M2 is the least crystalline of the three units. One possible explanation for that is an important effect of settling of crystals. We used the equations for velocity of hindered settling:

$$U_{hs} = U_{Stokes} \times f(c)$$

where  $U_{hs}$ , the hindered settling velocity, equals the Stokes settling velocity ( $U_{Stokes}$ ).

$$U_{Stokes} \frac{2r^2 g \Delta \rho}{9\mu}$$

Where  $r$  is radius of the crystal,  $g$  is the acceleration from gravity,  $\Delta \rho$  is the density contrast between crystal and melt, and  $\mu$  is the dynamic viscosity of the melt, and is corrected by the factor  $f(c)$ ,

$$f(c) = \frac{(1 - c)^2}{(1 + c^{1/3})^{[5c/3(1-c)]}}$$

$c$  being the crystal fraction (Barnea and Mizrahi, 1973). For density contrast we calculated a maximum melt density of  $2350 \text{ kg/m}^3$  and we defined density of crystal by using average density of plagioclase  $2680 \text{ kg/m}^3$ . We estimated maximum viscosity by Giordano et al. (2008), and the result was around  $4000 - 2000 \text{ Pa s}$ . The velocity estimated was a minimum of  $\sim 1 - 3 \text{ m/year}$ , which results in more than  $1000 - 3000 \text{ m}$  of settling in  $\sim 1200$  years (the gap between M1 and M2). So, it's a possible option to explain the poor crystallinity of this unit, besides, considering that M2 eruption was of a considerable lower volume, it could indicate that in this case there was a lower part of the chamber with eruptible magma and most crystals could be remaining under this zone. Taking into account this analysis was without considering convection processes that could be important and influence settling velocities.

## 2.5. Conclusions

Holocene activity of Melimoyu volcano has been characterized by low periodicity with respect to other volcanoes of the southern part of the SVZ, dominated by the two large size explosive eruptions (M1 and M2). Its explosive eruptions have different chemical compositions that show evidence of mingling behavior prior to the first eruption and mixing behavior prior to the second eruption. Our results show that these eruptions formed plinian eruptive columns of pumice and scoria juveniles and lava lithics with typical dispersion to E-SE, forming tephra layers up to ~ 60 kms to the E. M1 has a non-DRE volume of ~2.6 km<sup>3</sup> generated by a ~30-35 km height column. M2 has a non-DRE volume of ~1.6 km<sup>3</sup> generated by a ~25-30 km height column. Those volumes are greater than previous estimations, resulting in a IEV=5 i.e. Plinian eruptions.

Unlike some lava samples of Melimoyu that are only andesitic, these two eruptions have a variety of magma compositions. M1p is a trachydacite (64.3-65.4% SiO<sub>2</sub>) with plagioclases, amphiboles, orthopyroxenes and Fe-Ti oxides. M1s is a basalt (49.3-50.4% SiO<sub>2</sub>) with plagioclases, clinopyroxenes and olivines. M2 is a trachyandesite (59.5-61.3% SiO<sub>2</sub>) with plagioclases, amphiboles, clinopyroxenes, olivines, orthopyroxenes, Fe-Ti oxides and biotites. There are differences in textures between M1p and M1s due to variation in size and shape of vesicles that could be associated to a higher microlite content in M1s.

A cartoon showing the processes occurred during both eruptions is depicted in Fig. 29. We proposed that dacites from the first eruption M1p (~2.8 ka BP) were formed in moderately shallow depths (~ 2 kbar, ~ 7 km), where crystals could be formed without important magma injections. Basalts from M1s were formed in deeper conditions and injected during a short period triggering this eruption. It started with the output of dacitic pyroclasts with dispersion E-SE with an increasing intensity. The exit of the dacitic magma would cause an intense vesiculation in the basaltic magma and caused microlite crystallization. At the moment of the highest intensity of the eruption, the basaltic magma started to erupt.

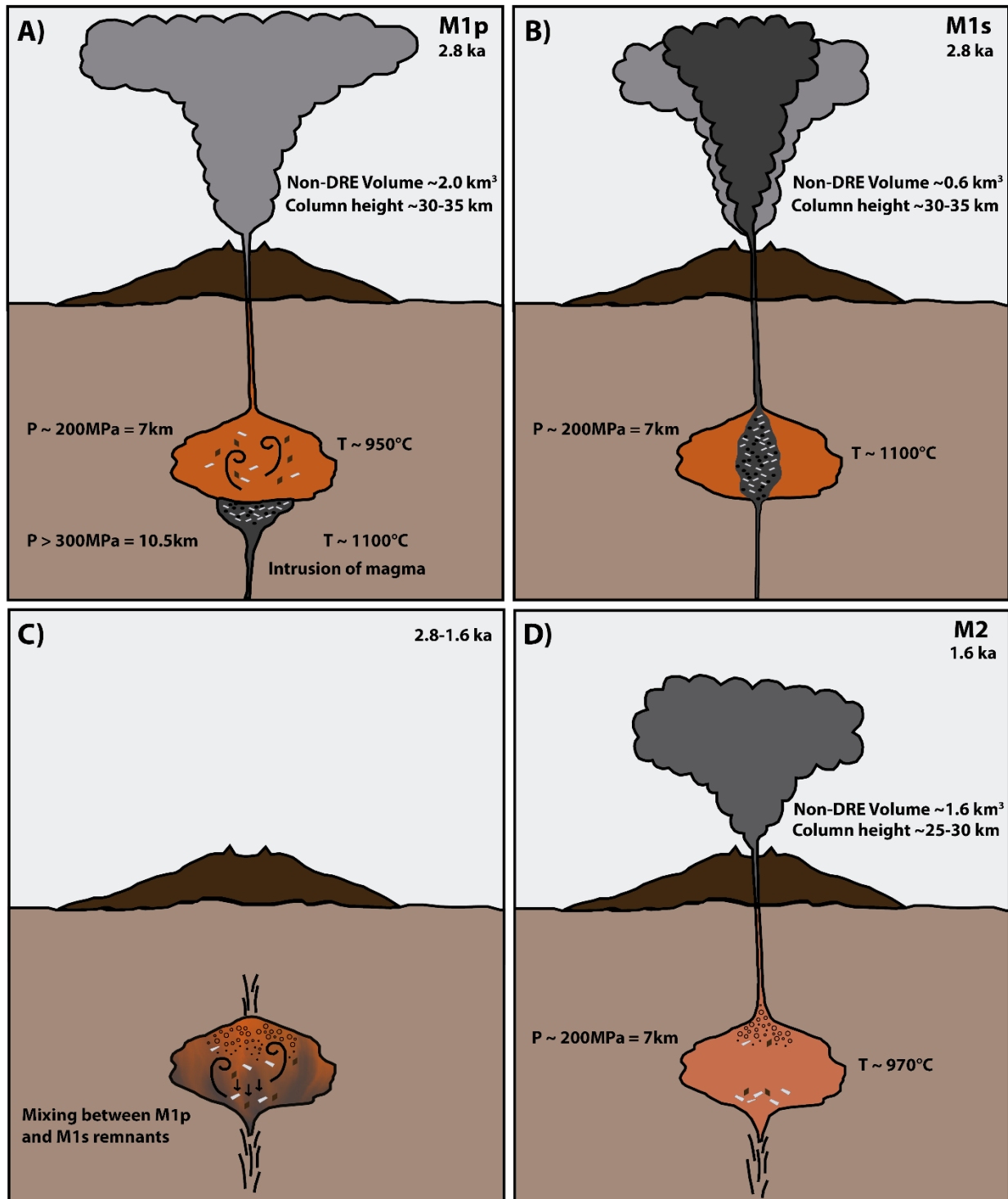


**Figure 29** Holocene eruptions of Melimoyu volcano. A) First phase of M1 eruption that initiates with the intrusion of the basalt M1s triggering the eruption; B) Second phase of M1 eruption with the emission of the basalt M1s; C)  $\sim 1.2$  kyrs of time, during which mixing between M1p and M1s remnants and crystallization generating volatile oversaturation occurred; D) M2 eruption with least amount of pyroclastic material erupted. For M1p and M2 we obtained temperatures and pressure in amphiboles. For M1s we obtained temperatures in olivines-clinopyroxenes and pressures in clinopyroxenes.

We suggest that for nearly 1200 years, remnants of those compositions had time to mix and form the andesitic magma of M2 (~1.6 ka BP). Its andesitic composition could be obtained by a mixing of ~77% of M1p dacite and ~23% of M1s basalt remnants and then a fractionated crystallization process of ~ 22-27%. M2 has a lower crystallinity and a smaller erupted volume, and it could be indicating crystals settling and a reduction of eruptible magma volume fraction inside the chamber. As there is no clear evidence of mafic injections we suggest that the triggering mechanism could be crystallization and volatile saturation (second-boiling).

Melimoyu eruptive record could be expanded if we consider our analysis of tephra layers observed by Stern et al. (2015) in which we determined that layers of ~4.6-4.8, ~8.3 and >19.7 ka could be associated to Melimoyu in addition to new pyroclastics deposits found in the western side of the volcano and described in this work. Western side deposits allowed us to increase the area covered by the eruption M2 and recognize that the eruption was greater than it was believed.

We expect the new data and analysis obtained on this work will be a contribution to improve the knowledge about volcanic processes of the southern SVZ where volcanoes without historic eruptions are poorly studied. Melimoyu volcano is currently monitored by the Observatorio Volcanológico de los Andes del Sur (OVDAS) with seismic stations and if we consider the last 3000 years, it would be one of the volcanoes with most erupted material in the southern SVZ. Considering these facts, together with the glacial cover of the edifice and population around their flanks, it is important to continue studies of petrologic and volcanic processes of this volcano.

### 3. BIBLIOGRAFÍA

- Alloway, B.V., Pearce, N.J.G., Moreno, P.I., Villarosa, G., Jara I., Ricardo De Pol-Holz, R. & Outes, V. (2017a) An 18,000 year-long eruptive record from Volcán Chaitén, northwestern Patagonia: paleoenvironmental and hazard-assessment implications. *Quaternary Science Reviews* 168, 151-181.
- Alloway, B.V., Moreno, P.I., Pearce, N., De Pol-Holz, Henríquez, W., Pesce, O., Sagredo E, Villarosa, G. & Outes, V. (2017b) Stratigraphy, age and correlation of Lepué tephra: a widespread c. 11,000 cal. a BP marker horizon sourced from the Chaitén Sector of southern Chile. *Journal of Quaternary Science* 32, 795–829.
- Alfano, F., Bonadonna, C., Volentik, A.C.M., Connor, C.B., Watt, S.F.L., Pyle, D.M. & Connor, L.J. (2011). Tephra stratigraphy and eruptive volume of the May, 2008, Chaitén eruption, Chile. *Bulletin of Volcanology* 73, 613–630.
- Amigo, Á., Lara, L.E. & Smith, V.C. (2013). Holocene record of large explosive eruptions from Chaitén and Michinmahuida Volcanoes, Chile. *Andean Geology*, 40(2), 227–248.
- Bacon, C. R. & Druitt, T. H. (1988). Compositional evolution of the zoned calc-alkaline magma chamber of Mount Mazama, Crater Lake, Oregon. *Contributions to Mineralogy and Petrology*, 98(2), 224-256.
- Barnea, E. & Mizrahi, J. (1973). A generalized approach to the fluid dynamics of particulate systems. Part I. General correlation for fluidization and sedimentation in solid multiparticulate systems. *Chemical Engineering Journal* 5, 171–189.
- Biass, S., Bagheri, G. & Bonadonna, C. (2015). A Matlab implementation of the Carey and Sparks (1986) model to estimate plume height and wind speed from isopleth maps. Department of Earth Sciences, University of Geneva, Switzerland.
- Blundy, J. & Cashman, K. (2008). Petrologic Reconstruction of Magmatic System Variables and Processes. *Reviews in Mineralogy and Geochemistry* 69, 179–239.
- Bonadonna, C. & Costa, A. (2012). Estimating the volume of tephra deposits: A new simple strategy. *Geology* 40, 415–418.
- Bonadonna, C., Cioni, R., Pistolesi, M., Connor, C., Scollo, S., Pioli, L. & Rosi, M. (2013). Determination of the largest clast sizes of tephra deposits for the characterization of explosive eruptions: a study of the IAVCEI commission on tephra hazard modelling. *Bulletin of Volcanology*, 75(1), 680.
- Brenan, J. M., Shaw, H. F., Ryerson, F. J. & Phinney, D. L. (1995). Mineral-aqueous fluid partitioning of trace elements at 900 C and 2.0 GPa: Constraints on the trace

element chemistry of mantle and deep crustal fluids. *Geochimica et Cosmochimica Acta*, 59(16), 3331-3350.

Carey, S. & Sparks, R. S. J. (1986). Quantitative models of the fallout and dispersal of tephra from volcanic eruption columns. *Bulletin of Volcanology*, 48(2), 109-125.

Cashman, K. V. & Sparks, R.S.J. (2013). How volcanoes work: A 25 year perspective. *Geological Society of America Bulletin* 125, 664–690.

Castruccio, A., Clavero, J., Segura, A., Samaniego, P., Roche, O., Le Pennec, J. L. & Drogueut, B. (2016). Eruptive parameters and dynamics of the April 2015 sub-Plinian eruptions of Calbuco volcano (southern Chile). *Bulletin of Volcanology* 78(9), 62.

Cembrano, J., Hervé, F. & Lavenu, A., 1996. The Liquiñe–Ofqui fault zone: long-lived intra-arc fault system in Southern Chile. *Tectonophysics* 259, 55–66.

Cembrano, J., Schermer, E., Lavenu, A. & Sanhueza, A. (2000). Contrasting nature of deformation along an intra-arc shear zone, the Liquiñe–Ofqui fault zone, southern Chilean Andes. *Tectonophysics* 319(2), 129-149.

Cembrano, J., Lavenu, A., Reynolds, P., Arancibia, G., López, G. & Sanhueza, A. (2002). Late Cenozoic transpressional ductile deformation north of the Nazca–South America–Antarctica triple junction. *Tectonophysics* 354(3), 289-314.

Clark, P.U., Dyke, A.S., Shakun, J.D., Carlson, A.E., Clark, J., Wohlfarth, B., Mitrovica, J.X., Hostetler, S.W. & McCabe, A.M. (2009). The last glacial maximum. *Science* 325, 710–714.

Costa, F. & Chakraborty, S. (2004). Decadal time gaps between mafic intrusion and silicic eruption obtained from chemical zoning patterns in olivine. *Earth and Planetary Science Letters* 227(3), 517-530.

de Silva, S. (2001). Magmas in collision: Rethinking chemical zonation in silicic magmas: Comment and Reply COMMENT. *Geology*, 29(11), 1063-1063.

Denton, G.H., Anderson, R.F., Toggweiler, J.R., Edwards, R.L., Schaefer, J.M. & Putnam, A.E. (2010). The last glacial termination. *Science* 328, 1652–1656.

Douglass, D. C., Singer, B. S., Kaplan, M. R., Ackert, R. P., Mickelson, D. M. & Caffee, M. W. (2005). Evidence of early Holocene glacial advances in southern South America from cosmogenic surface-exposure dating. *Geology* 33(3), 237-240.

Dunn, T., & Sen, C. (1994). Mineral/matrix partition coefficients for orthopyroxene, plagioclase, and olivine in basaltic to andesitic systems: a combined analytical and experimental study. *Geochimica et Cosmochimica Acta* 58(2), 717-733.

- Eichelberger, J.C., Chertkoff, D.G., Dreher, S.T., & Nye, C.J. (2000) Magmas in collision: Rethinking chemical zonation in silicic magmas. *Geology* 28, 603–606.
- Eichelberger, J. C., Chertkoff, D. G., Dreher, S. T., & Nye, C. J. (2001). Reply. *Geology* 29(11), 1063-1064.
- Ewart, A. & Griffin, W. L. (1994). Application of proton-microprobe data to trace-element partitioning in volcanic rocks. *Chemical Geology* 117(1), 251-284.
- Fierstein, J. & Nathenson, M. (1992). Another look at the calculation of fallout tephra volumes. *Bulletin of Volcanology* 54, 156–167.
- Fontijn, K., Lachowycz, S. M., Rawson H., Pyle D. M., Mather T. A., Naranjo J. A. & Moreno-Roa H. (2014). Late Quaternary tephrostratigraphy of southern Chile and Argentina. *Quaternary Science Reviews* 89, 70-84.
- Fujimaki, H., Tatsumoto, M. & Aoki, K. I. (1984). Partition coefficients of Hf, Zr, and REE between phenocrysts and groundmasses. *Lunar and Planetary Science Conference Proceedings* 14, B662-B672.
- Gill, J.B. (1981). Orogenic andesites and plate tectonics: New York, Springer-Verlag, 390 p.
- Giordano, D., Russell, J. K. & Dingwell, D. B. (2008). Viscosity of magmatic liquids: a model. *Earth and Planetary Science Letters*, 271(1), 123-134. Lange, R. L., & Carmichael, I. S. (1990). Thermodynamic properties of silicate liquids with emphasis on density, thermal expansion and compressibility. *Reviews in Mineralogy and Geochemistry* 24(1), 25-64.
- González-Ferrán, O. (1995). *Volcanes de Chile*. Instituto Geográfico Militar.
- Green, T.H. & Pearson, N.J. (1985). Experimental determination of REE partition coefficients between amphibole and basaltic to andesitic liquids at high pressure. *Geochimica et Cosmochimica Acta* 49(6), 1465-1468.
- Gutiérrez, F., Gioncada, A., González Ferran, O., Lahsen, A. & Mazzuoli, R. (2005). The Hudson Volcano and surrounding monogenetic centres (Chilean Patagonia): An example of volcanism associated with ridge-Trench collision environment. *Journal of Volcanology and Geothermal Research* 145, 207–233.
- Hawkesworth, C., George, R., Turner, S., & Zellmer, G. (2004). Time scales of magmatic processes. *Earth and Planetary Science Letters* 218(1), 1-16.
- Herman, F. & Brandon, M. (2015). Mid-latitude glacial erosion hotspot related to equatorial shifts in southern Westerlies. *Geology* 43(11), 987-990.

- Hervé, M. (1976). Estudio geológico de la falla Liquiñe-Reloncaví en el área de Liquiñe: Antecedentes de un movimiento transcurrente (Provincia de Valdivia). In *Congreso Geológico Chileno* (Vol. 1).
- Hervé, F., Pankhurst, R. J., Drake, R., Beck, M. E. & Mpodozis, C. (1993). Granite generation and rapid unroofing related to strike-slip faulting, Aysén, Chile. *Earth and Planetary Science Letters* 120(3-4), 375-386.
- Heusser, C.J., Heusser, L.E. & Hauser, A. (1992). Paleoecology of Late Quaternary Deposits in Chiloé Continental, Chile. *Revista Chilena de Historia Natural* 65, 235–245.
- Hildreth, W., & Drake, R.E. (1992). Volcán Quizapu, Chilean Andes. *Bulletin of Volcanology* 54(2), 93-125.
- Higuchi, H. & Nagasawa, H. (1969). Partition of trace elements between rock-forming minerals and the host volcanic rocks. *Earth and Planetary Science Letters*, 7(3), 281-287.
- Hogg, A.G., Hua, Q., Blackwell, P.G., Niu, M., Buck, C.E., Guilderson, T.P., Heaton, T.J., Palmer, J.G., Reimer, P.J., Reimer, R.W., Turney, C.S.M. & Zimmerman, S.R.H. (2013). SHCAL13 Southern Hemisphere calibration, 0-50,000 years cal BP. *Radiocarbon* 55, 2-15.
- Holland, T. & Blundy, J. (1994). Non-ideal interactions in calcic amphiboles and their bearing on amphibole-plagioclase thermometry. *Contribution to Mineralogy Petrology* 116, 433–447.
- Horwell, C.J. (2007). Grain-size analysis of volcanic ash for the rapid assessment of respiratory health hazard. *Journal of Environmental Monitoring* 9, 1107-1115.
- Irvine, T.N.J. & Baragar, W.R.A.F. (1971). A guide to the chemical classification of the common volcanic rocks. *Canadian Journal of Earth Sciences* 8(5), 523-548.
- Irving, A.J. & Frey, F.A. (1978). Distribution of trace elements between garnet megacrysts and host volcanic liquids of kimberlitic to rhyolitic composition. *Geochimica et Cosmochimica Acta* 42(6), 771-787.
- Kilian, R. & Lamy, F. (2012). A review of Glacial and Holocene paleoclimate records from southernmost Patagonia (49–55 S). *Quaternary Science Reviews* 53, 1-23.
- Kratzmann, D.J., Carey, S., Scasso, R. & Naranjo, J.A. (2009). Compositional variations and magma mixing in the 1991 eruptions of Hudson volcano, Chile. *Bulletin of Volcanology* 71, 419–439.
- Lange, R. A., Frey, H.M. & Hector, J. (2009). A thermodynamic model for the plagioclase-liquid hygrometer/thermometer. *American Mineralogist* 94, 494–506.

Le Bas, M.J., Le Maitre, R.W., Streckeisen, A., Zanettin, B. (1986). A chemical classification of volcanic-rocks based on the Total Alkali Silica diagram. *Journal of Petrology* 3, 745-750.

Leake, B. E., Woolley, A. R., Arps, C. E., Birch, W. D., Gilbert, M. C., Grice, J. D., Hawthorne, F.C., Kato, A., Kisch, H.J., Krivovichev, V.G., Linthout, K., Laird, J., Mandarino, J., Maresch, W.V., Nickel, E.H., Rock, N.M.S., Schumacher, J.C., Smith, D.C., Stephenson, N.C.N., Ungaretti, L., Whittaker, E.J.W. & Youzhi, G. (1997). Report. Nomenclature of Amphiboles: Report of the Subcommittee on Amphiboles of the International Mineralogical Association Commission on New Minerals and Mineral Names. *Mineralogical Magazine* 61(2), 295-321.

Lee, C.T.A. & Bachmann, O. (2014). How important is the role of crystal fractionation in making intermediate magmas? Insights from Zr and P systematics. *Earth and Planetary Science Letters* 393, 266-274.

Lopez-Escobar, L., Kilian, R., Kempton, P. & Tagiri, M. (1993) Petrography and geochemistry of Quaternary rocks from the Southern Volcanic Zone of the Andes between 41°30' and 46°00'S, Chile. *Revista Geológica de Chile* 20 (1), 33-55.

Lopez-Escobar, L., Cembrano, J. & Moreno, H. (1995) Geochemistry and tectonics of the Chilean Southern Andes basaltic Quaternary volcanism (37-46°S). *Revista Geológica de Chile* 22(2), 219-234.

Loucks, R.R. (1996). A precise olivine-augite Mg-Fe-exchange geothermometer. *Contributions to Mineralogy and Petrology* 125, 140–150.

Lowe, D.J. & Alloway, B.V. (2004) Tephrochronology. In: Rink, W.J., Thompson, J. (Eds.), *Encyclopedia of Scientific Dating Methods*. Springer, Netherlands, 1-26.

Luhr, J.F. & Carmichael, I.S. (1980). The Colima volcanic complex, Mexico. *Contributions to Mineralogy and Petrology* 71(4), 343-372.

Matsui, Y. (1977). Crystal structure control in trace element partition between crystal and magma. *Bulletin de la Société Française de Minéralogie et de Cristallographie* 100, 315-324.

McDonough, W.F. & Sun, S.S. (1995). The composition of the Earth. *Chemical geology* 120(3-4), 223-253.

Mella, M., Ramos, A., Kraus, S. & Duhart, P. (2004). Tefroestratigrafía, magnitud y geoquímica de erupciones holocenas mayores del volcán Mentolat, Andes del Sur (44°40'S), Chile. *Congreso Geológico Chileno* 580–582.

Moreno, P.I., Alloway, B.V., Henríquez, W.I., Villarosa, G., Outes, V., De Pol-Holz, R. & Pearce, N.J.G. (2015). A past millennium maximum in postglacial activity from Volcán Chaitén, southern Chile. *Geology* 43, 47-50.

- Nakamura, N. (1974). Determination of REE, Ba, Fe, Mg, Na and K in carbonaceous and ordinary chondrites. *Geochimica et Cosmochimica Acta* 38(5), 757-775.
- Naranjo, J.A. & Stern, C.R. (1998). Holocene explosive activity of Hudson Volcano, southern Andes. *Bulletin of Volcanology* 59, 291–306.
- Naranjo, J.A. & Stern, C.R. (2004). Holocene tephrochronology of the southernmost part ( $42^{\circ}30' - 45^{\circ}\text{S}$ ) of the Andean Southern Volcanic Zone. *Revista Geológica de Chile* 31, 225–240.
- Nash, W.P. & Crecraft, H.R. (1985). Partition coefficients for trace elements in silicic magmas. *Geochimica et Cosmochimica Acta*, 49(11), 2309-2322.
- Newhall, C.G. & Self, S. (1982). The volcanic explosivity index (VEI) an estimate of explosive magnitude for historical volcanism. *Journal of Geophysical Research: Oceans* 87(C2), 1231-1238.
- Nyland, R. E., Panter, K. S., Rocchi, S., Di Vincenzo, G., Del Carlo, P., Tiepolo, M., Field, B. & Gorrevski, P. (2013). Volcanic activity and its link to glaciation cycles: Single-grain age and geochemistry of Early to Middle Miocene volcanic glass from ANDRILL AND-2A core, Antarctica. *Journal of Volcanology and Geothermal Research* 250, 106-128.
- Pallister, J.S., Diefenbach, A. K., Burton, W.C., Munoz, J., Griswold, J.P., Lara, L., Lowenstein, J.B. & Valenzuela, C.E. (2013). The Chaitén rhyolite lava dome: Eruption sequence, lava dome volumes, rapid effusion rates and source of the rhyolite magma. *Andean Geology* 40, 277–294.
- Pankhurst, R.J., Weaver, S.D., Hervé, F. & Larrondo, P. (1999). Mesozoic – Cenozoic Evolution of the North Patagonian Batholith in Aysén, Southern Chile. *Journal of the Geological Society* 156 (4), 673–694.
- Parfitt, E.A. & Wilson, L. (2008). The role of volatiles. *Fundamentals of Physical Volcanology*, 64-76.
- Pearce, J.A. & Norry, M.J. (1979). Petrogenetic implications of Ti, Zr, Y, and Nb variations in volcanic rocks. *Contributions to Mineralogy and Petrology* 69(1), 33-47.
- Peccerillo, A. & Taylor, S.R. (1976). Geochemistry of Eocene calc-alkaline volcanic rocks from Kastamonu area, Northern Turkey. *Contributions to Mineralogy and Petrology* 58, 39-63.
- Philpotts, J. A. & Schnetzler, C.C. (1970). Phenocryst-matrix partition coefficients for K, Rb, Sr and Ba, with applications to anorthosite and basalt genesis. *Geochimica et Cosmochimica Acta* 34(3), 307-322.

- Putirka, K. D., Mikaelian, H., Ryerson, F. & Shaw, H. (2003). New clinopyroxene-liquid thermobarometers for mafic, evolved, and volatile-bearing lava compositions, with applications to lavas from Tibet and the Snake River Plain, Idaho. *American Mineralogist* 88(10), 1542-1554.
- Putirka, K.D. (2008). Thermometers and Barometers for Volcanic Systems. *Reviews in Mineralogy and Geochemistry* 69, 61–120.
- Pyle, D.M. (1989). The thickness, volume and grainsize of tephra fall deposits. *Bulletin of Volcanology* 51(1), 1-15.
- Pyle, D.M. (1995). Assessment of the minimum volume of tephra fall deposits. *Journal of Volcanology and Geothermal Research* 69(3-4), 379-382.
- Ramsey, C.B. (2009). Bayesian Analysis of Radiocarbon Dates. *Radiocarbon* 51(1), 337–360.
- Ridolfi, F. & Renzulli, A. (2012). Calcic amphiboles in calc-alkaline and alkaline magmas: thermobarometric and chemometric empirical equations valid up to 1,130° C and 2.2 GPa. *Contributions to Mineralogy and Petrology* 163(5), 877-895.
- Rojas, M., Moreno, P., Kageyama, M., Crucifix, M., Hewitt, C., Abe-Ouchi, A. & Hope, P. (2009). The Southern Westerlies during the last glacial maximum in PMIP2 simulations. *Climate Dynamics* 32(4), 525-548.
- Rojas, M. & Moreno, P.I. (2011). Atmospheric circulation changes and neoglacial conditions in the Southern Hemisphere mid-latitudes: insights from PMIP2 simulations at 6 kyr. *Climate Dynamics* 37(1-2), 357-375.
- Ruprecht, P., Bergantz, G. W., Cooper, K. M. & Hildreth, W. (2012). The crustal magma storage system of Volcán Quizapu, Chile, and the effects of magma mixing on magma diversity. *Journal of Petrology* 53(4), 801-840.
- Scaillet, B. & Evans, B.W. (1999). The 15 June 1991 eruption of Mount Pinatubo. I. Phase equilibria and pre-eruption P-T-f O<sub>2</sub>-f H<sub>2</sub>O conditions of the dacite magma. *Journal of Petrology*, 40(3), 381-411.
- Scandone R. & Giacomelli L. (2001) The slow boiling of magma chambers and the dynamics of explosive eruptions. *Journal of Volcanology and Geothermal Research* 110, 121–136.
- Schnetzler, C.C. & Philpotts, J.A. (1970). Partition coefficients of rare-earth elements between igneous matrix material and rock-forming mineral phenocrysts—II. *Geochimica et Cosmochimica Acta* 34(3), 331-340.

- Sellés, D., Rodríguez, A., Dungan, M.A., Naranjo, J.A., & Gardeweg, M. (2004). Geochemistry of Nevado de Longaví Volcano (36.2 S): a compositionally atypical arc volcano in the Southern Volcanic Zone of the Andes. *Revista geológica de Chile* 31(2), 293-315.
- Singer, B.S., Thompson, R.A., Dungan, M.A., Feeley, T.C., Nelson, S.T., Pickens, J.C., Brown, L.L., Wulff, A.W., Davidson, J.P., Metzger, J. (1997). Volcanism and erosion during the past 930 ky at the Tatara–San Pedro complex, Chilean Andes. *Geological Society of America Bulletin* 109, 127–142.
- Singer, B.S., Jicha, B.R., Harper, M.A., Naranjo, J.A., Lara, L.E., Moreno-Roa, H., (2008). Eruptive history, geochronology, and magmatic evolution of the Puyehue–Cordón Caulle volcanic complex, Chile. *Bulletin of the Geological Society of America* 120, 599–618.
- Smith, R.L. (1979). Ash-flow magmatism. *Geological Society of America Special Papers* 180, 5-28.
- Sparks, R.S.J., Bursik, M.I., Carey, S.N., Gilbert, J., Glaze, L.S., Sigurdsson, H. & Woods, A.W. (1997). *Volcanic plumes*. Wiley.
- Sun, S.S. & McDonough, W.S. (1989). Chemical and isotopic systematics of oceanic basalts: implications for mantle composition and processes. *Geological Society, London, Special Publications* 42(1), 313-345.
- Stern, C.R., Moreno, H., Lopez-Escobar, L., Clavero, J.E., Lara, L.E., Naranjo, J.A., Parada, M.A. & Skewes, M.A. (2007), Chilean volcanoes, in edited by T. Moreno and W. Gibbons, *The Geology of Chile.*, pp. 147–178, Geological Society of London, London, U. K.
- Stern, C., De Porras, M.E. & Maldonado, A. (2015). Tephrochronology of the upper Río Cisnes valley (44°S), southern Chile. *Andean Geology* 42, 173–189.
- Tait, S., Jaupart, C. & Vergniolle, S. (1989). Pressure, gas content and eruption periodicity of a shallow, crystallising magma chamber. *Earth and Planetary Science Letters* 92(1), 107-123.
- Taylor, S.R. & McLennan, S.M. (1985). *The Continental Crust: Its Composition and Evolution*. Blackwell, Oxford.
- Watt, S.F.L. (2010). Records of volcanism and controls on volcanic processes in southern Chile. D.Phil thesis Department of Earth Sciences, University of Oxford, U.K. (367 pp. (<http://ora.ouls.ox.ac.uk/>)).

- Watt, S.F.L., Pyle, D.M., Naranjo, J. a., Rosqvist, G., Mella, M., Mather, T. A. & Moreno, H. (2011). Holocene tephrochronology of the Hualaihue region (Andean southern volcanic zone, ~42°S), southern Chile. *Quaternary International* 246, 324–343.
- Watt, S.F.L., Pyle, D.M. & Mather, T.A. (2013a). The volcanic response to deglaciation: Evidence from glaciated arcs and a reassessment of global eruption records. *Earth-Science Reviews* 122, 77–102.
- Watt, S.F., Pyle, D.M., & Mather, T.A. (2013b). Evidence of mid-to late-Holocene explosive rhyolitic eruptions from Chaitén Volcano, Chile. *Andean Geology*, 40(2). 216-226.
- Weller, D., Miranda, C.G., Moreno, P.I., Villa-Martínez, R. & Stern, C.R. (2014). The large late-glacial Ho eruption of the Hudson volcano, southern Chile. *Bulletin of Volcanology* 76(6), 831.
- Weller, D.J., Miranda, C.G., Moreno, P.I., Villa-Martínez, R. & Stern, C.R. (2015). Tephrochronology of the southernmost Andean southern volcanic zone, Chile. *Bulletin of Volcanology* 77(12), 107.
- Wolff, J. A., Wörner, G., & Blake, S. (1990). Gradients in physical parameters in zoned felsic magma bodies: implications for evolution and eruptive withdrawal. *Journal of Volcanology and Geothermal Research* 43(1-4), 37-55.



MM-2-02	69.12	0.44	17.63	2.33	0.51	0.14	1.47	5.22	2.87	0.28
MM-2-03	69.07	0.41	17.74	2.17	0.55	0.15	1.40	5.43	2.74	0.35
MM-2-04	69.09	0.44	17.74	2.04	0.50	0.12	1.44	5.55	2.80	0.27
MM-2-05	69.26	0.44	17.58	2.33	0.45	0.15	1.50	5.32	2.75	0.23
MM-2-06	69.07	0.41	17.75	2.33	0.53	0.15	1.53	5.25	2.72	0.26
MM-2-08	69.01	0.41	17.68	2.33	0.52	0.15	1.47	5.31	2.86	0.26
MM-2-09	68.78	0.44	17.64	2.58	0.52	0.18	1.46	5.31	2.82	0.26
MM-2-10	69.25	0.43	17.58	2.33	0.53	0.13	1.49	5.22	2.78	0.27
MM-2-11	69.37	0.44	17.59	2.18	0.51	0.14	1.42	5.38	2.73	0.24
MM-2-12	68.97	0.46	17.67	2.26	0.52	0.15	1.48	5.37	2.84	0.27
MM-2-13	69.04	0.45	17.75	2.33	0.54	0.13	1.46	5.30	2.74	0.27
MM-2-14	69.08	0.40	17.67	2.33	0.54	0.18	1.46	5.25	2.84	0.24
MM-2-15	68.92	0.42	17.84	2.33	0.52	0.13	1.47	5.45	2.65	0.27
MM-2-16	69.00	0.43	17.59	2.36	0.51	0.13	1.44	5.45	2.79	0.28
MM-2-17	69.08	0.46	17.57	2.30	0.52	0.14	1.47	5.41	2.79	0.26
MM-2-18	68.97	0.46	17.58	2.21	0.50	0.14	1.50	5.48	2.89	0.27
MM-2-19	68.90	0.41	17.71	2.38	0.54	0.09	1.47	5.62	2.63	0.25
MM-2-20	69.23	0.42	17.59	2.36	0.53	0.12	1.50	5.17	2.84	0.24
MM-2-21	68.81	0.43	17.77	2.36	0.56	0.13	1.46	5.46	2.75	0.26
MM-2-22	68.81	0.43	17.47	2.33	0.53	0.14	1.64	5.58	2.82	0.25
MM-2-23	68.78	0.45	17.51	2.27	0.52	0.14	1.47	5.89	2.74	0.23
MM-2-24	69.22	0.44	17.77	2.14	0.53	0.13	1.56	5.17	2.76	0.28
MM-2-25	69.16	0.42	17.72	2.22	0.54	0.12	1.42	5.36	2.76	0.27
MM-3-01	69.09	0.44	17.77	2.37	0.56	0.15	1.48	5.08	2.82	0.25
MM-3-02	69.07	0.42	17.84	2.19	0.50	0.17	1.40	5.40	2.73	0.26
MM-3-03	69.06	0.43	17.63	2.30	0.52	0.17	1.51	5.28	2.86	0.25
MM-3-04	69.16	0.43	17.62	2.24	0.55	0.18	1.50	5.31	2.75	0.26
MM-3-05	69.03	0.45	17.71	2.35	0.52	0.18	1.44	5.30	2.75	0.27

MM-3-06	68.63	0.46	17.92	2.39	0.54	0.13	1.42	5.32	2.75	0.45
MM-3-07	69.36	0.44	17.81	2.34	0.50	0.12	1.47	5.00	2.72	0.24
MM-3-08	69.08	0.44	17.67	2.31	0.50	0.14	1.48	5.28	2.85	0.25
MM-3-10	69.19	0.42	17.68	2.31	0.49	0.15	1.43	5.24	2.84	0.25
MM-3-11	69.43	0.38	17.73	2.22	0.50	0.12	1.23	5.25	2.87	0.26
MM-3-12	68.66	0.43	17.61	2.43	0.54	0.12	1.40	5.73	2.83	0.26
MM-3-13	69.12	0.44	17.72	2.13	0.52	0.18	1.47	5.41	2.75	0.26
MM-3-14	68.69	0.44	17.79	2.38	0.54	0.17	1.47	5.48	2.82	0.24
MM-3-15	69.12	0.43	17.61	2.21	0.52	0.15	1.52	5.32	2.88	0.23
MM-3-16	68.89	0.44	17.57	2.34	0.56	0.15	1.52	5.37	2.90	0.27
MM-3-17	68.68	0.48	17.70	2.39	0.54	0.16	1.51	5.45	2.81	0.27
MM-3-18	68.74	0.48	17.70	2.31	0.54	0.13	1.49	5.51	2.83	0.27
MM-3-19	69.08	0.43	17.69	2.29	0.51	0.15	1.44	5.58	2.58	0.25
MM-3-20	69.24	0.44	17.68	2.12	0.54	0.17	1.48	5.26	2.81	0.26
MM-3-21	68.67	0.43	18.04	2.31	0.56	0.15	1.52	5.08	2.76	0.49
MM-3-22	68.31	0.43	18.10	2.39	0.53	0.18	1.50	5.45	2.64	0.46
MM-3-23	69.24	0.42	17.76	2.11	0.53	0.14	1.45	5.29	2.81	0.25
MM-3-24	68.85	0.45	17.60	2.25	0.51	0.15	1.48	5.68	2.78	0.25
MM-3-25	68.97	0.40	17.78	2.46	0.54	0.13	1.47	5.21	2.77	0.25
MM-4-02	69.33	0.42	17.42	2.18	0.47	0.12	1.44	5.48	2.90	0.25
MM-4-03	69.06	0.44	17.73	2.33	0.51	0.13	1.48	5.31	2.76	0.25
MM-4-04	69.04	0.46	17.60	2.25	0.51	0.15	1.44	5.52	2.72	0.30
MM-4-06	69.28	0.42	17.63	2.26	0.49	0.17	1.37	5.42	2.73	0.24
MM-4-07	68.92	0.43	17.61	2.23	0.54	0.16	1.56	5.46	2.81	0.27
MM-4-08	69.08	0.44	17.58	2.36	0.51	0.13	1.45	5.43	2.77	0.24
MM-4-09	68.93	0.45	17.67	2.31	0.55	0.16	1.50	5.44	2.75	0.25
MM-4-10	69.13	0.41	17.76	2.24	0.52	0.15	1.40	5.39	2.74	0.25
MM-4-11	68.84	0.43	17.87	2.36	0.51	0.11	1.43	5.48	2.66	0.31



MM-5-16	68.67	0.43	17.72	2.32	0.52	0.12	1.43	5.64	2.89	0.27
MM-5-17	69.02	0.42	17.72	2.31	0.52	0.15	1.48	5.28	2.85	0.25
MM-5-18	68.92	0.43	17.72	2.26	0.55	0.14	1.51	5.39	2.83	0.25
MM-5-19	68.80	0.42	17.71	2.37	0.49	0.16	1.38	5.72	2.69	0.26
MM-5-21	69.10	0.42	17.79	2.17	0.51	0.18	1.46	5.38	2.76	0.25
MM-5-22	68.67	0.43	17.63	2.45	0.55	0.15	1.44	5.64	2.79	0.26
MM-5-23	68.74	0.43	17.71	2.44	0.53	0.17	1.51	5.29	2.89	0.28
MM-5-24	68.86	0.43	17.74	2.25	0.53	0.15	1.49	5.53	2.76	0.27
MM-5-25	69.13	0.43	17.74	2.31	0.49	0.11	1.47	5.23	2.83	0.25
MM-6-01	69.14	0.44	17.38	2.35	0.54	0.12	1.43	5.48	2.82	0.29
MM-6-02	68.94	0.45	17.31	2.41	0.54	0.14	1.42	5.73	2.78	0.29
MM-6-03	69.95	0.41	17.00	2.28	0.44	0.10	1.24	5.32	2.96	0.31
MM-6-04	68.63	0.44	17.95	2.28	0.49	0.13	1.47	5.54	2.76	0.32
MM-6-05	68.99	0.42	17.43	2.48	0.47	0.13	1.45	5.35	3.01	0.29
MM-6-06	70.24	0.39	16.90	2.22	0.44	0.12	1.29	5.45	2.65	0.31
MM-6-07	70.05	0.42	16.94	2.62	0.39	0.21	1.13	4.98	2.98	0.28
MM-6-08	69.62	0.44	17.24	2.24	0.42	0.13	1.41	5.27	2.96	0.27
MM-6-09	68.84	0.46	17.56	2.53	0.46	0.12	1.43	5.43	2.90	0.29
MM-6-10	68.73	0.45	17.79	2.36	0.49	0.16	1.43	5.39	2.82	0.38
MM-6-11	68.92	0.43	17.83	2.21	0.52	0.14	1.56	5.35	2.77	0.26
MM-6-12	69.37	0.41	17.49	2.23	0.43	0.15	1.29	5.28	3.03	0.33
MM-6-14	69.19	0.42	17.85	2.23	0.50	0.12	1.42	5.12	2.85	0.30
MM-6-15	69.13	0.41	17.56	2.25	0.48	0.18	1.45	5.39	2.92	0.24
MM-6-16	69.76	0.41	17.14	2.19	0.43	0.13	1.34	5.27	3.01	0.33
MM-6-17	68.75	0.46	17.70	2.34	0.49	0.15	1.46	5.58	2.81	0.26
MM-6-18	68.97	0.42	17.58	2.33	0.53	0.16	1.54	5.30	2.90	0.27
MM-6-19	69.14	0.45	17.62	2.16	0.51	0.16	1.48	5.37	2.87	0.25
MM-6-20	69.05	0.47	17.71	2.32	0.52	0.15	1.43	5.26	2.80	0.30

MM-6-21	69.02	0.44	17.75	2.42	0.54	0.11	1.51	5.12	2.83	0.26	
MM-6-22	68.81	0.42	17.82	2.41	0.52	0.18	1.47	5.33	2.77	0.28	
MM-6-23	68.95	0.48	17.56	2.30	0.51	0.16	1.49	5.34	2.90	0.32	
MM-6-24	68.08	0.48	18.12	2.41	0.55	0.20	1.44	5.62	2.75	0.35	
MM-6-25	68.60	0.47	17.97	2.24	0.54	0.14	1.44	5.56	2.79	0.27	
MM-7-01	56.36	1.16	19.27	6.95	2.74	0.18	7.45	4.66	1.10	0.13	
MM-7-02	68.84	0.46	17.87	2.21	0.53	0.15	1.49	5.49	2.68	0.27	
MM-7-03	68.57	0.40	18.00	2.34	0.58	0.13	1.55	5.45	2.62	0.35	
MM-7-04	68.80	0.40	17.56	2.46	0.55	0.16	1.52	5.43	2.90	0.22	
MM-7-06	63.18	0.71	18.68	4.44	1.33	0.09	4.25	5.01	2.12	0.20	
MM-7-07	68.46	0.45	17.41	2.49	0.59	0.14	1.62	5.52	3.08	0.24	
MM-7-08	52.98	1.42	19.37	8.85	3.97	0.15	8.76	3.45	0.96	0.10	
MM-7-09	68.87	0.40	17.60	2.25	0.52	0.11	1.63	5.27	3.10	0.24	
MM-7-10	67.54	0.58	17.85	3.07	0.65	0.13	1.84	4.95	2.96	0.44	
MM-7-11	58.79	1.05	20.57	5.56	1.24	0.10	6.38	4.91	1.18	0.22	
MM-7-12	68.98	0.43	17.58	2.32	0.54	0.18	1.47	5.39	2.85	0.26	
MM-7-13	68.87	0.38	17.87	2.20	0.51	0.11	1.48	5.45	2.82	0.30	
MM-7-14	64.45	0.62	18.30	3.95	1.27	0.18	3.21	5.43	2.38	0.20	
MM-7-15	68.66	0.44	18.10	2.21	0.53	0.17	1.52	5.37	2.70	0.29	
MM-7-16	65.64	0.65	18.66	3.29	0.81	0.11	2.88	5.61	2.11	0.23	
MM-7-17	68.49	0.43	17.86	2.40	0.54	0.15	1.48	5.65	2.75	0.27	
MM-7-18	68.50	0.46	17.79	2.49	0.55	0.18	1.42	5.59	2.77	0.26	
MM-7-19	68.74	0.42	17.80	2.18	0.56	0.14	1.52	5.59	2.80	0.25	
MM-7-20	69.02	0.42	17.61	2.33	0.52	0.11	1.52	5.47	2.75	0.26	
MM-7-21	68.93	0.40	17.90	2.17	0.56	0.15	1.43	5.40	2.78	0.27	
MM-7-22	68.83	0.44	17.67	2.41	0.55	0.13	1.51	5.30	2.79	0.37	
MM-7-23	69.34	0.45	16.92	2.49	0.66	0.15	1.42	5.51	2.78	0.27	
M1s	MM-8-01	52.43	1.94	17.14	11.17	4.10	0.18	8.47	3.36	1.09	0.11

MM-8-02	53.79	2.02	17.94	8.71	4.22	0.18	8.48	3.35	1.16	0.15
MM-8-03	53.28	1.43	19.73	8.52	3.89	0.17	8.26	3.75	0.89	0.08
MM-8-04	51.99	1.80	17.17	12.61	4.30	0.25	7.84	2.70	1.22	0.12
MM-8-05	53.42	1.98	17.75	9.72	3.83	0.20	8.19	3.53	1.26	0.13
MM-8-06	52.67	1.69	17.37	11.26	5.17	0.21	7.41	2.99	1.10	0.12
MM-8-07	68.80	0.44	17.61	2.31	0.51	0.17	1.56	5.19	3.20	0.22
MM-8-08	53.17	1.92	16.60	8.90	5.17	0.20	8.06	4.19	1.62	0.17
MM-8-09	50.85	1.60	17.33	12.25	4.75	0.19	8.60	3.05	1.27	0.10
MM-8-10	52.84	2.15	15.38	11.79	5.16	0.28	7.78	2.92	1.55	0.16
MM-8-11	52.33	1.98	17.45	12.67	3.43	0.21	7.66	2.92	1.17	0.17
MM-8-12	51.94	1.76	17.24	13.83	3.85	0.21	6.62	3.19	1.24	0.12
MM-8-13	52.80	1.76	17.52	12.12	4.06	0.25	7.48	2.61	1.26	0.15
MM-8-14	52.69	1.71	17.96	8.72	5.10	0.18	9.39	3.21	0.90	0.13
MM-8-15	53.14	1.53	19.15	8.65	3.76	0.19	9.08	3.52	0.91	0.07
MM-8-16	53.30	1.98	17.47	9.38	4.68	0.16	7.84	3.76	1.29	0.14
MM-8-17	52.64	1.84	17.00	11.69	4.68	0.23	7.36	2.78	1.64	0.14
MM-8-18	53.08	2.13	15.28	11.44	5.13	0.26	8.05	2.90	1.54	0.18
MM-8-19	53.22	1.09	21.30	7.39	3.99	0.15	7.93	4.02	0.85	0.06
MM-8-20	53.31	1.74	18.48	9.25	3.81	0.19	8.42	3.67	1.01	0.12
MM-8-21	51.79	1.92	16.01	12.66	5.90	0.21	6.46	3.63	1.26	0.17
MM-8-22	53.40	1.91	17.15	11.74	3.84	0.20	7.26	3.09	1.27	0.16
MM-8-23	53.37	1.43	20.53	8.42	3.28	0.12	8.13	3.65	0.96	0.10
MM-8-24	52.29	2.20	15.46	13.79	4.93	0.27	7.24	1.87	1.77	0.18
MM-8-25	53.05	1.69	16.24	10.28	6.69	0.26	6.36	3.83	1.48	0.12
MM-9-01	52.77	1.95	16.43	12.12	4.93	0.15	7.38	2.90	1.26	0.12
MM-9-02	50.97	2.05	16.20	12.63	4.62	0.21	8.79	3.25	1.19	0.09
MM-9-03	52.56	1.93	16.76	10.88	4.51	0.18	8.60	3.50	0.99	0.08
MM-9-04	52.08	1.43	17.87	11.41	5.08	0.16	7.30	3.41	1.16	0.10

	MM-9-05	53.36	1.69	17.64	9.47	4.40	0.17	8.45	3.64	1.07	0.10
	MM-9-06	53.09	2.08	16.09	11.22	5.26	0.24	8.01	2.52	1.35	0.14
	MM-9-07	53.43	1.54	18.67	8.44	5.16	0.19	8.13	3.41	0.92	0.12
	MM-9-08	53.00	1.78	17.77	9.82	4.49	0.22	8.47	3.23	1.09	0.12
	MM-9-09	51.81	1.76	14.91	11.84	8.58	0.20	6.15	3.28	1.37	0.10
	MM-9-10	51.86	1.56	16.25	10.53	7.07	0.21	8.50	3.03	0.89	0.09
	MM-9-11	54.40	1.93	17.49	9.14	3.99	0.17	8.61	3.15	1.04	0.09
	MM-9-13	52.33	1.66	17.29	8.83	5.16	0.16	10.55	3.16	0.82	0.06
	MM-9-14	52.38	1.95	17.22	11.95	3.57	0.21	8.45	3.05	1.08	0.14
	MM-9-15	52.99	1.71	16.80	9.63	4.91	0.18	8.69	3.71	1.29	0.10
	MM-9-16	53.07	1.86	16.63	10.68	4.99	0.18	7.76	3.30	1.39	0.14
	MM-9-17	53.22	1.80	17.97	10.77	3.71	0.16	8.02	3.04	1.20	0.12
	MM-9-18	52.43	1.12	17.75	9.91	7.33	0.21	7.31	3.03	0.87	0.04
	MM-9-19	52.99	2.05	15.66	11.96	4.90	0.24	7.66	3.02	1.37	0.15
	MM-9-20	53.35	1.49	18.81	8.13	4.50	0.19	9.30	3.35	0.80	0.07
	MM-9-21	52.32	1.58	16.77	12.24	5.91	0.21	6.21	3.38	1.27	0.12
	MM-9-22	52.97	1.93	15.95	11.43	5.77	0.19	6.56	3.52	1.55	0.14
	MM-9-23	53.55	2.07	17.71	11.22	2.51	0.20	7.99	3.15	1.39	0.19
	MM-9-24	53.36	1.80	17.90	9.35	4.36	0.16	8.27	3.57	1.13	0.10
	MM-9-25	53.27	1.63	18.14	10.16	4.06	0.19	7.53	3.61	1.30	0.12
M2	MM-11-01	62.41	0.91	18.65	5.21	1.57	0.16	3.74	5.03	2.11	0.20
	MM-11-02	62.33	0.96	18.77	5.04	1.50	0.17	3.58	5.27	2.22	0.17
	MM-11-03	62.58	0.88	18.62	4.89	1.47	0.16	3.74	5.16	2.27	0.22
	MM-11-04	62.28	0.90	18.97	4.96	1.59	0.16	3.61	5.19	2.07	0.27
	MM-11-05	62.43	0.94	18.96	4.91	1.42	0.11	3.58	5.09	2.20	0.35
	MM-11-06	62.02	0.87	18.70	5.20	1.61	0.15	3.79	5.30	2.17	0.19
	MM-11-07	62.81	0.91	18.59	5.11	1.51	0.16	3.71	4.81	2.22	0.18
	MM-11-09	60.64	1.21	20.06	6.12	1.39	0.16	3.23	4.79	2.13	0.27

MM-11-10	62.61	0.96	18.72	4.84	1.52	0.18	3.84	4.93	2.20	0.21
MM-11-11	61.57	0.96	18.83	5.47	1.67	0.19	3.89	5.22	1.99	0.19
MM-11-12	61.75	0.94	18.97	5.20	1.63	0.18	3.92	5.12	2.10	0.19
MM-11-13	62.28	0.87	19.08	5.09	1.49	0.15	3.66	5.03	2.11	0.24
MM-11-14	62.32	0.95	18.80	5.27	1.45	0.15	3.86	4.87	2.14	0.19
MM-11-15	62.32	0.91	18.69	5.17	1.46	0.12	3.61	5.23	2.28	0.21
MM-11-16	62.45	0.92	18.90	5.17	1.43	0.17	3.57	4.94	2.16	0.28
MM-11-17	62.57	0.97	18.90	5.01	1.45	0.15	3.71	4.80	2.21	0.22
MM-11-18	62.43	0.87	19.13	5.22	1.43	0.20	3.49	4.74	2.13	0.36
MM-11-19	62.75	0.93	18.81	4.98	1.43	0.18	3.52	5.13	2.04	0.22
MM-11-20	62.19	0.95	18.93	5.05	1.46	0.15	3.52	5.16	2.23	0.35
MM-11-21	61.65	0.97	18.90	5.43	1.61	0.19	3.87	5.04	2.16	0.17
MM-11-22	62.20	0.94	19.27	5.11	1.44	0.17	3.68	4.65	2.20	0.35
MM-11-23	62.44	0.97	18.97	5.07	1.46	0.19	3.61	4.92	2.20	0.17
MM-12-01	63.16	0.85	18.72	4.89	1.30	0.16	3.26	5.21	2.26	0.19
MM-12-02	63.17	0.88	18.56	5.03	1.32	0.18	3.47	4.84	2.36	0.19
MM-12-03	62.44	0.92	19.02	4.88	1.53	0.15	3.65	4.92	2.21	0.29
MM-12-04	62.50	0.91	18.75	4.92	1.42	0.16	3.49	5.36	2.30	0.20
MM-12-05	62.49	0.95	18.77	5.19	1.56	0.18	3.53	4.86	2.25	0.23
MM-12-06	63.18	0.91	18.63	4.98	1.43	0.15	3.32	4.98	2.22	0.19
MM-12-08	62.98	0.82	19.12	4.68	1.28	0.17	3.56	5.03	2.16	0.21
MM-12-09	62.14	0.95	18.74	5.02	1.60	0.17	3.55	5.41	2.21	0.19
MM-12-10	63.43	0.84	18.59	5.01	1.29	0.16	3.23	4.93	2.26	0.26
MM-12-11	62.53	0.90	18.82	5.16	1.38	0.17	3.61	5.13	2.09	0.21
MM-12-12	62.79	0.94	18.68	5.04	1.44	0.14	3.52	4.92	2.35	0.19
MM-12-13	62.44	0.91	18.56	5.20	1.56	0.21	3.66	5.09	2.20	0.18
MM-12-14	62.66	0.87	18.77	4.99	1.38	0.19	3.63	5.05	2.26	0.19
MM-12-15	62.65	0.88	18.82	4.74	1.45	0.14	3.73	5.01	2.35	0.23



MM-13-20	63.78	0.85	18.76	4.88	1.31	0.17	3.38	4.34	2.31	0.22
MM-13-21	63.51	0.88	18.77	4.89	1.25	0.18	3.13	4.89	2.28	0.20
MM-13-22	64.40	0.59	18.53	4.70	1.09	0.16	2.92	4.94	2.42	0.24
MM-13-24	63.58	0.82	18.66	4.96	1.16	0.10	2.92	4.83	2.44	0.53
MM-13-25	64.16	0.80	18.44	4.55	1.16	0.18	2.94	4.97	2.54	0.26

**Table II Major element composition of minerals from M1p, M1s and M2 units acquired by electron microprobe (EMP) analysis conducted at Victoria University of Wellington, New Zealand (Analysts: Carolina Geoffroy-Gomez and Brent V. Alloway).**

Plagioclases										
Unit	Sample	SiO <sub>2</sub>	TiO <sub>2</sub>	Al <sub>2</sub> O <sub>3</sub>	FeO	CaO	Na <sub>2</sub> O	K <sub>2</sub> O	MgO	Total
M1p	ABR15-1D-P1-core	59.89	0.02	26.20	0.31	7.19	6.46	0.49	0.01	100.57
	ABR15-1D-P2-core	56.46	0.04	27.01	0.43	8.91	5.67	0.30	0.02	98.84
	ABR15-1D-P7-core	56.48	0.03	26.54	0.39	8.63	5.81	0.36	0.04	98.27
	ABR15-1DPM-P1-core	56.68	0.03	27.34	0.56	8.79	5.65	0.36	0.06	99.47
	ABR15-1DPM-P2-core	55.92	0.03	27.93	0.47	9.64	5.54	0.32	0.04	99.89
	ABR15-1DPM-P11-core	54.28	0.05	29.06	0.45	10.91	4.83	0.21	0.04	99.83
	ABR15-1DPM-P7-core	58.99	0.03	25.69	0.30	7.02	6.71	0.45	0.01	99.19
	ABR15-1DPM-P13-core	58.83	0.04	26.02	0.45	7.42	6.64	0.43	0.03	99.85
	ABR15-1A-P4-core	58.71	0.03	26.38	0.36	7.98	6.45	0.39	0.02	100.34
	ABR15-1A-P8-core1	59.92	0.03	25.51	0.31	6.86	7.08	0.52	0.03	100.26
	ABR15-1A-P8-core2	60.94	0.03	25.05	0.38	6.48	7.08	0.49	0.01	100.46
	ABR15-5ALFAPM-P1-core	53.37	0.04	28.86	0.45	11.03	4.83	0.19	0.04	98.81
	ABR15-5ALFAPM-P2-core	58.61	0.00	25.75	0.39	7.05	6.45	0.43	0.04	98.72
	ABR15-5ALFAPM-P3-core	55.42	0.04	27.58	0.44	9.21	5.61	0.32	0.04	98.67
	ABR15-5ALFAPM-P6-core	57.74	0.01	25.95	0.39	7.52	6.62	0.39	0.04	98.66
	ABR15-5ALFAPM-P7-core	59.21	0.03	25.43	0.40	6.58	6.72	0.47	0.03	98.87
	ABR15-5ALFA-P8-core	59.71	0.03	25.62	0.34	6.95	6.96	0.45	0.03	100.09
	ABR15-5ALFA-P4-core	59.85	0.02	25.39	0.31	6.71	7.14	0.44	0.03	99.89
	ABR15-5ALFA-P10-core	59.10	0.03	26.07	0.43	7.53	6.82	0.47	0.02	100.45
	ABR15-5ALFA-P6-core	56.22	0.03	27.67	0.46	9.73	5.68	0.29	0.04	100.12
	ABR15-1D-P1-rim1	59.88	0.03	26.05	0.38	7.00	6.60	0.43	0.01	100.38
	ABR15-1D-P1-rim2	57.56	0.03	27.44	0.51	8.75	6.03	0.41	0.02	100.76
	ABR15-1D-P1-rim3	60.02	0.02	25.85	0.34	6.95	6.56	0.52	0.03	100.29
	ABR15-1D-P1-rim4	62.42	0.01	24.65	0.27	5.38	7.03	0.63	0.01	100.40

ABR15-1D-P1-rim5	60.19	0.04	25.83	0.32	6.91	6.69	0.52	0.01	100.49
ABR15-1D-P1-rim6	61.17	0.01	25.50	0.39	6.31	6.73	0.53	0.02	100.66
ABR15-1D-P1-rim7	60.69	0.01	25.86	0.36	6.61	6.95	0.55	0.01	101.03
ABR15-1D-P2-rim1	59.00	0.01	25.34	0.38	6.91	6.50	0.45	0.01	98.62
ABR15-1D-P2-rim2	60.29	0.03	25.43	0.31	6.36	6.71	0.51	0.03	99.68
ABR15-1D-P2-rim3	60.16	0.03	25.48	0.35	6.80	6.49	0.49	0.01	99.82
ABR15-1D-P7-rim	59.53	0.01	25.59	0.38	6.74	6.88	0.47	0.03	99.63
ABR15-1DPM-P1-rim	56.19	0.05	28.54	0.47	9.90	5.32	0.28	0.03	100.78
ABR15-1DPM-P2-rim1	59.22	0.01	26.14	0.36	7.08	6.54	0.46	0.02	99.83
ABR15-1DPM-P2-rim2	59.20	0.02	25.61	0.32	6.79	6.42	0.51	0.03	98.91
ABR15-1DPM-P11-rim1	55.74	0.03	28.14	0.53	9.74	5.39	0.31	0.03	99.90
ABR15-1DPM-P11-rim2	59.82	0.01	25.80	0.32	6.61	6.69	0.50	0.02	99.76
ABR15-1DPM-P7-rim1	57.63	0.04	27.17	0.52	8.36	5.68	0.38	0.04	99.82
ABR15-1DPM-P7-rim2	59.52	0.03	25.69	0.34	6.83	6.72	0.47	0.04	99.64
ABR15-1DPM-P7-rim3	59.56	0.01	25.78	0.31	6.85	6.77	0.51	0.03	99.83
ABR15-1DPM-P7-rim4	58.17	0.03	26.31	0.36	7.55	6.56	0.43	0.03	99.44
ABR15-1DPM-P7-rim5	56.63	0.02	27.26	0.44	8.83	5.90	0.35	0.03	99.45
ABR15-1DPM-P7-rim6	59.35	0.01	25.97	0.37	6.89	6.81	0.45	0.03	99.88
ABR15-1DPM-P7-rim7	59.99	0.03	25.61	0.31	6.53	6.82	0.49	0.01	99.78
ABR15-1DPM-P13-rim	59.14	0.02	25.74	0.36	7.03	6.86	0.48	0.01	99.63
ABR15-1A-P4-rim1	58.64	0.05	26.42	0.46	8.07	6.51	0.40	0.03	100.58
ABR15-1A-P4-rim2	60.31	0.04	25.55	0.43	6.78	7.15	0.45	0.03	100.73
ABR15-1A-P4-rim3	60.06	0.03	25.82	0.41	7.23	7.00	0.44	0.02	101.01
ABR15-1A-P4-rim4	60.18	0.01	25.83	0.32	7.01	7.15	0.48	0.02	101.00
ABR15-1A-P4-rim5	61.14	0.02	25.78	0.36	6.69	7.16	0.47	0.01	101.64
ABR15-1A-P6-rim	49.71	0.03	32.92	0.72	15.75	2.62	0.11	0.09	101.94
ABR15-1A-P7-rim1	58.07	0.02	26.68	0.58	8.45	6.36	0.35	0.04	100.55
ABR15-1A-P7-rim2	57.12	0.04	27.68	0.48	9.34	5.83	0.31	0.04	100.83

ABR15-1A-P7-rim3	58.73	0.03	26.76	0.40	8.07	6.45	0.38	0.02	100.84
ABR15-1A-P7-rim4	57.11	0.02	27.59	0.42	9.28	5.95	0.31	0.02	100.69
ABR15-1A-P7-rim5	58.54	0.02	26.88	0.40	8.33	6.44	0.38	0.03	101.03
ABR15-1A-P7-rim6	57.32	0.03	27.61	0.41	9.21	5.90	0.32	0.02	100.82
ABR15-1A-P7-rim7	58.93	0.04	26.50	0.35	8.01	6.53	0.43	0.02	100.80
ABR15-1A-P8-rim1	61.51	0.03	24.89	0.29	5.81	7.41	0.57	0.02	100.54
ABR15-1A-P8-rim2	60.09	0.02	25.78	0.34	7.03	7.05	0.46	0.03	100.79
ABR15-5ALFAPM-P1-rim1	54.94	0.03	27.79	0.43	9.48	5.51	0.27	0.03	98.47
ABR15-5ALFAPM-P1-rim2	57.29	0.03	26.42	0.34	7.70	6.28	0.37	0.01	98.46
ABR15-5ALFAPM-P1-rim3	58.70	0.03	25.66	0.27	6.71	6.88	0.50	0.03	98.77
ABR15-5ALFAPM-P1-rim4	59.08	0.04	25.37	0.34	6.52	6.40	0.45	0.03	98.23
ABR15-5ALFAPM-P1-rim5	59.25	0.03	25.54	0.37	6.56	6.92	0.46	0.01	99.15
ABR15-5ALFAPM-P2-rim1	59.79	0.04	25.05	0.28	6.21	6.75	0.48	0.02	98.62
ABR15-5ALFAPM-P2-rim2	58.48	0.03	25.81	0.39	7.12	6.22	0.41	0.03	98.50
ABR15-5ALFAPM-P2-rim3	57.69	0.03	26.52	0.31	7.88	6.12	0.37	0.03	98.95
ABR15-5ALFAPM-P2-rim4	58.87	0.01	25.64	0.38	6.80	6.66	0.46	0.04	98.86
ABR15-5ALFAPM-P2-rim5	56.60	0.03	26.83	0.39	8.33	5.97	0.34	0.00	98.48
ABR15-5ALFAPM-P2-rim6	58.87	0.02	25.57	0.34	6.77	6.63	0.47	0.03	98.71
ABR15-5ALFAPM-P2-rim7	59.81	0.02	25.70	0.38	6.63	6.59	0.53	0.03	99.66
ABR15-5ALFAPM-P3-rim1	58.44	0.01	25.66	0.35	7.15	6.69	0.41	0.02	98.73
ABR15-5ALFAPM-P3-rim2	57.23	0.04	26.59	0.39	8.04	6.33	0.34	0.03	99.00
ABR15-5ALFAPM-P3-rim3	59.01	0.03	25.40	0.34	6.59	6.52	0.47	0.03	98.40
ABR15-5ALFAPM-P3-rim4	57.18	0.02	26.08	0.36	7.87	6.29	0.38	0.01	98.19
ABR15-5ALFAPM-P3-rim5	58.92	0.02	25.25	0.34	6.69	6.69	0.45	0.01	98.36
ABR15-5ALFAPM-P3-rim6	56.81	0.03	26.61	0.43	8.34	6.17	0.34	0.01	98.75
ABR15-5ALFAPM-P3-rim7	58.93	0.01	25.41	0.42	6.55	6.94	0.49	0.01	98.75
ABR15-5ALFAPM-P6-rim1	58.52	0.02	25.66	0.41	7.03	6.70	0.43	0.03	98.81
ABR15-5ALFAPM-P6-rim2	57.56	0.04	26.02	0.38	7.64	6.41	0.34	0.02	98.42

ABR15-5ALFAPM-P6-rim3	58.46	0.03	25.59	0.26	6.84	6.83	0.42	0.03	98.46	
ABR15-5ALFAPM-P6-rim4	58.59	0.01	25.33	0.28	6.80	6.84	0.45	0.01	98.29	
ABR15-5ALFAPM-P6-rim5	56.97	0.03	26.60	0.37	7.96	6.37	0.37	0.03	98.70	
ABR15-5ALFAPM-P6-rim6	58.86	0.01	25.16	0.34	6.42	6.76	0.50	0.00	98.04	
ABR15-5ALFAPM-P7-rim1	57.64	0.03	26.23	0.40	7.73	6.37	0.36	0.01	98.76	
ABR15-5ALFAPM-P7-rim2	56.83	0.04	26.48	0.43	8.19	6.18	0.35	0.02	98.52	
ABR15-5ALFAPM-P7-rim3	59.64	0.02	25.43	0.34	6.44	7.12	0.50	0.01	99.50	
ABR15-5ALFA-P8-rim	59.83	0.04	25.39	0.34	6.76	7.05	0.52	0.03	99.95	
ABR15-5ALFA-P4-rim1	59.21	0.02	25.84	0.32	7.32	6.79	0.47	0.02	99.99	
ABR15-5ALFA-P4-rim2	60.19	0.04	24.94	0.29	6.43	7.29	0.53	0.03	99.74	
ABR15-5ALFA-P4-rim3	60.13	0.00	25.59	0.30	6.75	7.20	0.51	0.03	100.51	
ABR15-5ALFA-P4-rim4	60.78	0.02	24.84	0.23	6.11	7.54	0.55	0.02	100.10	
ABR15-5ALFA-P4-rim5	60.12	0.01	25.17	0.26	6.57	7.30	0.49	0.02	99.95	
ABR15-5ALFA-P4-rim6	61.82	0.03	24.06	0.25	5.18	7.60	0.66	0.01	99.61	
ABR15-5ALFA-P4-rim7	60.68	0.02	25.21	0.31	6.40	6.32	0.50	0.03	99.47	
ABR15-5ALFA-P4-rim8	61.10	0.01	24.75	0.30	5.86	7.45	0.54	0.02	100.04	
ABR15-5ALFA-P4-rim9	60.38	0.02	25.58	0.33	6.79	7.18	0.53	0.02	100.84	
ABR15-5ALFA-P10-rim1	55.51	0.04	28.17	0.52	10.12	5.43	0.28	0.05	100.12	
ABR15-5ALFA-P10-rim2	57.84	0.04	26.73	0.48	8.56	6.21	0.39	0.04	100.28	
ABR15-5ALFA-P10-rim3	57.06	0.05	27.21	0.55	9.05	5.94	0.33	0.05	100.24	
ABR15-5ALFA-P10-rim4	54.36	0.03	29.17	0.74	11.35	4.96	0.20	0.05	100.87	
ABR15-5ALFA-P10-rim5	60.57	0.04	25.42	0.43	6.78	7.10	0.50	0.03	100.88	
ABR15-5ALFA-P6-rim1	57.04	0.04	27.28	0.33	8.94	6.14	0.30	0.04	100.11	
ABR15-5ALFA-P6-rim2	60.16	0.01	25.73	0.33	7.07	6.99	0.49	0.01	100.78	
ABR15-5ALFA-P6-rim3	56.92	0.03	27.41	0.44	9.25	5.90	0.35	0.03	100.33	
ABR15-5ALFA-P6-rim4	60.30	0.01	25.98	0.24	6.90	7.20	0.47	0.02	101.12	
ABR15-1A-P3-plagmicrolito	61.16	0.03	25.06	0.39	6.00	7.07	0.54	0.01	100.26	
<u>M1s</u>	ABR15-1E-P4-pl	45.26	0.00	34.36	0.45	18.07	1.15	0.04	0.12	99.46

ABR15-1F-P3-core2	46.97	0.03	33.09	0.77	16.40	2.03	0.04	0.07	99.42
ABR15-1F-P3-core1	46.34	0.03	33.62	0.81	16.87	1.68	0.07	0.07	99.49
ABR15-1F-P4-core	45.89	0.01	33.95	0.68	17.06	1.51	0.05	0.11	99.26
ABR15-1F-P2-core	46.41	0.03	33.50	0.58	16.63	1.70	0.07	0.05	98.97
ABR15-1FPM-P2-core	46.12	0.01	34.23	0.60	17.76	1.45	0.05	0.10	100.32
ABR15-1FPM-P1-core	46.12	0.02	34.58	0.43	17.92	1.42	0.07	0.13	100.69
ABR15-1F-P3-rim1	46.71	0.01	33.38	0.70	16.86	1.75	0.04	0.08	99.53
ABR15-1F-P3-rim2	50.53	0.03	30.44	0.76	13.61	3.40	0.14	0.09	99.01
ABR15-1F-P3-rim3	49.92	0.04	30.84	0.64	14.04	3.18	0.16	0.08	98.89
ABR15-1F-P3-rim4	47.07	0.02	32.44	0.59	16.14	2.08	0.07	0.09	98.49
ABR15-1F-P3-rim5	48.57	0.05	30.72	0.88	14.40	2.99	0.13	0.15	97.88
ABR15-1F-P4-rim1	48.20	0.03	32.40	0.77	15.37	2.40	0.10	0.11	99.39
ABR15-1F-P4-rim2	49.08	0.03	31.54	0.67	14.70	2.77	0.11	0.12	99.02
ABR15-1F-P4-rim3	48.27	0.03	32.31	0.64	15.61	2.41	0.10	0.09	99.45
ABR15-1F-P4-rim4	50.69	0.04	30.65	0.98	13.71	3.29	0.16	0.13	99.66
ABR15-1F-P2-rim	49.59	0.06	30.63	0.68	13.93	3.06	0.14	0.09	98.19
ABR15-1FPM-P2-rim1	48.42	0.02	32.90	0.72	16.04	2.30	0.09	0.09	100.59
ABR15-1FPM-P2-rim2	50.36	0.03	31.32	0.91	14.33	3.02	0.15	0.13	100.26
ABR15-1FPM-P1-rim1	48.00	0.03	33.50	0.65	16.52	2.16	0.17	0.09	101.11
ABR15-1FPM-P1-rim2	50.06	0.02	31.65	0.90	14.83	3.05	0.19	0.12	100.82
ABR15-1F-G3-2-1	50.47	0.07	30.48	0.95	13.69	3.32	0.15	0.12	99.24
ABR15-1F-G3-2-2	51.46	0.16	28.41	1.34	12.47	3.68	0.27	0.46	98.26
ABR15-1F-G3-2-3	52.73	0.69	22.83	4.49	10.74	4.04	0.61	1.88	98.00
ABR15-1F-G3-2-4	50.09	0.07	30.44	0.92	13.71	3.37	0.15	0.12	98.87
ABR15-1F-G3-2-5	51.65	0.08	29.74	1.01	12.96	3.62	0.17	0.14	99.35
ABR15-1F-G3-2-6	53.32	0.44	24.96	3.65	10.71	4.18	0.43	1.71	99.39
ABR15-1F-G3-2-7	53.61	0.58	22.94	4.02	9.20	4.23	0.93	1.94	97.45
ABR15-1F-G3-2-8	51.39	0.10	29.75	1.31	13.05	3.77	0.19	0.21	99.76

ABR15-1F-G3-2-10	53.15	0.62	23.14	4.22	10.25	3.97	0.53	2.33	98.20
ABR15-1F-G1-2	52.62	0.11	28.38	1.43	11.87	4.21	0.31	0.28	99.20
ABR15-1F-G1-6	49.96	0.05	30.97	0.91	13.98	3.31	0.13	0.10	99.41
ABR15-1FPM-G1-1	50.84	0.07	30.47	1.02	13.89	3.48	0.21	0.16	100.13
ABR15-1FPM-G1-2	50.95	0.08	30.27	1.18	13.35	3.59	0.21	0.14	99.77
ABR15-1FPM-G1-3	49.45	0.05	31.69	0.99	15.00	2.81	0.13	0.14	100.26
ABR15-1FPM-G1-4	50.70	0.05	31.06	0.99	14.31	3.40	0.15	0.13	100.79
ABR15-1FPM-G1-5	50.82	0.06	31.10	0.94	14.24	3.42	0.14	0.15	100.87
ABR15-1FPM-G2-1	50.54	0.07	30.73	0.99	13.94	3.18	0.13	0.12	99.71
ABR15-1FPM-G2-2	51.00	0.07	30.68	0.93	13.68	3.46	0.17	0.15	100.14
ABR15-1FPM-G2-3	51.00	0.07	30.99	0.96	14.01	3.20	0.17	0.13	100.54
ABR15-1FPM-G2-4	54.06	0.14	28.18	1.38	11.62	4.36	0.31	0.27	100.32
AGO14-4D-G1-1	55.20	0.15	27.26	1.42	10.75	4.66	0.39	0.22	100.04
AGO14-4D-G1-3	53.71	0.12	27.61	1.25	11.22	4.59	0.30	0.19	98.98
AGO14-4D-G1-4	51.54	0.07	30.99	0.96	13.71	3.43	0.17	0.15	101.01
AGO14-4D-G1-5	52.93	0.81	23.08	5.69	12.03	3.60	0.43	3.03	101.60
AGO14-4D-G1-6	51.19	0.06	31.32	0.98	14.15	3.21	0.15	0.13	101.20
AGO14-4D-G2-2	53.63	1.10	21.89	7.25	10.08	3.84	0.88	1.09	99.76
AGO14-4D-G2-3	53.61	1.10	22.66	6.59	10.42	3.83	0.81	1.19	100.21
AGO14-4D-G2-4	55.52	0.45	25.92	2.44	9.44	5.10	0.55	0.35	99.76
AGO14-4D-G2-5	55.93	0.34	25.85	2.22	9.54	5.09	0.56	0.32	99.85
AGO14-4D-G2-6	51.99	0.78	22.66	9.16	8.58	4.26	1.00	0.96	99.38
AGO14-4D-G2-7	54.12	0.13	28.20	1.30	11.47	4.48	0.28	0.20	100.16
AGO14-4D-G2-8	53.12	0.13	28.01	1.68	11.86	4.34	0.34	0.27	99.75
AGO14-4D-G2-9	55.02	0.14	26.56	1.68	10.55	4.84	0.38	0.24	99.42
AGO14-4D-G2-10	51.14	0.08	30.60	1.06	13.82	3.38	0.18	0.15	100.41
AGO14-4D-G2-11	51.48	0.07	30.63	1.01	13.84	3.35	0.18	0.14	100.69
AGO14-4D-G3-1	52.80	0.08	29.67	1.07	12.91	3.86	0.20	0.16	100.75

	AGO14-4D-G3-2	51.03	0.05	30.85	0.92	14.02	3.26	0.16	0.13	100.43
	AGO14-4D-G3-3	51.60	0.04	30.96	0.84	13.90	3.32	0.21	0.13	101.00
	AGO14-4D-G3-4	51.16	0.07	30.87	0.88	13.96	3.37	0.17	0.14	100.61
	AGO14-4D-G3-5	51.28	0.03	30.87	0.90	13.86	3.38	0.22	0.13	100.66
	AGO14-4D-G3-6	51.67	0.07	30.01	1.00	13.34	3.64	0.24	0.19	100.15
	AGO14-4D-G3-7	50.65	0.05	30.84	0.99	14.16	3.24	0.23	0.15	100.30
	AGO14-4D-G3-8	52.40	0.08	29.71	1.10	12.69	3.96	0.27	0.15	100.36
	AGO14-4D-G4-1	50.32	0.06	30.84	1.03	14.34	3.15	0.14	0.12	100.02
	AGO14-4D-G4-2	50.06	0.07	31.75	0.99	14.88	2.95	0.15	0.12	100.96
	AGO14-4D-G4-3	50.95	0.06	30.88	0.98	14.13	3.25	0.12	0.13	100.49
M2	ABR15-5C-P2-core	58.21	0.00	27.23	0.07	8.62	6.24	0.18	0.00	100.54
	ABR15-5C-P1-core	58.64	0.02	26.93	0.34	8.38	6.08	0.40	0.04	100.84
	ABR15-5C-P3-core	54.02	0.03	29.67	0.58	11.79	4.52	0.27	0.07	100.94
	ABR15-5D-P1-core2	50.80	0.04	27.94	0.44	10.63	4.44	0.23	0.06	94.58
	ABR15-5DPM-P7-core	57.74	0.03	26.35	0.28	8.16	5.80	0.46	0.03	98.85
	ABR15-5B-P1-core	59.17	0.02	25.86	0.27	7.28	6.68	0.53	0.02	99.83
	ABR15-5B-P3-core	56.24	0.01	26.88	0.31	9.28	5.80	0.33	0.02	98.85
	ABR15-5B-P4-core	57.28	0.02	27.40	0.32	9.11	6.00	0.36	0.02	100.50
	ABR15-5C-P2-rim1	55.19	0.00	29.19	0.05	11.23	4.95	0.04	0.01	100.66
	ABR15-5C-P1-rim	56.64	0.06	26.31	0.66	8.74	5.59	0.43	0.07	98.49
	ABR15-5C-P3-rim	57.54	0.07	27.69	0.60	9.56	5.72	0.33	0.08	101.59
	ABR15-5D-P1-rim1	54.89	0.07	25.92	0.50	8.08	5.83	0.35	0.09	95.73
	ABR15-5DPM-P7-rim	58.22	0.02	27.07	0.30	8.48	5.91	0.44	0.02	100.45
	ABR15-5B-P1-rim1	59.39	0.02	25.57	0.35	7.27	6.50	0.52	0.02	99.63
	ABR15-5B-P1-rim2	57.84	0.02	26.50	0.31	8.29	6.27	0.46	0.01	99.71
	ABR15-5B-P1-rim3	59.13	0.02	25.92	0.28	7.38	6.68	0.53	0.01	99.95
	ABR15-5B-P1-rim4	58.06	0.04	26.52	0.35	8.19	6.43	0.48	0.02	100.08
	ABR15-5B-P1-rim5	55.69	0.06	27.58	0.58	9.93	5.48	0.36	0.04	99.72

ABR15-5B-P3-rim	54.48	0.04	28.49	0.50	10.93	4.83	0.24	0.06	99.57
ABR15-5B-P4-rim1	56.69	0.03	27.79	0.39	9.68	5.70	0.34	0.03	100.65
ABR15-5B-P4-rim2	53.95	0.04	29.09	0.55	11.51	4.69	0.22	0.07	100.11
ABR15-5B-P4-rim3	59.63	0.08	26.10	0.58	7.60	6.90	0.50	0.07	101.46
ABR15-5C-G2-3-1	58.04	0.06	27.00	0.64	8.65	6.02	0.40	0.04	100.86
ABR15-5C-G2-3-2	58.60	0.07	26.62	0.64	8.36	6.22	0.44	0.03	100.97
ABR15-5C-G2-4-1	60.85	0.11	24.71	0.89	6.76	6.38	0.78	0.11	100.60
ABR15-5C-G2-4-2	60.12	0.10	24.92	0.88	6.94	6.48	0.71	0.11	100.26
ABR15-5C-G2-4-3	58.49	0.03	26.68	0.49	8.18	6.19	0.45	0.03	100.54
ABR15-5B-G1-pl1	57.72	0.10	24.86	0.72	7.69	6.43	0.56	0.10	98.18
ABR15-5B-G1-pl3	57.03	0.04	27.36	0.61	9.33	5.79	0.42	0.06	100.63
ABR15-5B-G2-pl1	58.32	0.06	25.94	0.77	7.94	6.29	0.56	0.08	99.96
ABR15-5B-G2-pl2	56.12	0.09	27.45	0.59	9.58	5.56	0.34	0.08	99.82
ABR15-5B-G2-pl3	56.90	0.08	27.03	0.59	9.15	5.98	0.40	0.05	100.17
ABR15-5B-G3-pl1	58.18	0.06	26.24	0.51	8.14	6.54	0.46	0.05	100.19
ABR15-5B-G3-pl2	58.19	0.15	24.77	1.01	7.52	6.37	0.69	0.14	98.83

Clinopyroxenes												
Unit	Sample	SiO <sub>2</sub>	TiO <sub>2</sub>	Al <sub>2</sub> O <sub>3</sub>	Cr <sub>2</sub> O <sub>3</sub>	FeO	MnO	MgO	CaO	Na <sub>2</sub> O	K <sub>2</sub> O	Total
M1s	ABR15-1E-P6-core	50.39	0.67	4.65	0.42	5.24	0.15	15.40	21.56	0.33	0.01	98.82
	ABR15-1E-P3-core	49.55	0.95	4.76	0.00	6.60	0.15	14.49	21.63	0.37	0.00	98.50
	ABR15-1E-P4-core	49.92	0.93	3.97	0.02	6.42	0.19	14.77	21.28	0.39	0.00	97.89
	ABR15-1E-P5-1-core	50.40	0.59	4.34	0.27	5.05	0.13	15.80	21.50	0.29	0.01	98.38
	ABR15-1FPM-P3-core	51.60	0.65	4.11	0.22	5.35	0.14	16.17	21.79	0.31	0.00	100.34
	ABR15-1FPM-P5-core	51.53	0.56	4.06	0.32	4.81	0.16	16.26	22.02	0.30	0.01	100.03
	AGO14-4D-P1-core	48.84	1.09	5.18	0.11	6.85	0.18	14.16	20.87	0.37	0.03	97.69
	AGO14-4D-P3-core	49.75	0.90	3.91	0.00	6.57	0.17	14.75	21.24	0.37	0.01	97.67
	AGO14-4D-P4-core	50.06	0.72	4.29	0.08	5.77	0.16	15.23	21.15	0.36	0.00	97.82
	MEL115-1F-P2-core	47.99	0.89	4.63	0.06	6.33	0.15	13.94	20.61	0.31	0.00	94.91

	ABR15-1E-P6-rim	50.50	0.76	4.17	0.21	6.31	0.16	15.25	21.47	0.37	0.00	99.18
	ABR15-1E-P3-rim	48.98	1.08	5.28	0.08	6.86	0.19	14.30	21.18	0.34	0.00	98.28
	ABR15-1E-P4-rim	49.91	0.88	3.97	0.02	6.28	0.19	14.86	21.48	0.33	0.00	97.93
	ABR15-1E-P5-1-rim	49.96	0.72	3.93	0.22	6.05	0.17	15.05	21.36	0.39	0.01	97.86
	ABR15-1FPM-P3-rim	50.08	0.86	5.08	0.27	5.80	0.14	15.10	21.50	0.36	0.01	99.20
	ABR15-1FPM-P5-rim	50.36	0.85	4.27	0.13	6.40	0.18	15.33	21.23	0.29	0.00	99.03
	AGO14-4D-P1-rim	50.64	0.48	4.04	0.27	4.81	0.15	16.06	21.56	0.28	0.03	98.32
	AGO14-4D-P3-rim	50.58	0.66	3.45	0.14	6.02	0.21	15.36	21.19	0.31	0.00	97.93
	AGO14-4D-P4-rim	49.53	0.94	4.90	0.03	6.72	0.14	14.52	21.37	0.40	0.03	98.57
	MEL115-1F-P2-rim	49.19	0.61	3.94	0.15	5.14	0.13	14.98	20.91	0.30	0.01	95.36
M2	ABR15-5C-P6-Cpx1-core	50.40	0.69	3.87	0.06	6.48	0.20	15.10	21.36	0.32	0.01	98.48
	ABR15-5C-P6-Cpx2-core	50.85	0.63	4.12	0.13	5.57	0.12	15.74	21.83	0.32	0.02	99.33
	ABR15-5D-P4-core	49.39	0.56	2.08	0.00	5.73	0.32	15.12	18.69	0.33	0.01	92.24
	ABR15-5C-P6-Cpx1-rim1	51.59	0.64	4.19	0.08	5.33	0.16	15.76	21.85	0.31	0.00	99.91
	ABR15-5C-P6-Cpx1-rim2	48.87	0.90	5.30	0.19	6.76	0.17	14.21	21.36	0.32	0.02	98.11
	ABR15-5C-P6-Cpx2-rim	51.14	0.67	3.33	0.02	6.75	0.17	15.60	21.21	0.32	0.00	99.22
	ABR15-5D-P4-rim	48.82	0.74	2.67	0.00	5.96	0.34	14.50	18.80	0.38	0.01	92.23

Orthopyroxenes										
Unit	Sample	SiO <sub>2</sub>	TiO <sub>2</sub>	Al <sub>2</sub> O <sub>3</sub>	Cr <sub>2</sub> O <sub>3</sub>	FeO	MnO	MgO	CaO	Total
	ABR15-1D-P4-core	53.29	0.16	0.57	0.00	18.57	1.88	24.08	1.30	99.84
	ABR15-1DPM-P4-core	52.10	0.24	0.65	0.00	16.58	1.90	23.84	1.01	96.31
	ABR15-1A-P1-core	54.02	0.22	0.81	0.01	18.47	1.90	24.78	1.10	101.32
	ABR15-1A-P5-core	53.62	0.21	0.86	0.01	18.60	2.15	24.24	1.08	100.76
M1p	ABR15-5ALFAPM-P8-core	52.73	0.17	0.64	0.00	16.79	1.83	24.63	0.81	97.60
	ABR15-5ALFAPM-P5-core	52.83	0.19	0.70	0.02	17.59	1.95	24.24	1.01	98.53
	ABR15-5ALFAPM-P10-core	53.31	0.13	0.41	0.00	17.81	2.10	24.25	1.01	99.02
	ABR15-5ALFAPM-P5-core2	52.76	0.16	0.52	0.00	17.57	2.18	24.15	1.00	98.34
	ABR15-5ALFA-P7-core	53.94	0.14	0.46	0.01	15.38	1.87	24.62	0.98	97.41

	ABR15-1D-P4-rim	54.06	0.18	0.77	0.00	19.02	2.12	24.31	1.24	101.70
	ABR15-1DPM-P4-rim	52.68	0.19	0.69	0.01	16.38	1.81	24.17	1.07	97.01
	ABR15-5ALFAPM-P10-rim	53.79	0.18	0.74	0.03	17.50	1.86	25.03	1.15	100.28
	ABR15-5ALFAPM-P5-rim2	53.09	0.19	0.59	0.00	17.13	1.89	24.76	1.03	98.67
	ABR15-5ALFA-P7-rim	53.74	0.17	0.60	0.00	15.95	1.81	24.59	0.93	97.79
M2	ABR15-5C-P8-core	51.83	0.21	0.75	0.02	24.04	1.38	19.88	1.71	99.82
	ABR15-5DPM-P7-core	51.85	0.23	0.74	0.00	24.18	1.33	19.61	1.81	99.75
	ABR15-5DPM-P7-rim	51.75	0.13	0.52	0.00	25.99	1.50	18.47	1.79	100.16

Olivines										
Unit	Sample	SiO <sub>2</sub>	TiO <sub>2</sub>	Cr <sub>2</sub> O <sub>3</sub>	FeO	MnO	MgO	NiO	CaO	Total
	abr15_1E_1_core (P1)	38.67	0.00	0.00	17.31	0.26	42.74	0.03	0.09	99.11
	abr15_1E_2_core (P1)	38.48	0.00	0.01	19.32	0.31	41.11	0.03	0.08	99.35
	ABR15-1E-P5-2-core	38.74	0.00	0.03	16.65	0.26	42.87	0.06	0.09	98.70
	ABR15-1F-P6-core	38.29	0.00	0.02	18.53	0.32	42.18	0.04	0.08	99.45
	ABR15-1FPM-P7-core	39.01	0.00	0.01	17.80	0.24	43.53	0.06	0.09	100.73
	ABR15-1FPM-P6-core	39.19	0.00	0.01	17.12	0.26	43.25	0.11	0.08	100.02
	ABR15-1FPM-P4-core	38.84	0.02	0.00	17.76	0.32	42.14	0.03	0.09	99.18
	ABR15-1FPM-P10-core	38.66	0.00	0.01	19.99	0.31	42.04	0.00	0.10	101.11
M1s	ABR15-1FPM-P11-core	38.48	0.00	0.01	21.43	0.31	40.70	0.07	0.10	101.11
	ABR15-1E-P8-core	38.39	0.00	0.02	17.79	0.28	42.11	0.07	0.09	98.74
	ago14-4d-p1-core	38.21	0.01	0.03	19.92	0.30	41.26	0.01	0.07	99.79
	ago14-4d-p5-core	38.41	0.01	0.01	16.59	0.20	42.80	0.08	0.09	98.18
	ago14-4d-p2-core	39.04	0.01	0.02	15.45	0.24	44.62	0.10	0.08	99.56
	ago14-4d-p2-core2	39.12	0.00	0.02	15.69	0.23	44.63	0.10	0.08	99.87
	ago14-4d-p6-core	38.39	0.00	0.00	17.24	0.28	42.27	0.07	0.07	98.31
	MEL115-1F-p1-core	37.76	0.00	0.00	15.65	0.21	41.96	0.08	0.08	95.75
	abr15_1E_1_rim	38.13	0.01	0.02	20.16	0.32	40.82	0.02	0.09	99.55

	abr15_1E_2_rim	37.89	0.03	0.01	21.94	0.36	39.07	0.01	0.10	99.42
	ABR15-1E-P5-2-rim	37.90	0.02	0.03	20.41	0.31	39.66	0.00	0.12	98.45
	ABR15-1F-P6-rim	38.09	0.02	0.00	20.08	0.30	40.68	0.00	0.09	99.26
	ABR15-1FPM-P7-rim	38.27	0.01	0.02	21.16	0.34	40.01	0.04	0.10	99.94
	ABR15-1FPM-P6-rim	38.22	0.01	0.01	21.69	0.36	39.63	0.09	0.09	100.10
	ABR15-1FPM-P4-rim	38.28	0.00	0.03	21.22	0.34	39.43	0.02	0.09	99.40
	ABR15-1FPM-P11-rim	38.53	0.01	0.02	21.22	0.37	39.74	0.04	0.13	100.07
	ABR15-1E-P8-rim	37.71	0.03	0.00	20.09	0.39	38.96	0.11	0.11	97.39
	ago14-4d-p1-rim	38.27	0.00	0.04	18.72	0.30	41.16	0.07	0.07	98.63
	ago14-4d-p5-rim	38.22	0.03	0.01	20.43	0.33	39.97	0.03	0.10	99.12
	ago14-4d-p2-rim2	38.77	0.00	0.02	21.00	0.29	40.12	0.03	0.10	100.34
	ago14-4d-p2-rim	39.13	0.04	0.00	20.58	0.31	40.27	0.00	0.10	100.43
	ago14-4d-p6-rim	37.86	0.13	0.03	22.18	0.31	37.99	0.02	0.09	98.61
	MEL115-1F-p1-rim	36.84	0.01	0.03	20.79	0.33	37.74	0.03	0.09	95.85
	abr15_1E_P4-microlite7	37.79	0.03	0.01	20.62	0.32	38.83	0.00	0.11	97.70
	abr15_1E_P4-microlite5	37.93	0.02	0.00	20.43	0.35	39.73	0.03	0.11	98.59
	ABR15-1F-G3-2	37.64	0.04	0.02	20.63	0.36	39.18	0.00	0.13	97.99
	ABR15-1F-G1-1	38.17	0.02	0.00	19.85	0.34	40.49	0.00	0.10	98.99
	ABR15-1F-G1-2	37.84	0.02	0.01	19.44	0.33	40.07	0.06	0.12	97.89
	ABR15-1FPM-G2	38.33	0.03	0.01	21.80	0.36	39.85	0.00	0.10	100.48
	AGO14-4D-G3-10	37.75	0.03	0.02	20.67	0.32	39.37	0.01	0.13	98.30
	AGO14-4D-G3-9	37.70	0.04	0.00	21.72	0.35	38.80	0.06	0.11	98.79
	AGO14-4D-G4-4	37.42	0.04	0.01	21.28	0.35	38.65	0.03	0.13	97.90
	AGO14-4D-G4-5	37.55	0.04	0.02	21.99	0.31	38.86	0.00	0.12	98.90
	AGO14-4D-G4-6	37.61	0.05	0.01	21.47	0.35	38.85	0.06	0.10	98.50
M2	ABR15-5C-P6-Ol1	36.99	0.01	0.02	24.25	0.37	37.44	0.00	0.11	99.18
	ABR15-5C-P6-Ol2	37.84	0.01	0.01	24.78	0.38	37.52	0.00	0.10	100.64
	ABR15-5C-P6-Ol3	37.82	0.01	0.01	24.65	0.38	37.78	0.00	0.11	100.78

Amphiboles												
Unit	Sample	SiO <sub>2</sub>	TiO <sub>2</sub>	Al <sub>2</sub> O <sub>3</sub>	Cr <sub>2</sub> O <sub>3</sub>	FeO	MnO	MgO	CaO	Na <sub>2</sub> O	K <sub>2</sub> O	Total
M1p	ABR15-1D-P8-core	43.65	3.16	9.67	0.00	12.52	0.75	14.39	10.63	2.70	0.43	97.90
	ABR15-1D-P9-core2	42.50	2.94	10.50	0.03	12.86	0.57	14.13	10.86	2.79	0.43	97.60
	ABR15-1D-P10-core	41.82	3.01	10.71	0.00	12.87	0.43	13.71	10.88	2.87	0.41	96.70
	ABR15-1D-P11-core	42.14	3.36	10.70	0.00	12.78	0.60	13.72	10.80	2.79	0.42	97.32
	ABR15-1D-P5-core	42.48	3.20	9.61	0.00	12.43	0.70	14.09	10.78	2.63	0.42	96.34
	ABR15-1D-P12-core	42.87	3.21	9.48	0.00	12.34	0.71	14.11	10.67	2.66	0.43	96.47
	ABR15-1D-P6-core	41.55	3.54	10.79	0.00	12.16	0.44	13.74	10.65	2.76	0.39	96.01
	ABR15-1D-P3-core	42.59	3.14	9.49	0.00	12.39	0.68	13.81	10.36	2.45	0.41	95.32
	ABR15-1DPM-P1-core	41.81	3.61	10.66	0.00	12.29	0.46	14.22	11.03	2.76	0.41	97.23
	ABR15-1DPM-P2-core	42.99	3.17	9.73	0.00	12.35	0.67	14.76	10.62	2.62	0.44	97.35
	ABR15-1DPM-P11-core	42.94	3.12	9.81	0.00	12.15	0.59	14.78	10.60	2.64	0.46	97.09
	ABR15-1DPM-P7-core	43.07	3.16	9.58	0.00	12.01	0.61	14.65	10.62	2.63	0.43	96.75
	ABR15-1DPM-P6-core	43.94	3.15	9.82	0.03	12.50	0.70	15.25	10.67	2.94	0.44	99.45
	ABR15-1DPM-P12-core2	41.85	2.97	10.90	0.01	13.23	0.63	13.94	10.81	2.75	0.47	97.56
	ABR15-1DPM-P14-core	43.25	3.16	9.81	0.02	12.38	0.65	14.84	10.74	2.73	0.45	98.01
	ABR15-1A-P2-core	42.95	3.43	10.36	0.00	12.77	0.60	14.62	11.10	2.77	0.41	99.01
	ABR15-1A-P3-core	42.39	4.10	11.08	0.00	12.21	0.38	14.61	11.42	2.60	0.42	99.20
	ABR15-1A-P7-core	43.25	3.17	9.99	0.00	12.79	0.66	14.64	10.95	2.63	0.47	98.55
	ABR15-1A-P6-hb1	40.44	3.42	12.15	0.01	14.31	0.20	12.53	11.48	2.44	0.40	97.38
	ABR15-1A-P6-hb2	39.19	4.08	12.15	0.04	17.59	0.26	10.75	11.53	2.49	0.45	98.52
	ABR15-5ALFAPM-P3-core	40.16	3.72	12.38	0.00	11.54	0.29	13.88	11.04	3.00	0.39	96.40
	ABR15-5ALFAPM-P6-core	42.34	3.23	10.05	0.00	11.78	0.57	14.55	10.57	2.81	0.42	96.32
	ABR15-5ALFAPM-P4-core	41.82	3.15	10.48	0.01	12.07	0.55	14.38	10.60	2.72	0.40	96.17
	ABR15-5ALFAPM-P7-core	42.12	3.07	10.12	0.02	11.40	0.49	14.62	10.63	2.86	0.39	95.73
	ABR15-5ALFAPM-P9-core2	42.03	3.12	10.50	0.00	11.31	0.49	14.31	10.53	2.86	0.44	95.60
	ABR15-5ALFA-P1-core	41.57	3.50	10.75	0.00	12.14	0.39	14.30	11.22	2.79	0.40	97.06

ABR15-5ALFA-P2-core	41.82	3.61	10.64	0.01	12.52	0.52	14.13	11.06	2.85	0.37	97.53
ABR15-5ALFA-P3-core	41.91	3.72	10.44	0.00	12.18	0.45	14.46	10.91	2.75	0.40	97.23
ABR15-5ALFA-P10-core	41.93	3.94	10.48	0.01	11.52	0.40	14.56	10.98	2.73	0.41	96.93
ABR15-5ALFA-P5-core	43.01	3.18	9.46	0.00	12.16	0.63	14.55	10.67	2.67	0.41	96.75
ABR15-1D-P8-rim	43.37	3.23	9.70	0.00	12.14	0.69	14.17	10.60	2.70	0.46	97.05
ABR15-1D-P9-rim	43.03	3.40	10.20	0.00	12.25	0.58	14.32	10.71	2.77	0.42	97.68
ABR15-1D-P10-rim	42.57	3.22	10.51	0.01	12.50	0.56	13.95	10.70	2.89	0.41	97.31
ABR15-1D-P11-rim	42.82	3.00	10.41	0.04	12.58	0.60	13.98	10.64	2.81	0.38	97.27
ABR15-1D-P5-rim	42.93	3.13	9.60	0.00	12.33	0.58	14.08	10.63	2.62	0.47	96.37
ABR15-1D-P12-rim	42.90	3.16	9.49	0.00	12.57	0.70	14.42	10.63	2.68	0.43	96.97
ABR15-1D-P6-rim	43.27	3.06	9.46	0.01	11.98	0.69	14.29	10.58	2.73	0.43	96.50
ABR15-1D-P3-rim	42.48	3.11	9.55	0.00	12.27	0.66	13.80	10.55	2.65	0.43	95.50
ABR15-1DPM-P1-rim	42.34	3.27	10.25	0.01	11.99	0.51	14.46	11.04	2.73	0.39	96.99
ABR15-1DPM-P2-rim	43.19	3.06	9.42	0.00	12.40	0.56	14.54	10.54	2.60	0.44	96.75
ABR15-1DPM-P11-rim	43.46	3.13	9.76	0.00	12.42	0.68	14.72	10.62	2.73	0.44	97.97
ABR15-1DPM-P7-rim	42.31	3.30	10.21	0.00	11.89	0.63	14.15	10.61	2.68	0.40	96.19
ABR15-1DPM-P6-rim	43.48	3.13	9.68	0.00	12.51	0.64	14.93	10.70	2.73	0.46	98.26
ABR15-1DPM-P12-rim	43.03	3.06	9.61	0.01	11.94	0.68	14.55	10.61	2.58	0.44	96.52
ABR15-1DPM-P14-rim	43.32	3.07	9.64	0.00	12.24	0.67	14.79	10.62	2.87	0.48	97.71
ABR15-1A-P2-rim	43.57	3.22	9.89	0.01	12.67	0.67	14.83	10.88	2.74	0.43	98.90
ABR15-1A-P3-rim	43.28	3.23	10.23	0.00	12.30	0.66	15.10	10.86	2.80	0.36	98.81
ABR15-1A-P7-rim	44.27	3.10	9.49	0.00	12.35	0.70	15.07	10.78	2.73	0.45	98.94
ABR15-5ALFAPM-P3-rim	43.68	2.96	9.26	0.00	11.58	0.65	15.18	10.39	2.69	0.41	96.80
ABR15-5ALFAPM-P6-rim	41.90	3.47	10.52	0.00	11.48	0.42	14.60	10.80	2.88	0.40	96.45
ABR15-5ALFAPM-P4-rim	42.20	2.97	10.43	0.00	11.47	0.58	14.33	10.59	2.73	0.41	95.71
ABR15-5ALFAPM-P7-rim	42.52	2.43	10.27	0.01	11.67	0.58	14.76	10.58	2.81	0.43	96.04
ABR15-5ALFAPM-P9-rim	42.48	3.10	9.83	0.01	11.32	0.60	14.58	10.45	2.77	0.42	95.56
ABR15-5ALFA-P1-rim	43.07	3.12	9.38	0.00	12.28	0.65	14.50	10.57	2.75	0.42	96.75
ABR15-5ALFA-P2-rim	43.72	3.16	9.47	0.00	12.52	0.69	14.59	10.47	2.78	0.41	97.80
ABR15-5ALFA-P10-rim	41.35	3.86	10.98	0.03	11.57	0.24	14.52	11.17	2.46	0.41	96.59

	ABR15-5ALFA-P5-rim	43.28	3.09	9.65	0.02	12.56	0.63	14.52	10.61	2.81	0.40	97.58
M2	ABR15-5C-P4-core	41.27	3.98	10.65	0.01	13.36	0.32	13.21	10.70	2.65	0.43	96.58
	ABR15-5C-P5-core2	41.34	4.12	10.54	0.00	11.64	0.22	14.13	11.01	2.58	0.39	95.98
	ABR15-5B-P2-core	41.39	4.04	10.47	0.03	12.54	0.32	13.63	10.91	2.69	0.44	96.46
	ABR15-5B-P5-core	41.50	3.98	11.04	0.00	12.86	0.31	14.00	10.99	2.65	0.43	97.76
	ABR15-5C-P4-rim	40.79	4.57	11.03	0.02	11.09	0.24	13.93	11.32	2.65	0.43	96.05
	ABR15-5B-P2-rim	40.44	4.45	10.87	0.00	11.66	0.26	13.84	11.06	2.66	0.40	95.63
	ABR15-5B-P5-rim	41.31	4.33	11.14	0.00	12.35	0.25	13.82	11.16	2.71	0.44	97.50
M1s	ABR15-P72-1-core (1E)	41.98	3.08	10.12	0.00	12.31	0.56	14.07	10.56	2.83	0.38	95.91
	ABR15-P72-2-core (1E)	42.62	3.17	9.42	0.00	12.42	0.66	14.21	10.53	2.70	0.43	96.15
	ABR15-P72-4-core (1E)	40.90	3.56	10.94	0.00	12.67	0.52	13.35	10.87	2.88	0.45	96.14
	ABR15-1F-P5-core	41.95	3.12	10.24	0.02	11.89	0.45	14.15	10.60	2.77	0.38	95.58
	ABR15-1F-P5-rim1	40.97	3.54	11.17	0.01	13.33	0.57	12.91	10.72	2.76	0.44	96.42

Oxides									
Unit	Sample	SiO <sub>2</sub>	Al <sub>2</sub> O <sub>3</sub>	MgO	TiO <sub>2</sub>	FeO	MnO	Cr <sub>2</sub> O <sub>3</sub>	Total
M1p	ABR15-1D-P4-2	0.08	2.02	1.43	12.35	78.34	0.23	0.00	94.45
	ABR15-1D-mg1	0.06	2.12	1.46	12.54	77.66	0.21	0.01	94.06
	ABR15-1D-mg2	0.08	2.10	1.45	12.27	78.20	0.22	0.00	94.32
	ABR15-1D-P4-1	0.02	0.20	3.43	45.39	48.32	1.85	0.00	99.22
	ABR15-1D-ilm1	0.04	0.21	3.46	44.69	46.96	1.71	0.00	97.06
	ABR15-1D-ilm2	0.04	0.19	3.49	45.34	48.73	1.77	0.00	99.56
	ABR15-1DPM-P6-2	0.04	1.95	1.34	11.82	76.19	0.21	0.01	91.56
	ABR15-1A-P5-2	0.04	2.02	1.29	12.03	78.69	0.21	0.01	94.29
	ABR15-1DPM-mg1	0.07	2.80	1.63	12.40	74.98	0.17	0.01	92.06
	ABR15-1DPM-mg3	0.08	2.05	1.34	11.61	77.20	0.21	0.02	92.50
	ABR15-1DPM-mg5	0.06	2.07	1.24	11.77	76.72	0.21	0.01	92.07
	ABR15-1DPM-mg6	0.06	2.06	1.27	11.65	77.73	0.21	0.00	92.98
	ABR15-5ALFAPM-mg1	0.08	2.05	1.31	11.52	73.24	0.20	0.00	88.40

ABR15-5ALFAPM-mg2	0.08	2.17	1.35	11.18	71.84	0.19	0.00	86.81
ABR15-5ALFAPM-mg3	0.08	2.21	1.17	11.53	71.59	0.17	0.01	86.76
ABR15-5ALFAPM-mg4	0.08	2.04	1.29	11.16	71.35	0.19	0.00	86.12
ABR15-5ALFAPM-mg5	0.03	2.10	1.24	11.16	72.14	0.19	0.03	86.88
ABR15-5ALFAPM-mg7	0.06	2.04	1.29	11.46	74.22	0.20	0.01	89.28
ABR15-5ALFAPM-mg8	0.04	2.08	1.32	11.58	74.25	0.19	0.01	89.47
ABR15-5ALFAPM-mg9	0.07	2.15	1.21	11.21	73.75	0.21	0.00	88.59
ABR15-5ALFAPM-mg10	0.04	2.02	1.18	11.52	74.67	0.20	0.00	89.64
ABR15-1DPM-P6-1	0.02	0.21	3.85	43.53	47.66	1.57	0.00	96.84
ABR15-1A-P5-1	0.01	0.20	3.81	45.30	48.99	1.66	0.00	99.97
ABR15-1DPM-ilm1	0.07	0.27	4.39	42.71	48.33	1.28	0.00	97.05
ABR15-1DPM-ilm3	0.07	0.21	3.69	43.26	48.27	1.66	0.01	97.17
ABR15-1DPM-ilm5	0.00	0.20	3.83	44.32	47.51	1.64	0.01	97.49
ABR15-1DPM-ilm6	0.02	0.17	3.79	43.60	48.02	1.73	0.00	97.34
ABR15-5ALFAPM-ilm1	0.03	0.18	3.89	43.08	45.21	1.58	0.00	93.97
ABR15-5ALFAPM-ilm2	0.14	0.23	4.33	42.00	44.12	1.80	0.00	92.61
ABR15-5ALFAPM-ilm3	0.07	0.20	3.96	41.49	44.96	1.62	0.01	92.30
ABR15-5ALFAPM-ilm4	0.00	0.21	3.94	41.97	44.13	1.58	0.01	91.85
ABR15-5ALFAPM-ilm5	0.04	0.20	3.83	41.96	42.98	1.60	0.00	90.61
ABR15-5ALFAPM-ilm7	0.01	0.18	3.86	43.26	45.93	1.59	0.01	94.85
ABR15-5ALFAPM-ilm8	0.04	0.21	3.91	43.39	45.91	1.64	0.02	95.13
ABR15-5ALFAPM-ilm9	0.07	0.18	3.72	42.54	45.05	1.69	0.00	93.25
ABR15-5ALFAPM-ilm10	0.00	0.20	3.91	43.34	46.51	1.61	0.00	95.57
ABR15-5ALFA-mg1	0.07	2.12	2.75	14.66	79.26	0.30	0.00	99.15
ABR15-5ALFA-mg3	0.06	2.07	2.96	14.70	77.54	0.28	0.03	97.65
ABR15-5ALFA-mg2	0.09	2.00	2.89	14.59	77.73	0.29	0.03	97.61
ABR15-5ALFA-mg4	0.06	2.05	3.02	14.96	78.47	0.28	0.00	98.85
ABR15-5ALFA-mg5	0.06	2.13	3.03	15.09	78.81	0.30	0.00	99.41
ABR15-5ALFA-mg6	0.06	2.18	2.92	14.93	78.30	0.27	0.01	98.68

	ABR15-5ALFA-mg7	0.07	2.11	2.97	14.66	77.67	0.30	0.04	97.81
	ABR15-5ALFA-ilm1	0.03	0.22	3.75	44.71	47.26	1.83	0.00	97.80
	ABR15-5ALFA-ilm2	0.03	0.16	3.75	44.57	47.61	1.82	0.00	97.95
	ABR15-5ALFA-ilm3	0.03	0.21	3.83	44.19	46.97	1.68	0.01	96.91
	ABR15-5ALFA-ilm4	0.00	0.20	3.91	45.19	47.52	1.75	0.00	98.57
	ABR15-5ALFA-ilm5	0.02	0.19	3.96	45.05	47.66	1.70	0.00	98.58
	ABR15-5ALFA-ilm6	0.00	0.21	3.92	45.30	45.42	1.72	0.01	96.57
	ABR15-5ALFA-ilm7	0.00	0.21	4.03	44.98	47.78	1.68	0.00	98.69
M2	ABR15-5DPM-P7-2	0.07	2.16	1.23	19.39	72.32	0.17	0.00	95.34
	ABR15-5DPM-P2-2	0.07	2.21	1.33	19.43	72.84	0.15	0.00	96.03
	ABR15-5DPM-mg1	0.07	2.15	1.34	18.82	72.62	0.14	0.01	95.15
	ABR15-5DPM-mg2	0.09	2.27	1.33	17.50	72.05	0.15	0.00	93.39
	ABR15-5DPM-P7-1	0.01	0.16	2.82	47.69	46.34	1.23	0.02	98.28
	ABR15-5DPM-P2-1	0.02	0.15	3.09	48.42	46.51	1.17	0.00	99.36
	ABR15-5DPM-ilm1	0.00	0.16	3.10	48.40	45.40	1.15	0.01	98.21
	ABR15-5DPM-ilm2	0.03	0.36	4.65	45.69	46.83	0.71	0.03	98.29